

Modular Learning of Deep Causal Generative Models for High-dimensional Causal Inference

Md Musfiqur Rahman, Murat Kocaoglu

School of Electrical and Computer Engineering
Purdue University
{rahman89, mkocaoglu}@purdue.edu

January 4, 2024

Abstract

Pearl’s causal hierarchy establishes a clear separation between observational, interventional, and counterfactual questions. Researchers proposed sound and complete algorithms to compute identifiable causal queries at a given level of the hierarchy using the causal structure and data from the lower levels of the hierarchy. However, most of these algorithms assume that we can accurately estimate the probability distribution of the data, which is an impractical assumption for high-dimensional variables such as images. On the other hand, modern generative deep learning architectures can be trained to learn how to accurately sample from such high-dimensional distributions. Especially with the recent rise of foundation models for images, it is desirable to leverage pre-trained models to answer causal queries with such high-dimensional data. To address this, we propose a sequential training algorithm that, given the causal structure and a pre-trained conditional generative model, can train a deep causal generative model, which utilizes the pre-trained model and can provably sample from identifiable interventional and counterfactual distributions. Our algorithm, called Modular-DCM, uses adversarial training to learn the network weights, and to the best of our knowledge, is the first algorithm that can make use of pre-trained models and provably sample from any identifiable causal query in the presence of latent confounders with high-dimensional data. We demonstrate the utility of our algorithm using semi-synthetic and real-world datasets containing images as variables in the causal structure.

1 Introduction

Evaluating the causal effect of an intervention on a system of interest, or understanding what would have happened to a sub-population had a different intervention been taken are fundamental questions that arise across disciplines. Pearl’s structural causal models (SCMs) provide a principled approach to answering such queries from data. Using SCMs, today we have a clear understanding of which causal queries can be answered from data on a fundamental level, and which cannot without further assumptions Pearl (1995); Shpitser and Pearl (2008); Huang and Valtorta (2012); Bareinboim and Pearl (2012a). The associated *identification algorithms* find a closed-form expression for an interventional distribution using only observational data, by making use of the causal structure via do-calculus rules Pearl (1995). With sufficient data, these functionals can be evaluated by first estimating the observational joint distribution, then evaluating these expressions.

Today, most of our datasets contain high-dimensional variables, such as images. Modern deep learning architectures can handle high dimensional data and solve machine learning problems such as prediction or learning the data distribution effectively. However, they fail to generalize where there exists spurious correlations in the data. Even though causal inference algorithms can deal with such issues but are unable to handle high-dimensional variables, i.e., there is no general causal inference algorithm for arbitrary causal structures that can use high-dimensional data. The aforementioned identification algorithms are not applicable since it is practically impossible to obtain a closed-form expression of the joint distribution with high-dimensional image datasets.

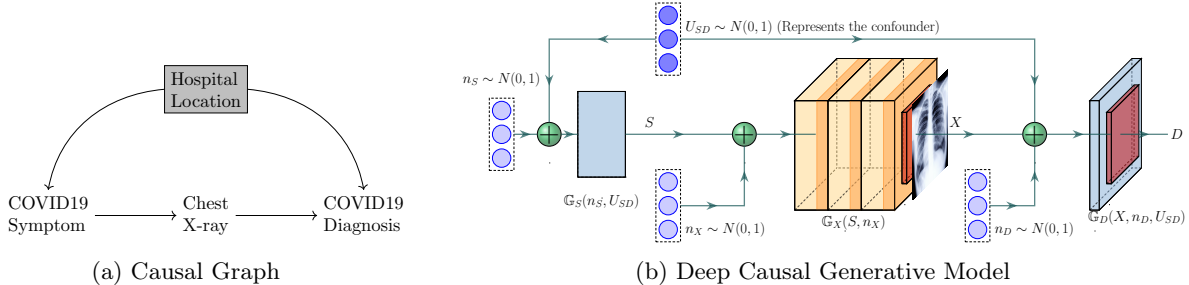


Figure 1: A causal graph for XrayImage example (left) and its deep generative model representation (right). For each variable, a NN (ex: G_S, G_X, G_D) is trained on datasets to mimic the true mechanism.

As an example, consider a healthcare dataset where we observe Symptoms, Diagnosis and XrayImage of a collection of patients. Suppose our dataset contains a mixture data from two hospitals in different cities, which we do not observe to ensure patient privacy. One of the cities is more wealthy, where patients are less likely to fall sick on average, and have access to better-trained doctors who are less likely to misdiagnose them. Then, hospital location acts as a latent confounder that affect both the Symptoms and Diagnosis. Suppose the medical X-ray device is standardized by the World Health Organization and is not affected by the wealth of the cities. In this realistic scenario, the data-generating process can be summarized by the causal graph in Figure 1. We would like to understand how likely an average person across the two cities is to be diagnosed if they get the symptom. This is the well-known *front-door* graph Pearl (2009) where the causal effect of Symptom on Diagnosis can be computed from the observational distribution over Symptom, Diagnosis and XrayImage as follows: $\sum_{x,s'} p(x|s)p(d|x,s')p(s')$. However, it is not possible to reliably estimate $p(x|s)$, i.e., the probability of observing a *specific X-ray image*, given Symptom = s . To the best of our knowledge, no existing causal inference algorithm can address this causal inference problem.

In this paper, we propose a modular sampling-based solution to address this problem. For causal queries with scalar, or low-dimensional targets, we can collect observational samples and use these samples to estimate the interventional distribution. For high-dimensional targets, our method can be used to obtain samples from the interventional distribution, which is implicitly modeled. Our solution uses deep learning architectures that mimic the causal structure of the system, see Figure 1b. Although the use of such structured deep generative models has been explored recently, the existing solutions either assume no unobserved confounders Kocaoglu et al. (2018); Pawlowski et al. (2020), assume all variables are low-dimensional Xia et al. (2021, 2023) or are suitable for specific graphs Louizos et al. (2017); Zhang et al. (2021). On the other hand, our solution is general and not limited to any back-door/front-door graph. Furthermore, these methods do not have the flexibility to use pre-trained models without affecting their weights whereas modularity in our method allows such flexibility. This is useful since state-of-the-art deep models such as image generators can only be successfully trained by a few industrial research labs with expensive resources DALL-E (2022); ChatGPT (2022); Bard (2023). Our algorithm paves the way to utilize these foundation models for causal inference. Finally, our method also enjoys efficient re-training of deep causal generative model, due to our proposed modularity.

We offer efficient training and flexibility in architecture with our key contribution: a modular training algorithm that can identify which parts of the deep causal generative models, can be trained separately (such as G_X in Figure 1b), and which parts should be trained together ($\{G_S, G_D\}$ in Figure 1b). We show that after this modularization, there is a *correct* training order for each sub-network, which our algorithm identifies and follows, freezing the weights of networks already trained in the previous steps of the algorithm. The following are our main contributions:

- We propose an adversarial learning algorithm for training deep causal generative models with latent confounders for high-dimensional variables. We show that, after convergence, our model can produce high-dimensional samples according to interventional or counterfactual queries that are identifiable from the data distributions.
- We propose an algorithm to train deep causal generative models in a modular manner using both observational and interventional datasets while preserving their theoretical guarantees after convergence.

To the best of our knowledge, this is the first algorithm that can modularize the training process in the presence of latent confounders, thereby enabling the use of large pre-trained models for causal effect estimation.

- We demonstrate the utility of Modular-DCM with experiments on high-dimensional semi-synthetic datasets Colored-MNIST and real-world COVIDx CXR-3 dataset. Modular training converges better and can correctly sample from interventional and counterfactual distributions compared to two of our closest benchmarks.

2 Related Works

There are many principled algorithms for estimating interventional or counterfactual distributions in different settings. Shpitser and Pearl (2008) estimate causal effects from observational data using their sound and complete identification algorithms. Bareinboim and Pearl (2012a) proposes zID that utilizes observational and all combinations of experimental datasets to identify causal effects that are not possible to estimate from only observations. Lee et al. (2020) covers both of these problems and suggests the gID algorithm that can make use of arbitrary sets of observational and interventional datasets to estimate a causal query. Similarly, Correa et al. (2021) employs arbitrary combinations of datasets for complete counterfactual identification.

Louizos et al. (2017); Nemirovsky et al. (2020) offer to solve the causal inference problem using deep generative models. Yet, they do not offer theoretical guarantees of causal estimation in general, but for some special cases. Researchers have recently focused on imposing causal structures within neural network structures. Particularly, Kocaoglu et al. (2018) introduces a deep causal model that produces interventional image samples after training on observational data. Pawlowski et al. (2020) applies normalizing flows and variational inference to predict exogenous noise for counterfactual inference. However, a major limitation is the causally sufficiency assumption, i.e., each observed variable is caused by independent unobserved variables. In contrast, the semi-Markovian model having shared unobserved confounders between variables, is quite common in the real world.

For semi-Markovian models, Xia et al. (2021); Balazadeh Meresht et al. (2022) follow a similar approach as Kocaoglu et al. (2018) to arrange neural models as a causal graph. They propose a minimization-maximization method to identify and estimate causal effects. However, these methods use only observational data and do not consider interventional data and hence cannot estimate most counterfactuals. Xia et al. (2023) extends these to identify and estimate counterfactual queries.

Most of the existing methods described above can only handle low-dimensional discrete variables except Bica et al. (2020) and it is not clear how to extend their results to continuous high-dimensional image data. Moreover, if these methods are given a pre-trained neural network model, they do not have the ability to incorporate them in their training. Our approach, to the best of our knowledge, is the first and only solution to address this problem in the presence of unobserved confounders, unlocking the potential of large pre-trained models for causal inference.

3 Background

In this section, we describe the definitions and the concepts used in this paper.

Definition 3.1 (Structural causal model (SCM) (Pearl, 2009)). An SCM \mathcal{M} is a 5-tuple $\mathcal{M} = (\mathcal{V}, \mathcal{N}, \mathcal{U}, \mathcal{F}, P(\cdot))$, where each observed variable $V_i \in \mathcal{V}$ is realized as an evaluation of the function $f_i \in \mathcal{F}$ which looks at a subset of the remaining observed variables $Pa_i \subset \mathcal{V}$, an unobserved exogenous noise variable $E_i \in \mathcal{N}$, and an unobserved confounding variable $U_i \in \mathcal{U}$. $P(\cdot)$ is a product joint distribution over all unobserved variables $\mathcal{N} \cup \mathcal{U}$.

Each SCM induces a directed graph called the *causal graph*, or acyclic directed mixed graph (ADMG) with \mathcal{V} as the vertex set. The directed edges are determined by which variables directly affect which other variable by appearing explicitly in that variable’s function. Thus the causal graph is $G = (V, E)$ where $V_i \rightarrow V_j$ iff $V_i \in Pa_j$. The set Pa_j is called the parent set of V_j . We assume this directed graph is acyclic (DAG). Under the semi-Markovian assumption, each unobserved confounder can appear in the equation of

exactly two observed variables. We represent the existence of an unobserved confounder between X, Y in the SCM by adding a bidirected edge $X \leftrightarrow Y$ to the causal graph. These graphs are no longer DAGs although still acyclic.

V_i is called an ancestor for V_j if there is a directed path from V_i to V_j . Then V_j is said to be a descendant of V_i . The set of ancestors of V_i in graph G is shown by $An_G(V_i)$. A do-intervention $do(v_i)$ replaces the functional equation of V_i with $V_i = v_i$ without affecting other equations. The distribution induced on the observed variables after such an intervention is called an interventional distribution, shown by $P_{v_i}(\mathcal{V})$. $P_\emptyset(\mathcal{V}) = P(\mathcal{V})$ is called the observational distribution. In this paper, we use \mathcal{L}_1 , \mathcal{L}_2 , and \mathcal{L}_3 distributions as notation for observational, interventional, and counterfactual distributions respectively. We follow the same for datasets and queries.

Definition 3.2 (c-components). A subset of nodes is called a c-component if it is a maximal set of nodes in G that are connected by bi-directed paths.

4 Deep Causal Generative Models with Unobserved Confounders

The basic idea behind Kocaoglu et al. (2018) that also motivates our work is the following: Suppose the ground truth data-generating SCM is made up of functions $X_i = f_i(Pa_i, E_i)$. If we have these equations, we can simulate an intervention on, say $X_5 = 1$, by evaluating the remaining equations. However, we can never hope to learn the functions and unobserved noise terms from data. The fundamental observation of Pearl is that even then there are some causal queries that can be uniquely identified as some *deterministic function* of the causal graph and the joint distribution between observed variables, e.g., $p(d|do(s)) = \xi(G, p(s, d, x))$ in Figure 1a for some deterministic ξ . This means that, if we can, somehow, train a causal model made up of neural networks that fits to the data, and has the same causal graph, then it has to induce the same interventional distribution $p(d|do(s))$ as the ground truth SCM, *irrespective of what functions the neural network uses*. This is a very strong idea that allows mimicing the causal structure, and opens up the possibility of using deep learning algorithms for performing causal inference through sampling even with high-dimensional variables.

Xia et al. (2021) took this idea one step further to *check identifiability of a causal query* by maximizing and minimizing the causal effect, which is now a differentiable function since neural nets are used. However, training such networks with high-dimensional data is challenging, and their work is limited to low-dimensional variables. Generative models have been successfully applied to approximately fit high-dimensional image data, which is our training algorithm choice in this paper to handle high-dimensional data. We first define a *deep causal generative model* and show identifiability results, formalizing the simple observation above that allows us to use deep learning to answer causal queries.

We first define a *deep causal generative model* for the unknowns SCM and show identifiability¹ results, formalizing the simple observation above that allows us to use deep learning to answer causal queries.

Definition 4.1. A neural net architecture \mathbb{G} is called a deep causal generative model (DCM) for an ADMG $G = (\mathcal{V}, \mathcal{E})$ if it is composed of a collection of neural nets, one \mathbb{G}_i for each $V_i \in \mathcal{V}$ such that

1. each \mathbb{G}_i accepts a sufficiently high-dimensional noise vector N_i ,
2. the output of \mathbb{G}_j is input to \mathbb{G}_i iff $V_j \in Pa_G(V_i)$,
3. $N_i = N_j$ iff $V_i \leftrightarrow V_j$.

We also define Q as the distribution induced by the DCM. Noise vectors N_i replace both the exogenous noise terms in the true SCM and the unobserved confounders. They need to have sufficiently high dimension to be able to induce the observed distribution. We say a DCM is *representative enough for an SCM* if the neural networks have sufficiently many parameters to induce the observed distribution induced by the true SCM (Assumption 3). We use Conditional Generative Adversarial Nets (Mirza and Osindero, 2014) as neural architectures for the variables in the same c-component that share the same confounders. We choose GANs for this purpose since GANs are effective in matching a joint distribution by feeding the same prior noise into

¹Identifiability here refers to our ability to uniquely sample from an interventional distribution. See Definition C.1 for details.

multiple generators. For variables that are not confounded with others, we can use any architecture such as diffusion models Ho and Salimans (2022). With Definition 4.1, we have the following, similar to Xia et al. (2021):

Theorem 4.2. *Consider any SCM $\mathcal{M} = (G, \mathcal{N}, \mathcal{U}, \mathcal{F}, P(\cdot))$. A DCM \mathbb{G} for G entails the same identifiable interventional distributions as the SCM \mathcal{M} if it entails the same observational distribution.*

Although the theorem focuses on interventional distributions, it can trivially be generalized to any counterfactual distribution by expanding the notion of identifiability to use a given collection of interventional distributions, and requiring the DGM to entail the same interventional distributions for the said collection. Please see Theorem C.3 in Appendix C.2 for the general statement and proof.

Thus, even with high-dimensional variables in the true SCM, given a causal graph, any identifiable interventional query can, in principle, be sampled from by training a DCM that fits the observational distribution. In order to learn the DCM, Kocaoglu et al. (2018); Xia et al. (2021) suggested training all neural nets in the DCM together. However, such an approach to match the joint distribution containing all low and high-dimensional variables is empirically challenging in terms of convergence. Any modularization not only is expected to help train more efficiently for better solution quality but also allow the flexibility to use pre-trained image generative models. We focus on uncovering how to achieve such modularization to improve the training phase and illustrate our contribution along these two aspects.

4.1 Modular-DCM Intuitive Explanation

Consider the graph G in Figure 2. Suppose, we have an observational dataset $D \sim P(\mathcal{V})$. Our goal is to sample from different \mathcal{L}_2 distributions such as $P(X_2|do(X_1))$ and $P(Z_2|do(X_1))$ by training a DCM \mathbb{G} for G that fits the observational data $P(\mathcal{V})$, in accordance with Theorem 4.2. The DCM will contain one feed-forward neural net per observed variable, i.e., $\mathbb{G} = \{\mathbb{G}_{Z_1}, \mathbb{G}_{Z_2}, \mathbb{G}_{Z_3}, \mathbb{G}_{X_1}, \mathbb{G}_{X_2}\}$. The question we are interested in is, which neural nets can be trained separately, and which need to be trained together *to be able to fit the joint distribution*.

Suppose we first train the causal generative model \mathbb{G}_{Z_1} , i.e., learn a mapping that can sample from $P(Z_1|Z_3, X_1)$. Even if we provide the unobserved confounder N_1 (see Definition 4.1), which also affects Z_2 and Z_3 , the neural network might learn a mapping that later makes it impossible to induce the correct dependence between Z_1, Z_2 , or Z_1, Z_3 no matter how \mathbb{G}_{Z_2} or \mathbb{G}_{Z_3} are trained later. This is because fitting the conditional $P(Z_1|Z_3, X_1)$ does not provide any incentive for the model \mathbb{G}_{Z_1} to induce the correct dependency through latent variables. If the model ignores the dependence due to the latent confounders, it cannot induce dependence between Z_3 and Z_2 conditioned on Z_1 . This observation suggests that the causal mechanisms of variables that are in the same c-component should be trained together. Therefore, we have to train $[\mathbb{G}_{Z_1}, \mathbb{G}_{Z_2}, \mathbb{G}_{Z_3}]$ together; similarly $[\mathbb{G}_{X_1}, \mathbb{G}_{X_2}]$ together.

Another issue is that it is very difficult to *condition* in feedforward models during training, which is the case in a DCM. To sample from $Q(z_1|z_3, x_1)$ it is not sufficient to feed z_3, x_1 to the network \mathbb{G}_{Z_1} . In fact, observe that this is exactly the intervention operation and we would give us a sample from $Q(Z_1|do(Z_3, X_1))$. Thus, while training DCMs, it is trivial to intervene on the inputs to a neural network, but highly non-trivial to condition since feedforward models cannot easily be used to correctly update the posterior via backdoor paths. This, together with the previous observation motivates us to fitting interventional distributions, a central part of our algorithm, as we explain below:

To match the joint $P(\mathcal{V})$ for semi-Markovian models while preserving the integrity of c-components, we propose using Tian’s factorization (Tian and Pearl, 2002). It factorizes $P(\mathcal{V})$ into c-factors: the joint distributions of each c-component C_j intervened on their parents, i.e., $P_{pa(C_j)}(C_j)$.

$$P(v) = P(x_1, x_2|do(z_1))P(z_1, z_2, z_3|do(x_1)) \quad (1)$$

Due to this factorization, matching $P(\mathcal{V})$ is equivalent to matching each of the c-factors. If we had access to the \mathcal{L}_2 distributions from $do(z_1)$ and $do(x_1), \forall z_1, x_1$, we could intervene on \mathbb{G}_{Z_1} and \mathbb{G}_{X_1} in the DCM to obtain $do(z_1)$ and $do(x_1)$ samples and train the generative models to match these \mathcal{L}_2 distributions. However, we only have access to the $P(\mathcal{V})$ dataset. Our key idea is to **leverage the do-calculus rule-2** (Pearl, 1995) to use observational samples and pretend that they are from these \mathcal{L}_2 distributions. This gives us a handle on how to modularize the training process of c-components.

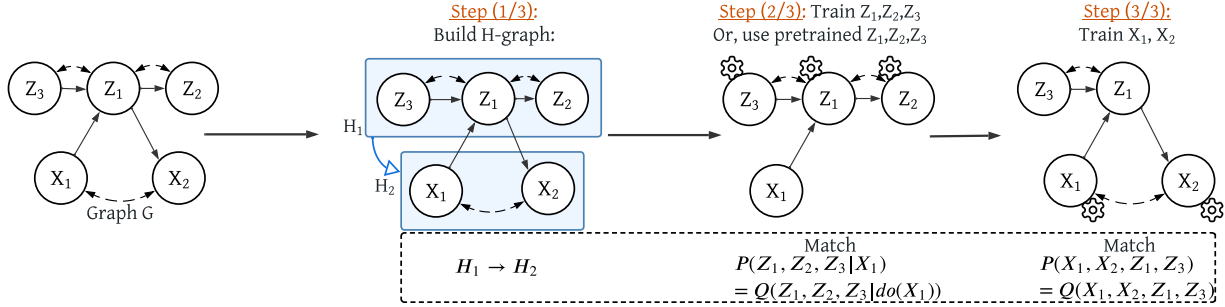


Figure 2: Modular training in 3 steps. Step 1: Since $P(X_1, X_2|do(Z_1)) \neq P(X_1, X_2|Z_1)$, we add an edge from c-component $H_1 : [Z_1, Z_2, Z_3]$ to c-component $H_2 : [X_1, X_2]$. Step 2: we train only the mechanisms in H_1 to match $P(Z_1, Z_2, Z_3|X_1) = Q(Z_1, Z_2, Z_3|do(X_1))$. Step 3: We train only H_2 while using pre-trained Z_1, Z_3 to match $P(X_1, X_2, Z_1, Z_3) = Q(X_1, X_2, Z_1, Z_3)$.

For example, in Figure 2, c-factor $P(z_1, z_2, z_3|do(x_1)) = P(z_1, z_2, z_3|x_1)$ since do-calculus rule-2 applies, i.e., intervening on X_1 is equivalent to conditioning on X_1 . We can then use the conditional distribution as a proxy/alternative to the c-factor to learn $Q(z_1, z_2, z_3|do(x_1))$ with the DCM. However, $P(x_1, x_2|do(z_1)) \neq P(x_1, x_2|z_1)$. To overcome this issue, we seek to fit a joint distribution that implies this c-factor, i.e., we find a superset of X_1, X_2 on which rule-2 applies. We can include Z_1 into the joint distribution that needs to be matched together with X_1, X_2 and check if the parent set of $\{X_1, X_2, Z_1\}$ satisfy rule-2. We continue including variables until we reach the joint $P(x_1, x_2, z_1, z_3)$ to be the alternative distribution for $\{X_1, X_2\}$'s c-factor.

After identifying which sub-networks of the DCM can be trained separately, we need to decide a *valid order* in which they should be trained. For the same example, we can first train $[\mathbb{G}_{Z_1}, \mathbb{G}_{Z_2}, \mathbb{G}_{Z_3}]$ together to induce $Q(z_1, z_2, z_3|do(x_1)) = P(z_1, z_2, z_3|x_1) = P(z_1, z_2, z_3|do(x_1))$. This is shown in step (2/3) in Figure 2: We can produce samples from the mechanisms of Z_1, Z_2, Z_3 by intervening on their parent X_1 with real observations from dataset D . Thus, we do not need \mathbb{G}_{X_1} to be pre-trained.

Now, we train mechanisms of the next c-component $[\mathbb{G}_{X_1}, \mathbb{G}_{X_2}]$ in our training order (step 3/3). As discussed, we need to ensure $Q(X_1, X_2, Z_1, Z_3|do(\emptyset)) = P(X_1, X_2, Z_1, Z_3|do(\emptyset)) = P(X_1, X_2, Z_1, Z_3|\emptyset)$. Since mechanisms of Z_1, Z_3 were trained in the previous step, we can freeze the neural network weights of $[\mathbb{G}_{Z_1}, \mathbb{G}_{Z_3}]$. These are used to correctly sample from Z_1 given X_1 , and feed this correctly sampled value into the network of X_2 . In Appendix D.1, we show that the c-factors in Equation 1 will correctly match the true c-factors after fitting these two conditional probabilities in this order. Therefore, DCM matches the joint distribution $P(\mathcal{V})$ as well. On the other hand, if we first trained the networks $[\mathbb{G}_{X_1}, \mathbb{G}_{X_2}]$, it would not be possible to match the joint distribution $P(x_1, x_2, z_1, z_3)$ as the mechanisms of Z_1, Z_3 are not yet trained. Thus, this order would not work.

Note that, without modularization, we have to match $P(X_1, X_2, Z_1, Z_2, Z_3)$ containing all low and high dimensional variables in a single training phase. Matching that joint distribution by training all models, at the same time, could be difficult since we are attempting to minimize a very complicated loss function. Our proposed method allows us to reduce the complexity of this problem by modularizing the training process to c-components X_1, X_2 and Z_1, Z_2, Z_3 . The size of a c-component is generally a lot smaller than the whole graph. Thus, even though we have to train mechanisms in a c-component together and match a joint distribution involving high and low dimensional variables, the complexity will be much lower. Without our approach, there is no existing work that can modularize and simplify the training process for a causal graph with latents. In the following, we generalize these ideas into an algorithm that can modularize the training process of different c-components, while identifying a valid training order to match the joint distribution.

4.2 Training Algorithm for Modular-DCM

To match the joint distribution $P(\mathcal{V})$ by training the DCMs in a modular way, we have to: 1) arrange the c-components in a valid training order and 2) train (sets of) c-components to match their c-factors.

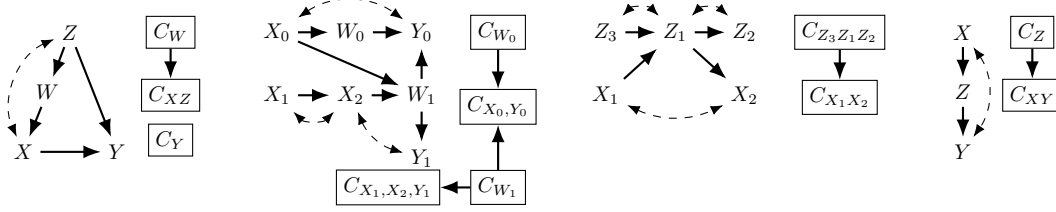


Figure 3: Causal graphs and their corresponding h-graphs that show modularization of the training process. The rectangular box represents each h-node and which networks we have to train together. The partial order of the h-graph represents in which order we should train the mechanisms.

Arranging the c-components: Consider a c-component C_t . When should a c-component C_s be trained before C_t ? Since we need rule 2 of do-calculus to hold on the parents of C_t for training, if C_s contains some parents of C_t that are located on the backdoor paths between any two variables in C_t , then C_s must be pre-trained before C_t . Conditioning and intervening on those parents of C_t in C_s is not the same, i.e., $P(C_t|do(pa(C_t) \cap C_s)) \neq P(C_t|pa(C_t) \cap C_s)$. Thus we include $pa(C_t) \cap C_s$ in the joint distribution that we want to match for C_t , which requires those parents in C_s to be pre-trained. For the front-door graph, (rightmost) in Figure 3, we observe that $P(X, Y|do(Z)) \neq P(X, Y|Z)$. Thus, we train G_X, G_Z, G_Y in $C_Z = \{G_Z\} \rightarrow C_{X,Y} = \{G_X, G_Y\}$ order. To obtain a partial order among all c-components, we construct a directed graph structure called \mathcal{H} -graph that contains c-components as nodes. While adding edges, if any cycle is formed, we merge c-components on that cycle into a single h-node indicating that they will need to be trained jointly. Thus some h-nodes may contain more than one c-component. The final structure is a DAG and gives us a valid partial order \mathcal{T} for modular training (Proposition D.14). Formally an \mathcal{H} -graph is defined as:

Definition 4.3 (\mathcal{H} -graph). Given a causal graph G with c-components $\mathcal{C} = \{C_1, \dots, C_n\}$, let $\{H_k\}_k$ be some partition of \mathcal{C} . The directed graph $(V_{\mathcal{H}}, E_{\mathcal{H}})$ where $V_{\mathcal{H}} = \{H_k\}_k$ and $H_s \rightarrow H_t \in E_{\mathcal{H}}$ iff $P(H_t|do(pa_G(H_t) \cap H_s)) \neq P(H_t|pa_G(H_t) \cap H_s)$, is called an \mathcal{H} -graph for G if it is acyclic.

We run the subroutine `Construct_Hgraph()` in Algorithm 1 to build an \mathcal{H} -graph. We check the edge condition in line 5 and merge cycles in line 7 if any. In Figure 2 step (1/3), we build the \mathcal{H} -graph $H_1 : [Z_1, Z_2, Z_3] \rightarrow H_2 : [X_1, X_2]$ for G . We provide more examples in Figure 3. For a larger example, please see Appendix E.2. Note that, we only use the \mathcal{H} -graph to obtain a partial training order via h-nodes. $An(H_k)$ and $Pa(H_k)$ below refer to ancestors and parents in the causal graph G , not in the \mathcal{H} -graph, for any h-node H_k .

Training c-components: We follow \mathcal{H} -graph’s topological order and train the c-components in an h-node H_k to match their corresponding c-factors $P_{pa(C_j)}(C_j), \forall C_j \in H_k$ and matching $P_{pa(H_k)}(H_k)$ ensures this. Although we can generate fake interventional samples from $Q_{pa(H_k)}(H_k)$ induced by the DCM, they can not be used to train \mathbb{G}_{H_k} as we do not have access to real data samples from the interventional distribution $P_{pa(H_k)}(H_k)$. Thus, we train \mathbb{G}_{H_k} to learn a larger joint distribution that can be obtained from the observational dataset as an alternative to its c-factors. We search for a set \mathcal{A}_k that can be added to the joint with H_k such that $P_{Pa(H_k, \mathcal{A}_k)}(H_k, \mathcal{A}_k) = P(H_k, \mathcal{A}_k|Pa(H_k, \mathcal{A}_k))$, i.e., true interventional and conditional distribution are the same. This enables us to take conditional samples from the input dataset and use them as interventional data samples and match their distribution with the DCM-generated fake interventional samples from $Q_{Pa(H_k, \mathcal{A}_k)}(H_k, \mathcal{A}_k)$ to train \mathbb{G}_{H_k} . The above condition is generalized into a **modularity condition** below:

Definition 4.4. Let H_k be an h-node in the \mathcal{H} -graph. A set $\mathcal{A}_k \subseteq An_G(H_k) \setminus H_k$ satisfies the modularity condition if it is the smallest set with $P(H_k, \mathcal{A}_k|do(Pa(H_k, \mathcal{A}_k))) = P(H_k, \mathcal{A}_k|Pa(H_k, \mathcal{A}_k))$.

As mentioned, such \mathcal{L}_1 and \mathcal{L}_2 distributional equivalence holds when the do-calculus rule-2 applies.

$$P_{Pa(H_k, \mathcal{A}_k)}(H_k, \mathcal{A}_k) = P(H_k, \mathcal{A}_k|Pa(H_k, \mathcal{A}_k)), \quad (2)$$

$$\text{if } (H_k, \mathcal{A}_k \perp\!\!\!\perp Pa(H_k, \mathcal{A}_k))_{G_{Pa(H_k, \mathcal{A}_k)}}$$

Algorithm 1 Construct \mathcal{H} -graph(G)

```

1: Input: Causal Graph  $G$ 
2:  $\mathcal{C} \leftarrow \text{get\_ccomponents}(G)$ 
3: Create nodes  $H_k = C_k$  in  $\mathcal{H}$ ,  $\forall C_k \in \mathcal{C}$ 
4: for each  $H_s, H_t \in \mathcal{H}$  such that  $s \neq t$  do
5:   if  $P(H_t|\text{do}(pa(H_t) \cap H_s))$ 
      $\neq P(H_t|pa(H_t) \cap H_s)$  then
6:      $\mathcal{H}.\text{add}(H_s \rightarrow H_t)$ 
7:  $\mathcal{H} \leftarrow \text{Merge}(\mathcal{H}, \text{cyc})$ ,  $\forall \text{cyc} \in \text{Cycles}(\mathcal{H})$ 
8: Return:  $\mathcal{H}$ 

```

Algorithm 2 Modular Training(G, \mathbf{D})

```

1: Input: Causal Graph  $G$ , Dataset  $\mathbf{D}$ .
2: Initialize DCM  $\mathbb{G}$ 
3:  $\mathcal{H} \leftarrow \text{Construct\_Hgraph}(G)$ 
4: for each  $H_k \in \mathcal{H}$  in partial order do
5:   Initialize  $\mathcal{A}_k \leftarrow \emptyset$ 
6:   while  $\text{IsRule2}(H_k, \mathcal{A}_k) = 0$  do
7:      $\mathcal{A}_k \leftarrow Pa_G(H_k, \mathcal{A}_k)$ 
8:    $\mathbb{G}_{H_k} \leftarrow \text{TrainModule}(\mathbb{G}_{H_k}, G, H_k, \mathcal{A}_k, \mathbf{D})$ 
9: Return:  $\mathbb{G}$ 

```

This suggests a graphical criterion to find such a set \mathcal{A}_k . Intuitively, if the outgoing edges of $Pa(H_k, \mathcal{A}_k)$ are deleted ($G_{Pa(H_k, \mathcal{A}_k)}$), they become d-separated from $\{H_k, \mathcal{A}_k\}$, i.e., there exists no backdoor path from $Pa(H_k, \mathcal{A}_k)$ to $\{H_k, \mathcal{A}_k\}$. Therefore, for a specific H_k , we start with $\mathcal{A}_k = \emptyset$ and check if $Pa(H_k, \mathcal{A}_k)$ satisfies the conditions of rule-2 for $\{H_k, \mathcal{A}_k\}$. If not, we add parents of $\{H_k, \mathcal{A}_k\}$ in \mathcal{A}_k . We include the ancestors since only they can affect H_k 's mechanisms from outside of the c-component. We continue the process until $Pa(H_k, \mathcal{A}_k)$ satisfies the condition of rule-2.

After constructing the \mathcal{H} -graph at Algorithm 2 in line 3, we train each h-node H_k according to the partial order to match with the c-factors' alternative distribution for the c-components in H_k . (lines 4-8). We initialize a set $\mathcal{A}_k = \emptyset$ to keep track of the joint distribution we need to match to train each h-node H_k . We search for the set of ancestors \mathcal{A}_k of the current h-node H_k such that \mathcal{A}_k satisfies the modularity condition for H_k (line 6), which is checked by Algorithm 5: $\text{IsRule2}(\cdot)$. Finding a set \mathcal{A}_k satisfying the modularity condition implies that we can train \mathbb{G}_{H_k} by matching:

$$Q_{Pa(H_k, \mathcal{A}_k)}(H_k, \mathcal{A}_k) = P(H_k, \mathcal{A}_k | Pa(H_k, \mathcal{A}_k))$$

(3)

; Now training: H_k , Pre-trained: \mathcal{A}_k

We utilize adversarial training to train the generators in \mathbb{G}_{H_k} on observational dataset \mathbf{D} to match the above. This is done by Algorithm 4: $\text{TrainModule}()$ called in line 8. More precisely, this sub-routine uses all mechanisms in $\{H_k, \mathcal{A}_k\}$ to produce samples but only updates the mechanisms in \mathbb{G}_{H_k} corresponding to the current h-node and returns those models after convergence. Even though we will train only \mathbb{G}_{H_k} i.e., $\mathbb{G}_V, \forall V \in H_k$, \mathcal{A}_k appears together with H_k in the joint distribution that we need to match. Thus, we use pre-trained causal mechanisms of \mathcal{A}_k , i.e., $\mathbb{G}_V, \forall V \in \mathcal{A}_k$ here. Following the partial order of \mathcal{H} -graph ensures that we have already trained \mathcal{A}_k before H_k .

Training \mathbb{G}_{H_k} to match the conditional distribution of data with the interventional distribution of the DCM, as in Equation 3, is sufficient to learn the c-factors $P_{Pa(C_j)}(C_j), \forall C_j \in H_k$. After training each \mathbb{G}_{H_k} according to the partial order of \mathcal{H} -graph, Modular-DCM will learn a DCM that induces $Q(\mathcal{V}) = P(\mathcal{V})$ from data. For example, in Figure 2 we match $P(z_1, z_2, z_3 | x_1) = Q(z_1, z_2, z_3 | \text{do}(x_1))$ at step (2/3) and $P(x_1, x_2, z_1, z_3) = Q(x_1, x_2, z_1, z_3)$ at step (3/3). Thus, $P(\mathcal{V}) = Q(\mathcal{V})$ in this graph. Finally, the trained DCM can sample from \mathcal{L}_2 and \mathcal{L}_3 distributions identifiable from $P(\mathcal{V})$ such as $P(X_2 | \text{do}(X_1))$ or $P(Z_2 | \text{do}(X_1))$. These are formalized in Theorem 4.5. Proof is in Appendix D.6.

Sampling with Modular-DCM: For \mathcal{L}_2 sampling, we set the intervened variables to fixed values instead of using their neural networks and push forward those values to generate the rest of the variables.

We have the following assumptions, mainly that the causal graph is given² and that generative models can correctly learn the desired conditional data distribution for each h-node.

Assumption 1: The true causal graph with the location of latent confounders is known. **Assumption 2:** The causal graph G is semi-Markovian Tian et al. (2006). **Assumption 3:** For any h-node H_k in the \mathcal{H} -graph, DCM training on \mathbf{D} converges to sample from the conditional distribution $P(H_k, \mathcal{A}_k | pa(H_k, \mathcal{A}_k))$ for all H_k , where \mathcal{A}_k is from Algorithm 2.

Theorem 4.5. Consider any SCM $\mathcal{M} = (G, \mathcal{N}, \mathcal{U}, \mathcal{F}, P(\cdot))$. Suppose Assumptions 1-3 hold. Algorithm 2 on (G, \mathbf{D}) returns a DCM \mathbb{G} that entails i) the same observational distribution, and ii) the same identifiable interventional distributions as the SCM \mathcal{M} .

²Causal discovery is typically an orthogonal problem to inference, and is beyond our scope in this work.

Proof Sketch: Following the partial order of the H-graph and matching the distributions $P(H_k, \mathcal{A}_k | Pa(H_k, \mathcal{A}_k))$ corresponding to each h-node, eventually matches the whole joint distribution $P(\mathcal{V})$. Since the Modular-DCM matches the true joint distribution $P(\mathcal{V})$, it can correctly sample from any identifiable interventional distributions according to Theorem 4.2. We provide the formal proof in Appendix D.6.

Note that, without modularization, in a causal graph with N variables, we have to match the joint distribution containing N (might be large) number of low and high dimensional variables in a single training phase. Matching that joint distribution with deep-learning models, and a complicated confounded causal structure could be difficult since we are attempting to minimize a very complicated loss function for a very large neural network. Our proposed method allows us to reduce the complexity of this problem tremendously by modularizing the training process to c-components. The size of a c-component is generally a lot smaller than the whole graph (Figure 4). Thus, even though modular-DCM has to train mechanisms in a c-component together and match a joint distribution involving high and low dimensional variables, the complexity will be much lower compared to joint training. Without our approach, there is no existing work to our knowledge that can modularize and simplify the training process for a causal graph with latents.

5 Experimental Evaluation

We present Modular-DCM performance on semi-synthetic high-dimensional Colored-MNIST dataset (LeCun et al., 1998) and real-world COVIDx CXR-3 dataset Wang et al. (2020). We also evaluate Modular-DCM’s capability of \mathcal{L}_1 , \mathcal{L}_2 , and \mathcal{L}_3 sampling after training on another semi-synthetic Colored-MNIST-2 dataset. In Appendix F, we provide more details and further performance on 3 datasets: Sachs (real-world) and two synthetic datasets.

5.1 Complexity Evaluation

To achieve a deep causal generative model (DCM), given a causal graph of N nodes, it is required to train N neural networks. However, our nearest benchmark NCM (Xia et al. (2023)), trains all N networks together at the same time. While our method trains only the networks that belong to a single h-node. Thus, during a training phase, the maximum number of networks NCM has to train is $O(N)$ and in our case, it is $O(|\text{Largest h-node}|)$ which is in most cases $O(|\text{Largest c-component}|)$. In figure 4, we evaluated the largest number of networks that need to be trained in our method and in NCM with respect to the number of nodes varying from 15 to 50. We kept the arc-ratio and number of latents equal to $N/3$. We observe that the number of networks NCM trains together increases linearly with respect to the number of nodes whereas in our method the growth is smaller since it does not depend on the number of nodes but rather on the number of latents.

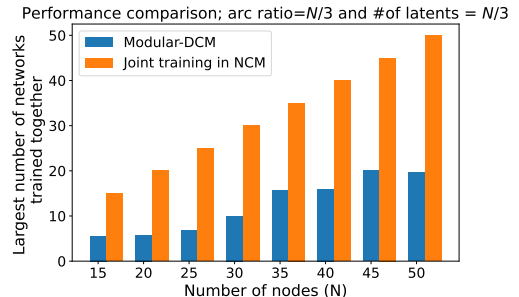


Figure 4: Evaluation of largest number of networks need to be trained together with respect to different number of nodes

5.2 Performance on Image Mediator Experiment and Benchmark Comparison

We show Modular-DCM performance in an experiment on the front-door graph in Figure 5a that involves both low and high-dimensional variables. We constructed a synthetic SCM where a hidden variable U affects both D and A . Image variable I contains the digit value of D , and A is some attribute of I obtained from a randomly chosen projection of the image. The digit color can be considered as exogenous noise. Suppose we are given a dataset sampled from $P(D, A, I)$. Our goal is to estimate the causal effect $P(A|do(D))$. We can use the backdoor criterion (Pearl, 1993), to evaluate the ground truth $P(A|do(D)) = \int_U P(A|D, U)P(U)$ since we know U in the true SCM. From the input \mathcal{L}_1 dataset, $P(A|do(D))$ is identifiable with the front-door criterion (Pearl, 2009).

The identification algorithm can not be applied since it requires image distribution. If we can train all mechanisms in the DCM to match $P(D, A, I)$, we can produce correct samples from $P(A|do(D))$. For this

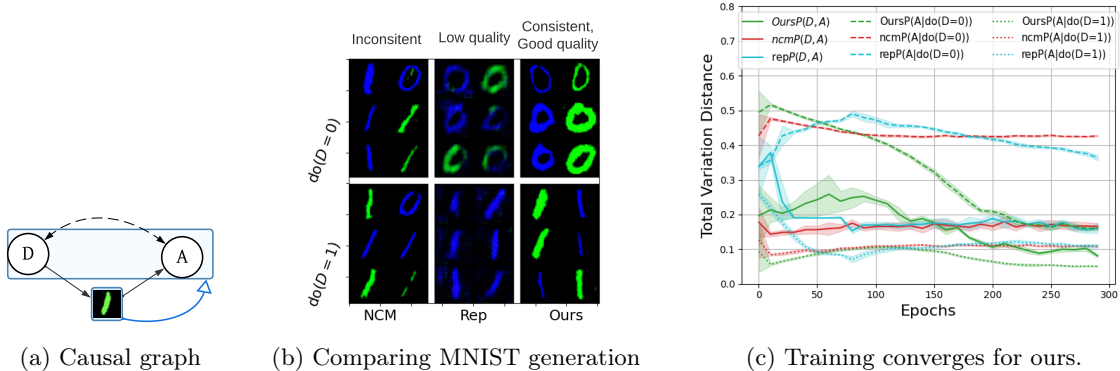


Figure 5: Performance on frontdoor. NCM produces good images but not consistent with $do(D)$. Modular-DCM without modular training (rep) produces consistent but low-quality images. Our modular approach with training order: $\{I\} \rightarrow \{D, A\}$ produces consistent, good images and converges faster.

purpose, we construct the Modular-DCM architecture with a neural network \mathbb{G}_D having fully connected layers to produce D , a CNN-based generator \mathbb{G}_I to generate images, and a classifier \mathbb{G}_A to classify MNIST images into variable A such that D and A are confounded. Now, for this graph, the corresponding \mathcal{H} -graph is $[I] \rightarrow [D, A]$. Thus, we first train \mathbb{G}_I by matching $P(I|D)$. Instead of training \mathbb{G}_I , we can also employ a pre-trained generative model that takes digits D as input and produces an MNIST image showing D digit in it. Thus in Fig 5b, Modular-DCM shows images of the digit 0 (top, right) and digit 1 (bottom, right) due to $do(D=0)$ and $do(D=1)$ intervention. Next, to train \mathbb{G}_D and \mathbb{G}_A , we should match the joint distribution $P(D, A, I)$ since $\{I\}$ is ancestor set \mathcal{A} for c-component $\{D, A\}$. Convergence of generative models becomes difficult using the loss of this joint distribution since the losses generated by low and high dimensional variables are not easily comparable and non-trivial to re-weight (see Appendix F.2). Thus, we map samples of I to a low-dimensional representation, RI with a trained encoder and match $P(D, A, RI)$ instead of the joint $P(D, A, I)$.

In Figure 5b, 5c, we compare our method with Xia et al. (2023): NCM and a version of our method: Modular-DCM-rep that does not use modular training, with respect to image quality and total variation distance from true $P(D, A)$ and $P(A|do(D))$. We implemented NCM on our architectures as it could not be directly used for images. Since NCM trains all mechanisms with the same loss function calculated from both low and high-dimensional samples, it learns marginal distribution $P(I)$ (Figure 5b left) but does not fully converge to match the joint $P(D, A, I)$ (all red-lines are not going down in Figure 5c). Thus, NCM produces good-quality images but is not consistent with $do(D)$ intervention. Modular-DCM-rep uses a low-dim representation of images: RI and matches the joint distribution $P(D, A, RI)$ as a proxy to $P(D, A, I)$ without modularization. We observe Modular-DCM-rep to converge (Figure 5c blue-lines) slower compared to the original Modular-DCM and produce consistent but low-quality images (Figure 5b middle) for $do(D)$ intervention. Finally, Modular-DCM modular training matches $P(D, A, RI)$ and converges faster (Figure 5c green-lines) for $P(D, A)$, $P(A|do(D))$ and produces good-quality, consistent $P(I|do(D))$ images (Figure 5b right).

5.3 Performance on Real-world COVIDx CXR-3 Dataset

In this section, we conduct a case study with the COVIDx CXR-3 (Wang et al., 2020) dataset. This dataset contains 30,000 chest X-ray images with Covid (C) and pneumonia (N) labels from over 16,600 patients located in 51 countries. The X-ray images are of healthy patients ($C=0, N=0$), patients with non-Covid pneumonia ($C=0, N=1$), and patients with Covid pneumonia ($C=1, N=1$). X-ray images for COVID non-pneumonia ($C=1, N=0$) are not present in this dataset as according to health experts those images do not contain enough signal for pneumonia detection.

There is no ground truth causal graph associated with this dataset. In order to demonstrate the convergence behavior of Modular-DCM on real high-dimensional datasets, we consider the causal graph shown in Figure 6a. Note that the causal effect estimates obtained via this graph may not reflect the true causal effect since the

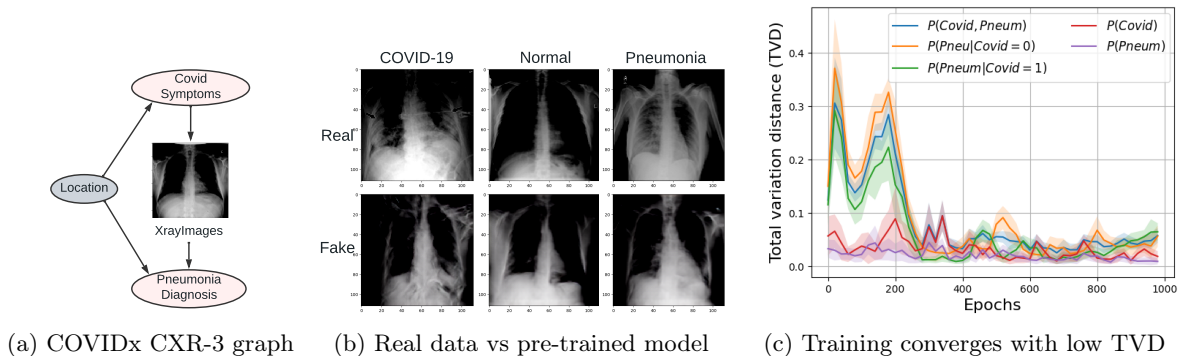


Figure 6: Modular-DCM converges with pre-trained model on COVIDx CXR-3 dataset.

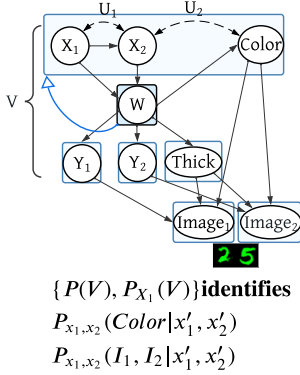
ground truth graph is unknown and there may be other violations of assumptions such as distribution shift and selection bias. However, observe that this graph does not impose conditional independence restrictions on the joint distribution $P(C, Xray, N)$. Therefore, we expect our modular training algorithm to correctly match the observational joint distribution.

Our reasoning for using this causal graph is as follows: we can assume that Covid symptoms determine the X-ray features and the pneumonia diagnosis is made based on the X-rays. Thus we can add direct edges between these variables. A patient’s location is hidden and acts as a confounder because a person’s socio-economic and health conditions in a specific location might affect both the likelihood of getting Covid and being properly diagnosed with Pneumonia by local health care. The X-ray images are done by chest radiography imaging examination. Due to the standardization of equipment, we assume the difference in X-ray data across hospital locations is minor and can be ignored. Thus, $Location \not\rightarrow XrayImages$. We aim to learn that if a patient is randomly picked and intervened with Covid (hypothetically), how likely will they be diagnosed with pneumonia, i.e., $P(N|do(C))$? If our mentioned assumptions (including no selection bias, etc.) are correct, we expect Modular-DCM to correctly sample from interventional distribution after training by Theorem 4.5.

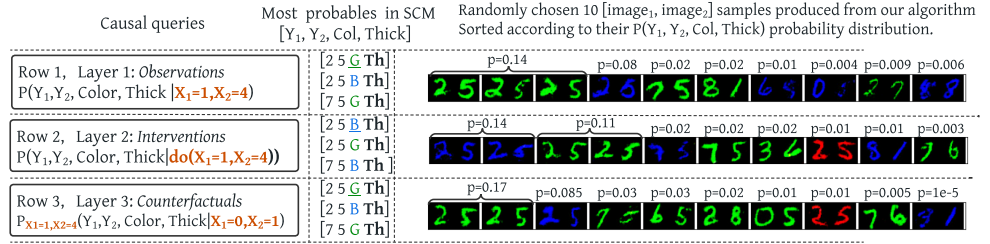
To match the joint distribution $P(C, Xray, N)$, we follow the modular training order: $[\mathbb{G}_{Xray}] \rightarrow [\mathbb{G}_C, \mathbb{G}_N]$. Instead of training \mathbb{G}_{Xray} from scratch, we use a pre-trained model (Giorgio Carbone, 2023) that can be utilized to produce Xray images corresponding to $C \in [0, 1]$ input. Figure 6b shows images for the original dataset and output images from the pre-trained model. Next, we train \mathbb{G}_C and \mathbb{G}_N together since they belong to the same c-component. Since the joint distribution contains both low and high-dimensional variables, we map Xray to a low-dimensional representation $Rxray$ with an encoder and match $P(C, Rxray, N)$. In Figure 6c, we plot the total variation distance (TVD) of $P(C), P(N), P(N|C), P(N, C)$. We observe that TVD for all distributions is decreasing. The average treatment effect, i.e., the difference between $E[P(N|do(C = 1))]$ and $E[P(N|do(C = 0))]$ is in $[0.05, 0.08]$ after convergence. This implies that intervention with Covid increases the likelihood of being diagnosed with Pneumonia. However, these results are based on this specific COVIDx CXR-3 dataset and should not be used to make medical inferences without expert opinion.

5.4 Interventional and Counterfactual Sampling with Colored-MNIST-2 Dataset

To evaluate Modular-DCM’s ability to produce \mathcal{L}_2 and \mathcal{L}_3 samples, we consider the graph in Figure 7a and run experiments on a synthetic SCM involving the Colored-MNIST dataset. Here, $W \in [0, 9]$ represents the sum of X_1, X_2 , and Y_1, Y_2 are the first and second digits of W^2 . Also, $Color \in [0(R), 1(G), 2(B)]$ and $Thick \in [0(th), 1(\mathbf{Th})]$. For, $V = \mathcal{V} \setminus \{Image_1, Image_2\}$, we generated three datasets, $D_1 \sim P(V), D_2 \sim P_{X_1=0}(V), D_3 \sim P_{X_1=1}(V)$. Next, we use $[Y_1, Color, Thick]$ and $[Y_2, Color, Thick]$ as parameters to produce dataset $D_4: [Image_1, Image_2]([I_1, I_2])$ by utilizing Colored MNIST dataset following Castro et al. (2019). Our goal is to sample from $\mathcal{L}_2: P_{x_1, x_2}(I_1, I_2)$ and $\mathcal{L}_3: P_{x_1, x_2}(I_1, I_2|do(x'_1, x'_2))$. In Figure 7a, we show the \mathcal{H} -graph with an edge $\{W\} \rightarrow \{X_1, X_2, Color\}$. We can combine multiple c-component mechanisms that follow the partial order



(a) Causal graph



(b) For each query, the top 3 occurred image samples match with true SCM.

Figure 7: Modular training on low and high dimensional variables to produce \mathcal{L}_1 , \mathcal{L}_2 , and \mathcal{L}_3 samples.

and train them together. Thus, we consider the training order $\{W, X_1, X_2, Color\}, \{Y_1, Y_2, Thick\}, \{I_1\}, \{I_2\}$. First, we train $[\mathbb{G}_{X_1}, \mathbb{G}_{X_2}, \mathbb{G}_W, \mathbb{G}_{Color}]$ together using both $\mathcal{L}_1, \mathcal{L}_2$ datasets: $\{D_1, D_2, D_3\}$. Next, we train $[\mathbb{G}_{Y_1}, \mathbb{G}_{Y_2}, \mathbb{G}_{Thick}]$ with only \mathcal{L}_1 dataset D_1 . Since $P(Y_1, Y_2, Thick|do(X_1)) = P(Y_1, Y_2, Thick|X_1)$, \mathcal{L}_1 dataset is sufficient for training. Next, we train I_1, I_2 mechanisms with dataset D_4 . If we have access to pre-trained models for I_1, I_2 , we can utilize them by plugging them with the models trained in the previous steps.

After training on $\{D_1, \dots, D_4\}$, Modular-DCM can produce correct $\mathcal{L}_1, \mathcal{L}_2$ samples from $P_{x_1, x_2}(I_1, I_2)$ and $P_{x_1, x_2}(I_1, I_2|do(x'_1, x'_2))$ since these distributions are identifiable from $P(V)$. We use the trained models to generate 40k samples for different \mathcal{L}_1 (row 1), \mathcal{L}_2 (row 2), and \mathcal{L}_3 (row 3) queries and present randomly selected 10 samples in Figure 7b. We sort them according to their occurrences. The first column represents the image sampling causal queries, according to which the image samples are produced. The second column represents the top 3 highest probability outcomes according to the true SCM. Finally, the 3rd column shows 10 samples of $[Image_1, Image_2]$ produced from Modular-DCM. We observe realistic sample images, produced from Modular-DCM corresponding to these queries after we feed generated samples of $[Y_1, Y_2, Color, Thick]$ into I_1, I_2 mechanisms. We calculated the numeric values of distributions considering the occurrences of each combination in the fake samples. We found that estimated distributions are very close to the true distributions for the top 3 combinations.

In row 1, for \mathcal{L}_1 -query, we condition on $X_1 = 1, X_2 = 4$ and get [2,5, G, Th] as the highest probable outcome which is the same as the true outcome in column 2. In row 2, for \mathcal{L}_2 -query, we intervene on $X_1 = 1, X_2 = 4$. X_2 and $Color$ are no longer confounded and the true SCM has [2 5 B Th] as the most probable, different from earlier. $Color$ shows different outcomes besides green with high probability, for example blue. As expected, our trained DCM also produces images with blue color with the highest probability. In row 3, for \mathcal{L}_3 -query we intervene on $X_1 = 1, X_2 = 4$ but condition on $X_1 = 0, X_1 = 1$. X_2 and $Color$ are not confounded after the intervention but due to the conditioning $[X_1 = 0, X_1 = 1]$, the posterior of the confounder U_2 changes the most likely counterfactual outcome to be [2 5 G Th]. Our model output is consistent with this outcome. Therefore, in all three queries, the top 3 combinations produced by our model match the outcomes of the true SCM. This depicts Modular-DCM's ability to produce high-dimensional $\mathcal{L}_1, \mathcal{L}_2$ and \mathcal{L}_3 samples. We provide the derivations associated with this experiment and more plots in Appendix F.4).

6 Conclusion

We propose a modular adversarial training algorithm called Modular-DCM for learning deep causal generative models for estimating causal effects with high-dimensional variables in the presence of unobserved confounders. After convergence, Modular-DCM can generate high-dimensional samples from identifiable interventional and counterfactual distributions. In this paper, we assume that we have access to a fully specified causal graph with latents and the causal model is semi-Markovian. We aim to deal with these limitations by relaxing the assumptions in our future work.

Acknowledgements

This research has been supported in part by NSF Grant CAREER 2239375.

References

- Balazadeh Meresht, V., Syrgkanis, V., and Krishnan, R. G. (2022). Partial identification of treatment effects with implicit generative models. *Advances in Neural Information Processing Systems*, 35:22816–22829.
- Bard (2023). Bard - chat based ai tool from google, powered by palm 2. <https://bard.google.com/chat>. Accessed: Sep 26, 2023.
- Bareinboim, E. and Pearl, J. (2012a). Causal inference by surrogate experiments: z-identifiability. *arXiv preprint arXiv:1210.4842*.
- Bareinboim, E. and Pearl, J. (2012b). Causal inference by surrogate experiments: Z-identifiability. In *Proceedings of the Twenty-Eighth Conference on Uncertainty in Artificial Intelligence, UAI'12*, page 113–120, Arlington, Virginia, USA. AUAI Press.
- Bica, I., Jordon, J., and van der Schaar, M. (2020). Estimating the effects of continuous-valued interventions using generative adversarial networks. *Advances in Neural Information Processing Systems*, 33:16434–16445.
- Castro, D. C., Tan, J., Kainz, B., Konukoglu, E., and Glocker, B. (2019). Morpho-mnist: quantitative assessment and diagnostics for representation learning. *Journal of Machine Learning Research*, 20(178):1–29.
- ChatGPT (2022). Chatgpt: A large language model trained by openai. <https://openai.com/blog/chatgpt/>. Accessed: Sep 26, 2023.
- Correa, J., Lee, S., and Bareinboim, E. (2021). Nested counterfactual identification from arbitrary surrogate experiments. *Advances in Neural Information Processing Systems*, 34:6856–6867.
- DALL-E (2022). Dall-e 2 is an ai system that can create realistic images and art from a description in natural language. <https://openai.com/dall-e-2>. Accessed: Sep 26, 2023.
- Giorgio Carbone, Remo Marconzini, G. C. (2023). Cxr-acgan: Auxiliary classifier gan (ac-gan) for conditional generation of chest x-ray images (pneumonia, covid-19 and healthy patients) for the purpose of data augmentation. <https://github.com/giocoal/CXR-ACGAN-chest-xray-generator-covid19-pneumonia>.
- Gulrajani, I., Ahmed, F., Arjovsky, M., Dumoulin, V., and Courville, A. C. (2017). Improved training of wasserstein gans. *Advances in neural information processing systems*, 30.
- Ho, J. and Salimans, T. (2022). Classifier-free diffusion guidance. *arXiv preprint arXiv:2207.12598*.
- Huang, Y. and Valertorta, M. (2012). Pearl’s calculus of intervention is complete. *arXiv preprint arXiv:1206.6831*.
- Jaber, A., Zhang, J., and Bareinboim, E. (2019). Causal identification under markov equivalence: Completeness results. In *International Conference on Machine Learning*, pages 2981–2989. PMLR.
- Jang, E., Gu, S., and Poole, B. (2017). Categorical reparameterization with gumbel-softmax. In *International Conference on Learning Representations*.
- Kocaoglu, M., Snyder, C., Dimakis, A. G., and Vishwanath, S. (2018). Causalgan: Learning causal implicit generative models with adversarial training. In *International Conference on Learning Representations*.
- LeCun, Y., Bottou, L., Bengio, Y., and Haffner, P. (1998). Gradient-based learning applied to document recognition. *Proceedings of the IEEE*, 86(11):2278–2324.
- Lee, S., Correa, J. D., and Bareinboim, E. (2020). General identifiability with arbitrary surrogate experiments. In *Uncertainty in artificial intelligence*, pages 389–398. PMLR.

- Louizos, C., Shalit, U., Mooij, J. M., Sontag, D., Zemel, R., and Welling, M. (2017). Causal effect inference with deep latent-variable models. *Advances in neural information processing systems*, 30.
- Mirza, M. and Osindero, S. (2014). Conditional generative adversarial nets. *arXiv preprint arXiv:1411.1784*.
- Nemirovsky, D., Thiebaut, N., Xu, Y., and Gupta, A. (2020). CounterGAN: generating realistic counterfactuals with residual generative adversarial nets. *arXiv preprint arXiv:2009.05199*.
- Pawlowski, N., Coelho de Castro, D., and Glocker, B. (2020). Deep structural causal models for tractable counterfactual inference. *Advances in Neural Information Processing Systems*, 33:857–869.
- Pearl, J. (1993). [bayesian analysis in expert systems]: comment: graphical models, causality and intervention. *Statistical Science*, 8(3):266–269.
- Pearl, J. (1995). Causal diagrams for empirical research. *Biometrika*, 82(4):669–688.
- Pearl, J. (2009). *Causality*. Cambridge university press.
- Sachs, K., Perez, O., Pe’er, D., Lauffenburger, D. A., and Nolan, G. P. (2005). Causal protein-signaling networks derived from multiparameter single-cell data. *Science*, 308(5721):523–529.
- Scutari, M. and Denis, J.-B. (2021). *Bayesian networks: with examples in R*. Chapman and Hall/CRC.
- Shpitser, I. and Pearl, J. (2007). What counterfactuals can be tested. In *Proceedings of the Twenty-Third Conference on Uncertainty in Artificial Intelligence*, pages 352–359.
- Shpitser, I. and Pearl, J. (2008). Complete identification methods for the causal hierarchy. *Journal of Machine Learning Research*, 9:1941–1979.
- Shpitser, I. and Pearl, J. (2009). Effects of treatment on the treated: Identification and generalization. In *Proceedings of the 25th Conference on Uncertainty in Artificial Intelligence, UAI 2009*, pages 514–521. AUAI Press.
- Tian, J., Kang, C., and Pearl, J. (2006). A characterization of interventional distributions in semi-markovian causal models. In *AAAI*, pages 1239–1244.
- Tian, J. and Pearl, J. (2002). *A general identification condition for causal effects*. eScholarship, University of California.
- van Breugel, B., Kyono, T., Berrevoets, J., and van der Schaar, M. (2021). Decaf: Generating fair synthetic data using causally-aware generative networks. *Advances in Neural Information Processing Systems*, 34:22221–22233.
- Wang, L., Lin, Z. Q., and Wong, A. (2020). Covid-net: a tailored deep convolutional neural network design for detection of covid-19 cases from chest x-ray images. *Scientific Reports*, 10(1):19549.
- Xia, K., Lee, K.-Z., Bengio, Y., and Bareinboim, E. (2021). The causal-neural connection: Expressiveness, learnability, and inference. *Advances in Neural Information Processing Systems*, 34:10823–10836.
- Xia, K. M., Pan, Y., and Bareinboim, E. (2023). Neural causal models for counterfactual identification and estimation. In *The Eleventh International Conference on Learning Representations*.
- Xu, D., Wu, Y., Yuan, S., Zhang, L., and Wu, X. (2019). Achieving causal fairness through generative adversarial networks. In *Proceedings of the Twenty-Eighth International Joint Conference on Artificial Intelligence*.
- Zhang, W., Liu, L., and Li, J. (2021). Treatment effect estimation with disentangled latent factors. In *Proceedings of the AAAI Conference on Artificial Intelligence*, volume 35, pages 10923–10930.

Contents

1	Introduction	1
2	Related Works	3
3	Background	3
4	Deep Causal Generative Models with Unobserved Confounders	4
4.1	Modular-DCM Intuitive Explanation	5
4.2	Training Algorithm for Modular-DCM	6
5	Experimental Evaluation	9
5.1	Complexity Evaluation	9
5.2	Performance on Image Mediator Experiment and Benchmark Comparison	9
5.3	Performance on Real-world COVIDx CXR-3 Dataset	10
5.4	Interventional and Counterfactual Sampling with Colored-MNIST-2 Dataset	11
6	Conclusion	12
A	Broader Impacts	16
B	Limitations and Future work	16
C	Appendix: Modular-DCM: Adversarial Training of Deep Causal Generative Models	16
C.1	Modular-DCM Interventional and Counterfactual Sampling after Training	16
C.2	Modular-DCM: Adversarial Training of Deep Causal Generative Models (Full Training) . . .	17
C.3	Training with Multiple Datasets	18
C.4	Non-Markovianity	19
D	Appendix: Modular-DCM Modular Training	19
D.1	Tian’s Factorization for Modular Training	19
D.2	Modular Training for Interventional Dataset	20
D.2.1	Modular Training Basics	20
D.2.2	Training Process of Modular Modular-DCM	23
D.2.3	Learn $P(\mathcal{V})$ -factors from Interventional Datasets	23
D.3	Training following the H-graph	24
D.4	Essential Theoretical Statements Required for Distributions Matching by Modular-DCM Modular Training	24
D.5	Theoretical Proofs of Distributions Matching by Modular-DCM Modular Training	27
D.5.1	Matching Observational Distributions with Modular Training on observational dataset	28
D.5.2	Matching Observational Distributions with Modular Training on interventional dataset	30
D.5.3	Matching Interventional Distributions with Modular Training	32
D.6	Identifiability of Algorithm 7:Modular-DCM Modular Training	36
E	Modular Training on Different Graphs	37
E.1	Modular Training Example 1	37
E.2	Modular Training Example 2	38
F	Experimental Analysis	39
F.1	Training Details and Compute	39
F.2	Image Mediator Experiment	39
F.3	Performance on Real-world COVIDx CXR-3 Dataset	41
F.4	MNIST Experiment 2: interventional and counterfactual Sampling from MNIST Dataset . . .	42
F.4.1	MNIST Experimental Setup	42
F.4.2	MNIST Low Dimensional Variables	42

F.4.3	MNIST High Dimensional Variables	44
F.4.4	MNIST Derivation	44
F.5	Asia/Lung Cancer Dataset	46
F.6	Real-world: Sachs Protein Dataset	46
F.7	Synthetic Experiment	47
G	Algorithms & Pseudo-codes	49
H	Questions and Answers about Modular-DCM	49

A Broader Impacts

Our proposed algorithm Modular-DCM, can sample from high-dimensional observational, interventional, and counterfactual distributions. As a result, it can be used to explore different creative directions such as producing realistic interventional and counterfactual images that we can not observe in real-world. We can train Modular-DCM models on datasets and perform intervention on sensitive attributes to detect any bias towards them or any unfairness against them (Xu et al., 2019; van Breugel et al., 2021). However, an adversary might apply our method to produce realistic images which are causal. As a result, it will be harder to detect fake data generated by DCM from real data.

B Limitations and Future work

Similar to most causal inference algorithms, we had to make the assumption of having a fully specified causal graph with latents, as prior. With the advancements in causal discovery with latents, it might be possible to reliably learn part of the structure and leverage the partial identifiability results from the literature. Indeed, this would be one of the future directions we are interested in. Another limitation of this work is that we assumed each confounder to cause only two observed variables which is considered as semi-Markovian in literature. We aim to extend our work for non-Markovian causal models where confounders can cause any number of observed variables. In this paper, we do not consider conditional sampling. Also, we perform rejection sampling for counterfactual sampling which is practical if the evidence variables are low-dimensional. We aim to resolve these limitations in our future works.

C Appendix: Modular-DCM: Adversarial Training of Deep Causal Generative Models

Definition C.1 (Identifiability (Shpitser and Pearl, 2007)). Given a causal graph, G , let \mathbf{M} be the set of all causal models that induce G and objects ϕ and θ are computable from each model in \mathbf{M} . We define that ϕ is θ -identifiable in G , if there exists a deterministic function g_G determined by the graph structure, such that ϕ can be uniquely computable as $\phi = g_G(\theta)$ in any $M \in \mathbf{M}$.

Definition C.2 (Causal Effects z-Identifiability). Let $\mathbf{X}, \mathbf{Y}, \mathbf{Z}$ be disjoint sets of variables in the causal graph G . If $\phi = P_{\mathbf{x}}(\mathbf{y})$ is the causal effect of the action $\text{do}(\mathbf{X}=\mathbf{x})$ on the variables in \mathbf{Y} , and θ contains $P(\mathbf{V})$ and interventional distributions $P(\mathbf{V} \setminus \mathbf{Z}' | \text{do}(\mathbf{Z}'))$, for all $\mathbf{Z}' \subseteq \mathbf{Z}$, where ϕ and θ satisfies the definition of Identifiability, we define it as z-identifiability. (Bareinboim and Pearl, 2012b) proposes a z-identification algorithm to derive g_G for these ϕ and θ

C.1 Modular-DCM Interventional and Counterfactual Sampling after Training

After Modular-DCM training, to perform hard intervention and produce samples accordingly, we manually set values of the intervened variables instead of using their neural network. Then, we feed forward those values into its children’s mechanisms and generate rest of the variable like as usual. Figure 8(b) is the Modular-DCM network for the causal graph in Figure 8(a). Now, in Figure 8(c), we performed $\text{do}(X = x)$. Exogenous variables U_1 and n_X are not affecting X anymore as we manually set $X = x$.

For counterfactual sampling of $P_x(Y|x')$, we follow the three steps, *i*) Abduction: With rejection sampling, we record the posterior exogenous n_X , confounding U and the gumbel noises responsible for producing $X = x'$ in the DCM's no intervention forward propagation (Figure 8c). We collect Gumbel Noise as we performed Gumbel-softmax (Jang et al., 2017) to deal with discrete variables. *ii*) Action: We intervene on \mathbb{G}_X with $X = x$ *iii*) Prediction: We use pre-recorded exogenous variable values as input to rest of the variable's neural network and push forward through the neural networks. (Figure 8c).

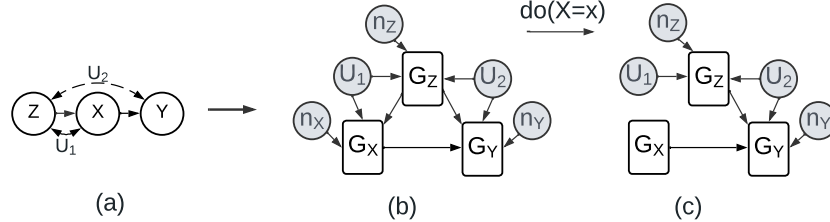


Figure 8: (a) Causal Graph with latents. (b), (c) DCM before and after intervention.

C.2 Modular-DCM: Adversarial Training of Deep Causal Generative Models (Full Training)

Full training of the DCM indicates the setup when we update all mechanisms in the causal graph with the same common loss. In this section, we prove that a trained DCM can sample from identifiable causal queries from any causal layer. We assume M_1 as true SCM and M_2 as DCM of Modular-DCM.

Theorem C.3. *Let $\mathcal{M}_1 = (G = (\mathcal{V}, \mathcal{E}), \mathcal{N}, \mathcal{U}, \mathcal{F}, P(\cdot))$ be an SCM. If a causal query $\mathcal{K}_{\mathcal{M}_1}(\mathcal{V})$ is identifiable from a collection of observational and/or interventional distributions $\{P_i(\mathcal{V})\}_{i \in [m]}$ for graph G , then any SCM $\mathcal{M}_2 = (G, \mathcal{N}', \mathcal{U}', \mathcal{F}', Q(\cdot))$ entails the same answer to the causal query if it entails the same input distributions. Therefore, for any identifiable query \mathcal{K} , if $\{P_i(\mathcal{V})\}_{i \in [m]} \vdash \mathcal{K}_{\mathcal{M}_1}(\mathcal{V})$ and $P_i(\mathcal{V}) = Q_i(\mathcal{V}), \forall i \in [m]$, then $\mathcal{K}_{\mathcal{M}_1}(\mathcal{V}) = \mathcal{K}_{\mathcal{M}_2}(\mathcal{V})$.*

Proof. By definition of identifiability, we have that $\mathcal{K}_{\mathcal{M}_1} = g_G(\{P_i(\mathcal{V})\}_{i \in [m]})$ for some deterministic function g_G that is determined by the graph structure. Since \mathcal{M}_2 has the same causal graph, the query $\mathcal{K}_{\mathcal{M}_2}$ is also identifiable and through the same function g_G , i.e., $\mathcal{K}_{\mathcal{M}_2} = g_G(\{Q_i(\mathcal{V})\}_{i \in [m]})$. Thus, the query has the same answer in both SCMs, if they entail the same input distributions over the observed variables, i.e., $P_i(\mathcal{V}) = Q_i(\mathcal{V}), \forall i$. \square

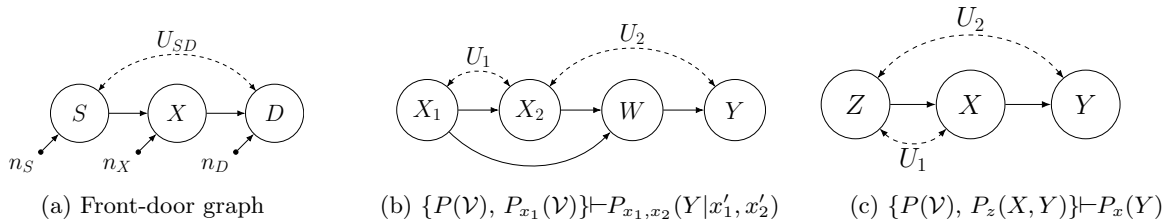


Figure 9: Causal graphs with latents and respective identifiable causal queries. θ identifies $\phi : \theta \vdash \phi$

Corollary C.4. *Let $\mathcal{M}_1 = (G = (\mathcal{V}, \mathcal{E}), \mathcal{N}, \mathcal{U}, \mathcal{F}, P(\cdot))$ and $\mathcal{M}_2 = (G, \mathcal{N}', \mathcal{U}', \mathcal{F}', Q(\cdot))$ be two SCMs. If $\{P(\mathcal{V})\} \vdash P_x(Y)$ for $X, Y \subset \mathcal{V}$, $X \cap Y = \emptyset$ and $P(\mathcal{V}) = Q(\mathcal{V})$ then $P_x(Y) = Q_x(Y)$*

For example, in Figure 9(b), the interventional query $P_{x_1, x_2}(W)$ is identifiable from $P(\mathcal{V})$. According to the Corollary C.4, after training on $P(\mathcal{V})$ dataset, Modular-DCM will produce correct interventional sample from $P_{x_1, x_2}(W)$ and along with other queries in $\mathcal{L}_2(P(\mathcal{V}))$.

Algorithm 3 Modular-DCM Training on Multiple Datasets

```
1: Input: Causal Graph  $G = (\mathcal{V}, \mathcal{E})$ , Interventional datasets=  $(\mathbf{I}, \mathcal{D})$ , DCM  $\mathbb{G}$ , Critic  $\mathbb{D}$ , Parameters=  $\theta_1, \dots, \theta_n$ ,  $\lambda = 10$ 
2: while  $\theta_1, \dots, \theta_n$  has not converged do
3:   for each  $(X, D) \in (\mathbf{I}, \mathcal{D})$  do
4:      $compare\_var = \mathcal{V}$ 
5:     Sample real data  $\mathbf{v}_x^r \sim D$  following the distribution  $\mathbb{P}_x^r$  with intervention  $X$ .
6:      $\mathbf{x} \leftarrow X.values$  //  $X=(keys, values)$ 
7:      $\mathbf{v}_x^f = \text{RunGAN}(G, \mathbb{G}, X, compare\_var, \emptyset)$ 
8:      $\hat{\mathbf{v}}_x = \epsilon \mathbf{v}_x^r + (1 - \epsilon) \mathbf{v}_x^f$ 
9:      $L_x = \mathbb{D}_{w_x}(\mathbf{v}_x^f) - \mathbb{D}_{w_x}(\mathbf{v}_x^r) * \lambda(\|\nabla_{\hat{\mathbf{v}}_x} \mathbb{D}_{w_x}(\hat{\mathbf{v}}_x)\|_2 - 1)^2$ 
10:     $G_{loss} = G_{loss} + \mathbb{D}_{w_x}(\mathbf{v}_x^f)$ 
11:     $w_x = \text{Adam}(\nabla_{w_x} \frac{1}{m} \sum_{j=1}^m L_{\mathbb{D}_x}, w_x, \alpha, \beta_1, \beta_2)$ 
12:  for  $\theta \in \theta_1, \dots, \theta_n$  do
13:     $\theta = \text{Adam}(\nabla_{\theta} - G_{loss}, \theta, \alpha, \beta_1, \beta_2)$ 
14: Return:  $\theta_1, \dots, \theta_n$ 
```

Bareinboim and Pearl (2012a) showed that we can identify some \mathcal{L}_2 -queries with other surrogate interventions and \mathcal{L}_1 -distributions. Similarly, we can apply Theorem C.3:

Corollary C.5. *Let $\mathcal{M}_1 = (G = (\mathcal{V}, \mathcal{E}), \mathcal{N}, \mathcal{U}, \mathcal{F}, P(\cdot))$ and $\mathcal{M}_2 = (G, \mathcal{N}', \mathcal{U}', \mathcal{F}', Q(\cdot))$ be two SCMs and X, Y be disjoint, and $\{S_i\}_i$ arbitrary subsets of variables. If *i*) $\{P(\mathcal{V}), P_{s_1}(\mathcal{V}), P_{s_2}(\mathcal{V}) \dots\} \perp\!\!\!\perp P_x(Y)$, *ii*) $P(\mathcal{V}) = Q(\mathcal{V})$ and *iii*) $P_{s_i}(\mathcal{V}) = Q_{s_i}(\mathcal{V}), \forall i, s_i$ then $P_x(Y) = Q_x(Y)$.*

In Figure 9(c), the interventional query $P_x(Y)$ is identifiable from $P(\mathcal{V})$ and $P_z(X, Y)$. Therefore, after being trained on datasets sampled from these distributions, Modular-DCM will produce correct interventional sample from $P_x(Y)$ and all other queries in $\mathcal{L}_2(P(\mathcal{V}), P_z(X, Y))$. We apply Theorem C.3 to answer counterfactual queries:

Corollary C.6. *Let $\mathcal{M}_1 = (G = (\mathcal{V}, \mathcal{E}), \mathcal{N}, \mathcal{U}, \mathcal{F}, P(\cdot))$ and $\mathcal{M}_2 = (G, \mathcal{N}', \mathcal{U}', \mathcal{F}', Q(\cdot))$ be two SCMs and X, Y be disjoint, and $\{S_i\}_i$ arbitrary subsets of variables. If *i*) $\{P(\mathcal{V}), P_{s_1}(\mathcal{V}), P_{s_2}(\mathcal{V}), \dots\} \perp\!\!\!\perp P(Y_x|e)$, *ii*) $P(\mathcal{V}) = Q(\mathcal{V})$ and *iii*) $P_{s_i}(\mathcal{V}) = Q_{s_i}(\mathcal{V}), \forall i, s_i$ then $P(Y_x|e) = Q(Y_x|e)$.*

In Figure 9(b), the counterfactual query $P_{x_1, x_2}(Y|x'_1, x'_2)$ is identifiable from $P(\mathcal{V})$ and $P_{x_1}(\mathcal{V})$ (see Appendix F.4.4). After training on datasets sampled from $P_{x_1}(\mathcal{V})$ and $P(\mathcal{V})$, Modular-DCM will produce correct counterfactual samples from $P_{x_1, x_2}(Y|x'_1, x'_2)$ and queries in $\mathcal{L}_3(P(\mathcal{V}), P_{x_1}(\mathcal{V}))$.

C.3 Training with Multiple Datasets

We propose a method in Algorithm 3 for training Modular-DCM with both \mathcal{L}_1 and \mathcal{L}_2 datasets. We use Wasserstein GAN with penalized gradients (WGAN-GP) (Gulrajani et al., 2017) for adversarial training. We can also use more recent generative models such as diffusion models when variables are not in any c-component. \mathbb{G} is the DCM, a set of generators and $\{\mathbb{D}_x\}_{X \in \mathbf{I}}$ are a set of discriminators for each intervention value combinations. The objective function of a two-player minimax game would be

$$\min_{\mathbb{G}} \sum_x \max_{\mathbb{D}_x} L(\mathbb{D}_x, \mathbb{G}),$$
$$L(\mathbb{D}_x, \mathbb{G}) = \mathbb{E}_{v \sim \mathbb{P}_x^r} [\mathbb{D}_x(\mathbf{v})] - \mathbb{E}_{\mathbf{z} \sim \mathbb{P}_Z, \mathbf{u} \sim \mathbb{P}_U} [\mathbb{D}_x(\mathbb{G}^{(\mathbf{x})}(\mathbf{z}, \mathbf{u}))]$$

Here, for intervention $\text{do}(X = x)$, $X \in \mathbf{I}$, $\mathbb{G}^{(\mathbf{x})}(\mathbf{z}, \mathbf{u})$ are generated samples and $v \sim \mathbb{P}_x^r$ are real \mathcal{L}_1 or \mathcal{L}_2 samples. We train our models by iterating over all datasets and learn \mathcal{L}_1 and \mathcal{L}_2 distributions (line 3). We produce generated interventional samples by intervening on the corresponding node of our architecture. For this purpose, we call Algorithm 9 RunGAN(), at line 7. We compare the generated samples with the input \mathcal{L}_1 or \mathcal{L}_2 datasets. For each different combination of the intervened variables x , \mathbb{D}_x will have different losses, $L_{X=x}$ from each discriminator (line 9). At line 10, we calculate and accumulate the generator loss over each dataset. If we have $V_1, \dots, V_n \in \mathcal{V}$, then we update each variable's model weights based on the accumulated

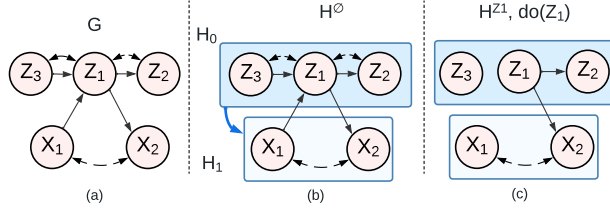


Figure 10: (a) Causal graph G , (b) \mathcal{H}^0 -graph, (c) H^{Z_1} -graph

loss (line 13). This will ensure that after convergence, Modular-DCM models will learn distributions of all the available datasets and according to Theorem C.3, it will be able to produce samples from same or higher causal layers queries that are identifiable from these input distributions. Following this approach, Modular-DCM Training in Algorithm 3, will find a DCM solution that matches to all the input distributions, mimicking the true SCM. Finally, we describe sampling method for Modular-DCM after training convergence in Appendix C.1.

Proposition C.7. *Let \mathcal{M}_1 be the true SCM and Algorithm 3: **Modular-DCM Training** converges after being trained on datasets: $\mathbf{D} = \{\mathcal{D}_i\}_i$, outputs the DCM \mathcal{M}_2 . If for any causal query $\mathcal{K}_{\mathcal{M}_1}(\mathcal{V})$ identifiable from \mathbf{D} then $\mathcal{K}_{\mathcal{M}_1}(\mathcal{V}) = \mathcal{K}_{\mathcal{M}_2}(\mathcal{V})$*

Proof. Let $\mathcal{M}_1 = (G = (\mathcal{V}, \mathcal{E}), \mathcal{N}, \mathcal{U}, \mathcal{F}, P(\cdot))$ be the true SCM and $\mathcal{M}_2 = (G, \mathcal{N}', \mathcal{U}', \mathcal{F}', Q(\cdot))$ be the deep causal generative model represented by Modular-DCM. Modular-DCM Training converges implies that $Q_i(\mathcal{V}) = P_i(\mathcal{V}), \forall i \in [m]$ for all input distributions. Therefore, according to Theorem C.3, Modular-DCM is capable of producing samples from correct interventional or counterfactual distributions that are identifiable from the input distributions. \square

C.4 Non-Markovianity

Note that, one can convert a non-Markovian causal model M_1 to a semi-Markovian causal model M_2 by taking the common confounder among the observed variables and splitting it into new confounders for each pair. Now, for a causal query to be unidentifiable in a semi-Markovian model M_2 , we can apply the Identification algorithm (Shpitser and Pearl, 2008) and check if there exists a hedge. The unidentifiability of the causal query does not depend on the confounder distribution. Thus, if the causal query is unidentifiable in the transformed semi-Markovian model M_2 , it will be unidentifiable in the original non-Markovian model M_1 as well.

Besides Semi-Markovian, Theorem 4.2 and Theorem C.3 holds for Non-Markovian models, with latents appearing anywhere in the graph and thus can be learned by Modular-DCM training. Jaber et al. (2019) performs causal effect identification on equivalence class of causal diagrams, a partial ancestral graph (PAG) that can be learned from observational data. Therefore, we can apply their method to check if an interventional query is identifiable from observational data in a Non-Markovian causal model and express the query in terms of observations and obtain the same result as Theorem C.3. We aim to explore these directions in more detail in our future work.

D Appendix: Modular-DCM Modular Training

D.1 Tian's Factorization for Modular Training

In Figure 10(a), We apply Tian's factorization (Tian and Pearl, 2002) to get,

$$P(v) = P(x_1, x_2 | \text{do}(z_1)) P(z_1, z_2, z_3 | \text{do}(x_1)) \quad (4)$$

We need to match the following distributions with the DCM.

$$\begin{aligned} P(x_1, x_2 | \text{do}(z_1)) &= Q(x_1, x_2 | \text{do}(z_1)) \\ P(z_1, z_2, z_3 | \text{do}(x_1)) &= Q(z_1, z_2, z_3 | \text{do}(x_1)) \end{aligned} \quad (5)$$

With modular training, we matched the following alternative distributions:

$$\begin{aligned} P(z_1, z_2, z_3|x_1) &= Q(z_1, z_2, z_3|\text{do}(x_1)) \\ P(x_1, x_2, z_1, z_3) &= Q(x_1, x_2, z_1, z_3) \end{aligned} \quad (6)$$

Now, for the graph in Figure 10(a),

$$\begin{aligned} P(x_1, x_2, z_1, z_2, z_3) &= P(x_1, x_2|\text{do}(z_1)) \times P(z_1, z_2, z_3|\text{do}(x_1)) \\ &= \frac{P(x_1, x_2, z_1, z_3)}{P(z_1, z_3|\text{do}(x_1))} \times P(z_1, z_2, z_3|x_1) \quad [\text{C-factorization of } P(x_1, x_2, z_1, z_3)] \\ &= \frac{P(x_1, x_2, z_1, z_3)}{P(z_1, z_3|x_1)} \times P(z_1, z_2, z_3|x_1) \quad [\text{Do-calculus rule-2 applies}] \\ &= \frac{P(x_1, x_2, z_1, z_3)}{\sum_{z_2} P(z_1, z_2, z_3|x_1)} \times P(z_1, z_2, z_3|x_1) \\ &= \frac{Q(x_1, x_2, z_1, z_3)}{\sum_{z_2} Q_{x_1}(z_1, z_2, z_3)} \times Q_{x_1}(z_1, z_2, z_3) \quad [\text{According to Equation 6}] \\ &= Q(x_1, x_2, z_1, z_2) \quad [\text{We can follow the same above steps as } P(\cdot) \text{ for } Q(\cdot)] \end{aligned} \quad (7)$$

Therefore, if we match the distributions in Equation 6 with the DCM, it will match $P(\mathcal{V})$ as well.

D.2 Modular Training for Interventional Dataset

D.2.1 Modular Training Basics

Suppose, for the graph in Figure 11, we have two datasets $D^\emptyset \sim P(\mathcal{V})$ and $D^{z_1} \sim P_{z_1}(V)$, i.e., intervention set $\mathcal{I} = \{\emptyset, Z_1\}$. Joint distributions in both dataset factorize like below:

$$\begin{aligned} P(v) &= P_{z_1}(x_1, x_2)P_{x_1}(z_1, z_2, z_3) \\ P_{z_1}(v) &= P_{z_1}(x_1, x_2)P(z_3)P_{z_1}(z_2) \\ &= P_{z_1}(x_1, x_2)P_{z_1}(z_2, z_3)[\text{Since } Z_2, Z_3 \text{ independent in } G_{\overline{Z_1}} \text{ graph}] \\ &= P_{z_1}(x_1, x_2)P_{x_1, z_1}(z_2, z_3)[\text{Ignores intervention using do calculus rule-2}] \end{aligned} \quad (8)$$

We change the c-factors for $P_{z_1}(V)$ to keep the variables in each c-factor same in all distributions. This factorization suggests that to match $P(\mathcal{V})$ and $P_{z_1}(V)$ we have to match each of the c-factors using D^\emptyset and D^{z_1} datasets. In Figure 2 graph G , $P_{x_1}(z_1, z_2, z_3) = P(z_1, z_2, z_3|x_1)$ since do-calculus rule-2 applies. And in $G_{\overline{Z_1}}$, $P(z_3)P_{z_1}(z_2)$ can be combined into $P_{x_1, z_1}(z_2, z_3)$. Thus we can use these distributions to train part of the DCM: $\mathbb{G}_{Z_1}, \mathbb{G}_{Z_2}, \mathbb{G}_{Z_3}$ to learn both $Q(z_1, z_2, z_3|\text{do}(x_1))$ and $Q(z_2, z_3|\text{do}(x_1, z_1))$. However, $P(x_1, x_2|\text{do}(z_1)) \neq P(x_1, x_2|z_1)$ in $P(\mathcal{V})$. But we have access to $P_{z_1}(\mathcal{V})$. Thus, we can train $\mathbb{G}_{X_1}, \mathbb{G}_{X_2}$ with only dataset $D^{Z_1} \sim P_{z_1}(\mathcal{V})$ (instead of both D^\emptyset, D^{Z_1}) and learn $Q(x_1, x_2|\text{do}(z_1))$. This will ensure the DCM has matched both $P(\mathcal{V})$ and $P_{z_1}(\mathcal{V})$ distribution.

Thus, we search proxy distributions to each c-factor corresponding to both $P(\mathcal{V})$ and $P_{z_1}(V)$ dataset, to train the mechanisms in a c-component \mathbf{Y} . For each of the c-factors corresponding to \mathbf{Y} in $P(\mathcal{V})$ and $P_{z_1}(V)$, we search for two ancestor sets $\mathcal{A}_\emptyset, \mathcal{A}_{Z_1}$ in both $P(\mathcal{V})$ and $P_{z_1}(V)$ datasets such that the parent set $Pa(\mathbf{Y} \cup \mathcal{A}_\emptyset)$ satisfies rule-2 for the joint $\mathbf{Y} \cup \mathcal{A}_\emptyset$ and $Pa(\mathbf{Y} \cup \mathcal{A}_{Z_1})$ satisfies rule-2 for the joint $\mathbf{Y} \cup \mathcal{A}_{Z_1}$ with $\text{do}(Z_1)$ intervention.

We update Definition 4.4as **modularity condition-I** for multiple interventional datasets as below:

Definition D.1 (Modularity condition-I). Given a causal graph G , an intervention $I \in \mathcal{I}$ and a c-component variable set \mathbf{Y} , a set $\mathcal{A} \subseteq An_{G_I}(\mathbf{Y}) \setminus \mathbf{Y}$ is said to satisfy the modularity condition if it is the smallest set that satisfies $P(\mathbf{Y} \cup \mathbf{X}|\text{do}(Pa(\mathbf{Y} \cup \mathbf{X})), \text{do}(I)) = P(\mathbf{Y} \cup \mathbf{X}|Pa(\mathbf{Y} \cup \mathbf{X}), \text{do}(I))$, i.e., do-calculus rule-2 (Pearl, 1995) applies.

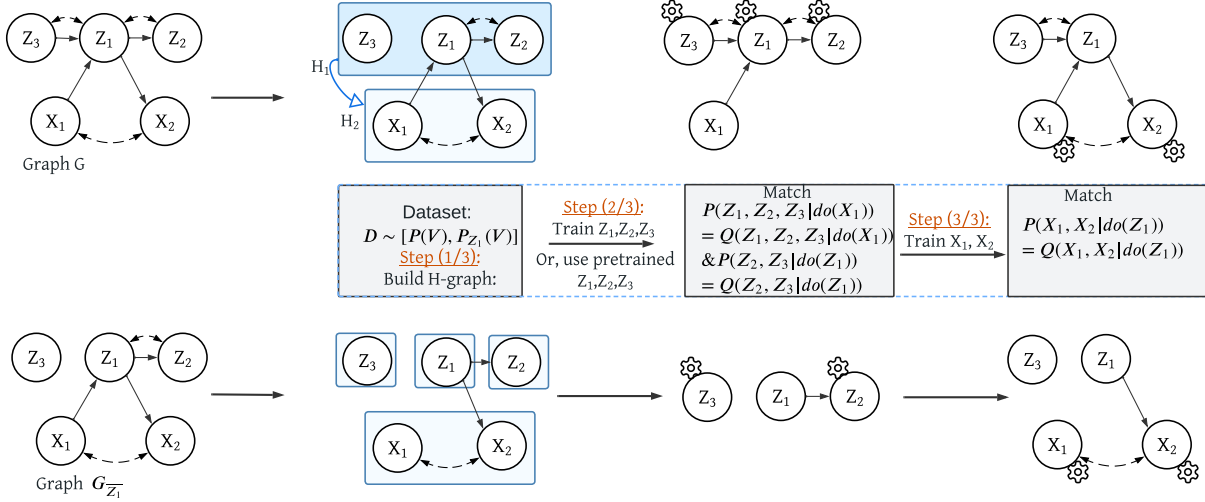


Figure 11: Modular training on H-graph: $H_1 : [Z_1, Z_2, Z_3] \rightarrow H_2 : [X_1, X_2]$ with dataset $D \sim P(V)$.

Unlike before, we have access to $P_{z_1}(V)$ and we can use that to match $P_{z_1}(x_1, x_2)$ in both cases. To match the \mathcal{L}_1 and \mathcal{L}_2 joint distributions according to (8), we train each c-component one by one. For each c-component, we identify the modularity conditions of all c-factors $P_{pa(\mathbf{Y}) \cup I}(\mathbf{Y})$, $\forall I \in \mathcal{I}$ and use them to train \mathbf{Y} . We train the mechanisms in \mathbf{Y} to learn an alternative to each c-factor $P_{pa(\mathbf{Y}) \cup I}(\mathbf{Y})$, $\forall I \in \mathcal{I}$. For some ancestor set \mathcal{A}_I , the alternative distribution is in the form $P(\mathbf{Y} \cup \mathcal{A}_I | do(Pa(\mathbf{Y} \cup \mathcal{A}_I)), do(I))$ which should be equivalent to $P(\mathbf{Y} \cup \mathcal{A} | Pa(\mathbf{Y} \cup \mathcal{A}), do(I))$. We will find an \mathcal{A}_I from the D^I , $\forall I \in \mathcal{I}$ such that we do not require $Pa(\mathbf{Y} \cup \mathcal{A})$ to be intervened on.

Now, to match $P(\mathbf{Y} \cup \mathcal{A} | Pa(\mathbf{Y} \cup \mathcal{A}), do(I)) = Q(\mathbf{Y} \cup \mathcal{A} | do(Pa(\mathbf{Y} \cup \mathcal{A})), do(I))$ with our generative models, we pick the observations of $Pa(\mathbf{Y} \cup \mathcal{A})$ from D^I dataset and intervene in our DCM with those values besides intervening on \mathbb{G}_I . Since we do not need generated samples for $Pa(\mathbf{Y} \cup \mathcal{A})$ from DCM, rather their observations from the given D^I dataset, we do not require them to be trained beforehand. However, the order in which we train c-components matters and we follow the partial order found for $P(V)$ dataset even though we train with multiple datasets.

For example, in Figure 2, we have two graphs G and G_{Z_1} . We follow G 's training order for both graphs to train the c-components, i.e., $[\mathbb{G}_{Z_1}, \mathbb{G}_{Z_2}, \mathbb{G}_{Z_3}] \rightarrow [\mathbb{G}_{X_1}, \mathbb{G}_{X_2}]$. Here, for the c-component $\mathbf{Y} = \{Z_1, Z_2, Z_3\}$, we match $P(V)$ c-factor $P_{x_1}(z_1, z_2, z_3)$ and $P_{z_1}(V)$ c-factor $P_{x_1, z_1}(z_2, z_3)$ thus have to find alternative distribution for them. We find the smallest ancestor set $\mathcal{A}_0, \mathcal{A}_{z_1}$ for these c-factors in both D^0 and D^{z_1} datasets. $\mathcal{A}_0 = \emptyset$ satisfies modularity condition for $P(V)$ c-factor and their $Pa(\mathbf{Y} \cup \mathcal{A}) = \{X_1\}$. $\mathcal{A}_{z_1} = \emptyset$ satisfies modularity condition for $P_{z_1}(V)$ c-factor and their $Pa(\mathbf{Y} \cup \mathcal{A}) = \emptyset$. At step (2/3) in Figure 2, We do not need \mathbb{G}_{X_1} to be pre-trained. $[\mathbb{G}_{Z_1}, \mathbb{G}_{Z_2}, \mathbb{G}_{Z_3}]$ converges by matching both $P(z_1, z_2, z_3 | x_1) = Q_{x_1}(z_1, z_2, z_3)$ and $P_{x_1, z_1}(z_2, z_3) = Q_{x_1, z_1}(z_2, z_3)$.

Now, we train mechanisms of the next c-component $[\mathbb{G}_{X_1}, \mathbb{G}_{X_2}]$ in our training order (step 3/3). We have to match $P(V)$ c-factor $P_{z_1}(x_1, x_2)$ and $P_{z_1}(V)$ c-factor $P_{z_1}(x_1, x_2)$. Ancestor set $\mathcal{A}_0 = \{Z_1, Z_3\}$ satisfies the modularity condition for $\mathbf{Y} = \{X_1, X_2\}$ with $P(V)$ dataset but $\mathcal{A}_{z_1} = \emptyset$ a smaller set, satisfies the modularity condition for same c-factor with $P_{z_1}(V)$ dataset. Also, $P_{z_1}(V)$ c-factor is $P_{z_1}(x_1, x_2)$. Thus if we train $[\mathbb{G}_{X_1}, \mathbb{G}_{X_2}]$ with only $P_{z_1}(V)$ dataset, it will learn both c-factors and converge with $P_{z_1}(x_1, x_2) = Q_{z_1}(x_1, x_2)$. Since we have matched all the c-factors, our DCM will match both $P(V)$ and $P_{z_1}(V)$ distributions. During training of $[\mathbb{G}_{X_1}, \mathbb{G}_{X_2}]$, we had $\mathcal{A} = \emptyset$ for both observation and interventional c-factors. Therefore, we do not need any pre-trained mechanisms, rather we can directly use the observations from $P_{z_1}(V)$ dataset as parent values. We define \mathcal{H}^I -graph for each $I \in \mathcal{I}$ as below:

Definition D.2 (\mathcal{H}^I -graph). For a post-interventional graph $G_{\bar{I}}$, let the set of c-components in $G_{\bar{I}}$ be $\mathcal{C} = \{C_1, \dots, C_t\}$. Choose a partition $\{H_k^I\}_k$ of \mathcal{C} such that the \mathcal{H}^I -graph $\mathcal{H}^I = (V_{\mathcal{H}^I}, E_{\mathcal{H}^I})$, defined as follows, is acyclic: $V_{\mathcal{H}^I} = \{H_k^I\}_k$ and for any s, t , $H_s^I \rightarrow H_t^I \in E_{\mathcal{H}^I}$, iff $P(H_t^I | do(pa(H_t^I) \cap H_s^I)) \neq P(H_t^I | pa(H_t^I) \cap H_s^I)$, i.e., do-calculus rule-2 does not hold. Note that one can always choose a partition of \mathcal{C} to ensure \mathcal{H}^I is acyclic:

Algorithm 4 TrainModule($\mathbb{G}, G, H_*, \mathcal{A}, \mathbf{D}$)

```
1: Input: DCM  $\mathbb{G}$ , Graph  $G(\mathcal{V}, \mathcal{E})$ , h-node  $H_*$ , Ancestor set  $\mathcal{A}$ , Data  $\mathbf{D}$ , Params  $\theta_H, \lambda = 10$ 
2: while  $\theta_{H_*}$  has not converged do
3:   for each  $(A_i, X_i, D_i) \in (\mathcal{A}, \mathbf{D})$  do
4:      $V_r = H_* \cup A_i \cup Pa(H_* \cup A_i) \cup X_i$ 
5:     Initialize critic  $\mathbb{D}_{w_i}$ 
6:     for  $t = 1, \dots, m$   $\{m \text{ samples}\}$  do
7:       Sample real data  $\mathbf{v}_x^r \sim D_i$ 
8:        $\mathbf{x}^r \leftarrow \text{get\_intv\_values}(X_i, D_i)$ 
9:        $\mathbf{v}_x^f = \text{RunGAN}(\mathbb{G}, \mathbf{x}^r, V_r, \theta_{H_*})$ 
10:       $\hat{\mathbf{v}}_x = \epsilon \mathbf{v}_x^r + (1 - \epsilon) \mathbf{v}_x^f$ 
11:       $L_i^{(t)} = \mathbb{D}_{w_i}(\mathbf{v}_x^f) - \mathbb{D}_{w_i}(\mathbf{v}_x^r) * \lambda (\|\nabla_{\hat{\mathbf{v}}_x} \mathbb{D}_{w_i}(\hat{\mathbf{v}}_x)\|_2 - 1)^2$ 
12:       $w_i = \text{Adam}(\nabla_{w_i} \frac{1}{m} \sum_{t=1}^m L_i^{(t)}, w_i)$ 
13:       $G_{loss} = G_{loss} + \frac{1}{m} \sum_{j=1}^m -\mathbb{D}_{w_i}(\mathbf{v}_x^f)$ 
14:      for  $\theta \in \theta_{H_*}$   $\{\text{All hnode mechanisms}\}$  do
15:         $\theta = \text{Adam}(\nabla_{\theta} G_{loss}, \theta)$ 
16: Return:  $\theta_1, \dots, \theta_n$ 
```

Algorithm 5 IsRule2($Y, X, I = \emptyset$ (by default))

```
1: Input: Variable sets  $Y$  and  $X$ , Intervention  $I$ .
2: Return:
3: if  $P(Y \cup X | \text{do}(Pa(Y \cup X)), \text{do}(I)) = P(Y \cup X | Pa(Y \cup X), \text{do}(I))$  then
4:   Return:1
5: else
6:   Return:0
```

Algorithm 6 Construct- \mathcal{H}^I -graph(G, \mathcal{I})

```
1: Input: Causal Graph  $G$ , Intervention set,  $\mathcal{I}$ 
2: for each  $I \in \mathcal{I}$  do
3:    $\mathcal{C} \leftarrow \text{get\_ccomponents}(G_{\bar{I}})$ 
4:   Construct graph  $\mathcal{H}^I$  by creating nodes  $H_j^I$  as  $H_j^I = C_j, \forall C_j \in \mathcal{C}$ 
5: for each  $I \in \mathcal{I}$  do
6:   for each  $H_s^I, H_t^I \in \mathcal{H}^I$  such that  $H_s^I \neq H_t^I$  do
7:     if  $P(H_t^I | \text{do}(pa(H_t^I) \cap H_s^I)) \neq P(H_t^I | pa(H_t^I) \cap H_s^I)$  then
8:        $\mathcal{H}^I.add(H_s^I \rightarrow H_t^I)$ 
9:      $\mathcal{H}^I \leftarrow \text{merge}(\mathcal{H}^I, cyc) \forall cyc \in Cycles(H^I)$ 
10: for each  $I \in \mathcal{I}$  do
11:   for each  $H_j^0 \in \mathcal{H}^0$  do
12:      $H_j^I = \bigcup_k H_k^I$  such that  $\mathcal{V}(H_k^I) \subseteq \mathcal{V}(H_j^0)$  [All variables in  $H_k^I$  h-node is contained in  $H_j^0$  h-node.]
13: Return:  $\{\mathcal{H}^I : I \in \mathcal{I}\}$ 
```

The \mathcal{H}^I graph with a single node $H_1^I = \mathcal{C}$ in $G_{\bar{I}}$. Even though \mathcal{H}^I for different I might have different partial order, during training, every \mathcal{H}^I follows the partial order of \mathcal{H}^0 . Since its partial order is valid for other H-graphs as well (Proposition D.14).

Here, \mathcal{H}^I is the \mathcal{H} -graph constructed from $G_{\bar{I}}$, for $I \in \mathcal{I}$ where \mathcal{I} is the intervention set. \mathcal{H}^0 is the \mathcal{H} -graph constructed from G for observational training. $H_k^I := k$ -th h-node in the \mathcal{H}^I graph. During \mathcal{H}^I -graphs construction, we resolve cycles by combining c-components on that cycle into a single h-node. Please check example in Figure 19. After merging all such cycles, $\mathcal{H}^I, \forall I \in \mathcal{I}$ will become directed acyclic graphs. The partial order of this graph will indicate the training order that we can follow to train all variables in G . For example in Figure 11, two given datasets D_1 and D_2 , imply two different graphs G and G_{Z_1} respectively. $[Z_3] \rightarrow [Z_1, Z_2] \rightarrow [X_1, X_2]$ is a valid training order for \mathcal{H}_{Z_1} , we follow the same order as \mathcal{H}^0 . We follow : $[Z_1, Z_2, Z_3] \rightarrow [X_1, X_2]$.

We run the subroutine **Construct- \mathcal{H}^I -graph()** in Algorithm 6 to build \mathcal{H} -graphs. We check the edge condition at line 5 and merge cycles at line 7 if any. In Figure 2 step (1/3), we build the \mathcal{H} -graph $H_1 : [Z_1, Z_2, Z_3] \rightarrow H_2 : [X_1, X_2]$ for G .

Algorithm 7 Modular Training-I($G, \mathcal{I}, \mathbf{D}$)

```
1: Input: Causal Graph  $G$ , Intervention set  $\mathcal{I}$ , Dataset  $\mathbf{D}$ .
2: Initialize DCM  $\mathbb{G}$ 
3:  $\mathcal{H}^I \leftarrow \mathbf{Construct-H-graphs}(G, \mathcal{I})$ 
4: for each  $H_k \in \mathcal{H}^0$  in partial order do
5:    $\mathcal{A}_\emptyset \leftarrow \mathcal{V}$  //Initialize with all nodes
6:   for each  $S \subseteq An_G(H_k)$  do
7:     if  $\text{IsRule2}(H_k, S, \emptyset) = 1$ 
       and  $|S| < |\mathcal{A}_\emptyset|$  then
8:        $\mathcal{A}_\emptyset \leftarrow S$ 
9:   for each  $I \in \mathcal{I} \cap H_k$  do
10:     $\mathcal{A}_I \leftarrow \mathcal{V}$  //Initialize with all nodes
11:    for each  $S \subseteq An_{G_{\bar{I}}}(H_k)$  do
12:      if  $\text{IsRule2}(H_k, S, I) = 1$ 
        and  $|S| < |\mathcal{A}_I|$  then
13:         $\mathcal{A}_I \leftarrow S$ 
14:     $\mathbb{G}_{H_k} \leftarrow \text{TrainModule}(\mathbb{G}_{H_k}, G, H_k, \mathcal{A}, \mathbf{D})$ 
15: Return:  $\mathbb{G}$ 
```

D.2.2 Training Process of Modular Modular-DCM

We construct the \mathcal{H}^I -graph for each $I \in \mathcal{I}$ at Algorithm 7 line 3. Next, we train each h-node H_k^\emptyset of \mathcal{H}^0 , according to its partial order \mathcal{T} . Since we follow the partial order of \mathcal{H}^0 -graph, we remove the superscript to address the hnode. Next, we match alternative distributions for $P_I(\mathcal{V})$ c-factors that correspond to the c-components in H_k . (lines 4-14) We initialize a set $\mathcal{A}_I = \{V : V \subseteq An_{G_{\bar{I}}}(H_k)\}, \forall I \in \mathcal{I}$ to keep track of the joint distribution we need to match to train each h-node H_k from D^I datasets. We iterate over each intervention and search for the smallest set of ancestors \mathcal{A}_I in $G_{\bar{I}}$ such that \mathcal{A}_I satisfies the modularity condition for H_k in D^I dataset tested by Algorithm 5: $\text{IsRule2}(\cdot)$ (line 7)

$\mathcal{A}_I, \forall I \in \mathcal{I}$ implies a set of joint distributions in Equation 9, which is sufficient for training the current h-node H_k to learn the c-factors $P_{Pa(C_i) \cup I}(C_i), \forall C_i \in H_k, \forall I \in \mathcal{I}$.

$$Q(H_k \cup \mathcal{A}_I | \text{do}(pa(H_k \cup \mathcal{A}_I)), \text{do}(I)) = P(H_k \cup \mathcal{A}_I | pa(H_k \cup \mathcal{A}_I), \text{do}(I)), \text{in } G_{\bar{I}}, \forall I \in \mathcal{I}. \quad (9)$$

Training: H_k , Pre-trained: \mathcal{A}_I , From D^I dataset: $pa(H_k \cup \mathcal{A}_I)$, Intervened: $\text{do}(I)$

Training H_k with the \mathcal{A}_\emptyset found at this step, is sufficient to learn the c-factors $P_{Pa(C_i)}(C_i), \forall C_i \in H_k$. Similarly, if we have an interventional dataset with $I \in H_k$ i.e., the intervened variable lies in the current h-node, we have to match c-factors $P_{Pa(C_i) \cup I}(C_i), \forall C_i \in H_k$. To find alternatives to these c-factors, we look for the ancestor set \mathcal{A}_I in the D^I dataset. For each \mathcal{A}_I , we train H_k to match the interventional joint distribution in Equation 9. We ignore intervention on any descendants of H_k since the intervention will not affect c-factors differently than the c-factor in the D^\emptyset observational dataset.

D.2.3 Learn $P(\mathcal{V})$ -factors from Interventional Datasets

When we need the alternative distribution for $P(\mathcal{V})$ c-factor, we search for the smallest ancestor set in D^\emptyset dataset. However, when we have a dataset D^I with $I \in An_G(H_j^\emptyset)$, we can search for an ancestor set in $An_{G_{\bar{I}}}(H_k)$ and train on D^I to match a distribution that would be a proxy to $P(\mathcal{V})$ c-factor. This is possible because when we factorize $P_I(\mathcal{V})$ for $I \in An_G(H_j^\emptyset)$, the c-factors corresponding to the descendant c-components of I are similar to $P(\mathcal{V})$ c-factors of the same c-components.

We update Theorem 4.5 for interventional datasets as below.

Theorem D.3. *Let $\mathcal{M}_1 = (G = (\mathcal{V}, \mathcal{E}), \mathcal{N}, \mathcal{U}, \mathcal{F}, P(\cdot))$ be the true SCM and $\mathcal{M}_2 = (G, \mathcal{N}', \mathcal{U}', \mathcal{F}', Q(\cdot))$ be the DCM. Suppose Algorithm 7: **Modular-DCM Modular Training-I** on observational and interventional datasets $\mathbf{D}^I \sim P_I(\mathcal{V}), \forall I \in \mathcal{I}$ converges for each h-node in the \mathcal{H}^0 -graph constructed from $G = (\mathcal{V}, \mathcal{E})$ and DCM induces the distribution $Q_I(\mathcal{V}), \forall I \in \mathcal{I}$. Then, we have i) $P_I(\mathcal{V}) = Q_I(\mathcal{V})$, and ii) for any interventional or counterfactual causal query $\mathcal{K}_{\mathcal{M}_1}(\mathcal{V})$ that is identifiable from $\mathbf{D}^I, \forall I \in \mathcal{I}$, we have $\mathcal{K}_{\mathcal{M}_1}(\mathcal{V}) = \mathcal{K}_{\mathcal{M}_2}(\mathcal{V})$.*

We provide the proof in Appendix D.6.

D.3 Training following the \mathcal{H} -graph

Modular-DCM utilizes conditional generative models such as diffusion models and Wasserstein GAN with penalized gradients (Gulrajani et al., 2017) for adversarial training on \mathcal{L}_1 and \mathcal{L}_2 datasets in Algorithm 4. \mathbb{G} is the DCM, a set of generators and $\{\mathbb{D}_{w_i}\}$ are a set of critics for each intervention dataset. Here, for intervention $\text{do}(X = x)$, $X \in \mathbf{I}$, $\mathbb{G}^{(x)}(\mathbf{z}, \mathbf{u})$ are generated samples and $v \sim \mathbb{P}_x^r$ are real \mathcal{L}_1 or \mathcal{L}_2 samples. We train our models by iterating over all datasets and learn \mathcal{L}_1 and \mathcal{L}_2 distributions (lines 3-15). We produce fake interventional samples at line 9 by intervening on the corresponding node of our architecture with Algorithm 9 RunGAN(). Each critic \mathbb{D}_x will obtain different losses, $L_{X=x}$ by comparing the generated samples with different true datasets (line 11). Finally, at line 15, we update each variable’s model weights located at the current hnode based on the accumulated generated loss over each dataset at line 13. After calling Algorithm 4: **TrainModule()** for each of the h-nodes according to the partial order of \mathcal{H}^θ -graph, Modular-DCM will find a DCM equivalent to the true SCM that matches all dataset distributions. According to, Theorem C.3, it will be able to produce correct $\mathcal{L}_1, \mathcal{L}_2$ and \mathcal{L}_3 samples identifiable from these input distributions (Appendix C.1).

D.4 Essential Theoretical Statements Required for Distributions Matching by Modular-DCM Modular Training

In this section and the following section, we prove some theoretical statements required for our algorithm. Figure 12, illustrates the statements we have to prove and the route we have to follow.

In proposition D.6, we prove the property of a sub-graph having the same set of c-components although we intervene on their parents outside that sub-graph. We use this proposition in Lemma D.7 to show that we can apply c-component factorization for any sub-graph under appropriate intervention. Therefore, in Corollary D.8, we can show that c-component factorization can be applied for h-nodes of the \mathcal{H} -graph as well.

We build the above theoretical ground and utilize the statements in section D.5. We show that c-factorization works for the \mathcal{H} -graph and Modular Training on h-nodes matches those c-factors. Thus, Modular-DCM will be able to match i) the observational joint distribution $P(\mathcal{V})$ after training on observational data (Proposition D.12) ii) the observational joint distribution $P(\mathcal{V})$ after training on partial observational data and interventional data (Proposition D.13) and iii) the interventional joint distribution $P_I(\mathcal{V}), \forall I \in \mathcal{I}$ after training on observational data and interventional data. (Proposition D.15). The last proposition requires the proof that for all intervention $I \in \mathcal{I}$, the generated \mathcal{H}^I graphs follows the same partial order.

Modular-DCM modular training can now match $P(\mathcal{V})$ and $P_I(\mathcal{V}), \forall I \in \mathcal{I}$ according to Proposition D.13 and Proposition D.15. We can now apply Theorem C.3 to say that Modular-DCM modular training can sample from identifiable interventional distributions after training on $D \sim P(V)$ and from identifiable counterfactual distributions after training on $D \sim P(V), P_I(V)$ (Theorem D.16). Finally, Theorem D.17 for observational case is a direct application of Proposition D.12 and TheoremD.16 while Theorem D.18 for interventional case is a direct application of Proposition D.13, Theorem D.15 and Theorem D.16.

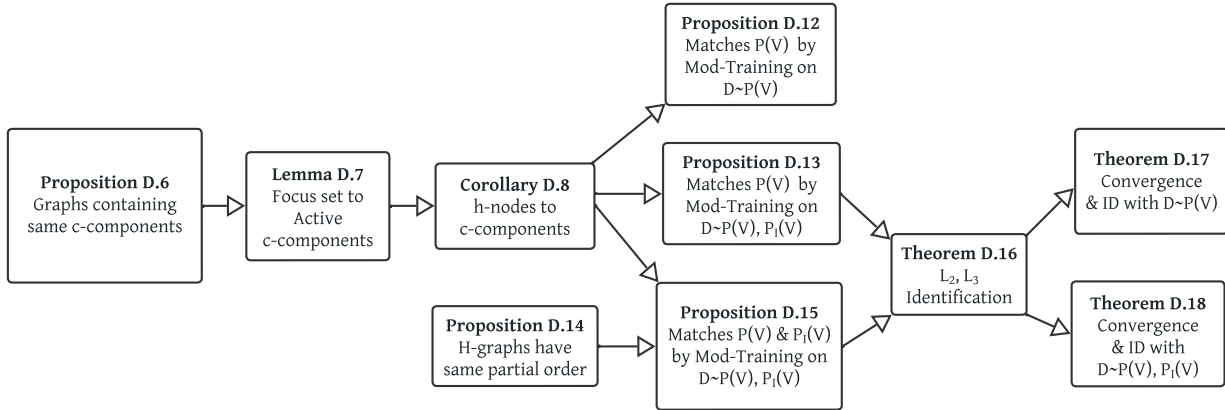


Figure 12: Flowchart of proofs

We start with some definitions that would be required during our proofs.

Definition D.4 (Intervention Set, \mathcal{I}). Intervention Set, \mathcal{I} represents the set of all available interventional variables such that after performing intervention $I \in \mathcal{I}$ on G , we observe $G_{\overline{I}}$. \mathcal{I} includes $I = \emptyset$, which refers to "no intervention" and implies the original graph G and the observational data $P(\mathcal{V})$.

Definition D.5 (Sub-graph, $(G_{\overline{I}})_V$). Let G_V be a sub-graph of G containing nodes in V and all arrows between such nodes. $(G_{\overline{I}})_V$ refers to the sub-graph of $G_{\overline{I}}$ containing nodes in V only, such that variable I is intervened on i.e., all incoming edges to I is cut off.

Proposition D.6. Let $V \in \mathcal{V}, I \in \mathcal{I}$ be some arbitrary variable sets. The set of c-components formed from a sub-graph $(G_{\overline{I}})_V$ with intervention I is not affected by additional interventions on their parents from outside of the sub-graph. Formally, $(G_{\overline{Pa(V) \cup I}})_{\overline{V}}$ and $(G_{\overline{I}})_V$ has the same set of c-components.

Proof. Let $C((G_{\overline{I}})_V)$ be the c-components which consists of nodes of V in graph $(G_{\overline{I}})_V$. In sub-graph $(G_{\overline{Pa(V) \cup I}})_{\overline{V}}$, no extra intervention is being done on any node in V rather only on $Pa(V)$ where V and $Pa(V)$ are two disjoint sets. Therefore, the c-components can be produced from this sub-graph will be same as for $G_{\overline{I}}$. i.e., $C(G_{\overline{Pa(V) \cup I}})_{\overline{V}} = C(G_{\overline{I}})$. \square

Lemma D.7. Let V' be a set called focus-set. V' and intervention I be arbitrary subsets of observable variables \mathcal{V} and $\{C_i\}_i$ be the set of c-components in $G_{\overline{I}}$. Let $\{Pa(V') \cup I\}$ be a set called action-set. and S be a set called remain-set, defined as $S := \mathcal{V} \setminus \{V' \cup Pa(V') \cup I\}$, $S(i)$ as $S(i) = S \cap C_i$ i.e., some part of the remain-set that are located in c-component C_i . Thus, $S = \bigcup_i S(i)$. We also define active c-components C_i^+ as $C_i^+ := C_i \setminus \{S(i) \cup Pa(V') \cup I\}$ i.e., the variables in focus-set that are located in c-component C_i . Given these sets, Tian's factorization can be applied to a sub-graph under proper intervention. Formally, we can factorize as below:

$$P_{Pa(V') \cup I}(V') = \prod_i P_{Pa(C_i^+) \cup I}(C_i^+)$$

Proof Sketch. Similar to the original c-factorization formula $P(\mathcal{V}) = \prod_i P_{Pa(C_i)}(C_i)$, we can factorize as $P_{Pa(V') \cup I}(V') = \prod_i P_{Pa(C_i) \cup Pa(V') \cup I}(C_i)$. Next, we can marginalize out unnecessary variables S located outside of V' from both sides of this expression. The left hand side of the expression is then $P_{Pa(V') \cup I}(V')$ that is what we need. For the right hand side, we can distribute the marginalization \sum_S among all terms and obtain $\prod_i \sum_{S(i)} P_{Pa(C_i) \cup Pa(V') \cup I}(C_i)$ from $\sum_S \prod_i P_{Pa(C_i) \cup Pa(V') \cup I}(C_i)$. Finally for each product term $P_{Pa(C_i) \cup Pa(V') \cup I}(C_i)$, we remove $S(i)$ from C_i to obtain C_i^+ and drop non parent interventions following do-calculus rule-3. This final right hand side expression becomes, $\prod_i P_{Pa(C_i^+) \cup I}(C_i^+)$. We provide the detailed proof below. \square

Proof. $(G_{\overline{Pa(V') \cup I}})_{V'}$ and $(G_{\overline{I}})_{V'}$ have the same c-components according to Proposition D.6. According to Tian's factorization for causal effect identification (Tian and Pearl, 2002), we know that

$$\begin{aligned} P_{Pa(V') \cup I}(\mathcal{V}) &= \prod_i P_{Pa(C_i) \cup Pa(V') \cup I}(C_i) \\ &\quad [\text{let } \eta = Pa(V') \cup I, \text{ i.e., action-set}] \\ \implies P_\eta(\eta) \times P_\eta(\mathcal{V} \setminus \eta | \eta) &= \prod_i P_{Pa(C_i) \cup \eta}(C_i) \\ \implies P_\eta(\mathcal{V} \setminus \{Pa(V') \cup I\}) &= \prod_i P_{Pa(C_i) \cup \eta}(C_i) \end{aligned} \tag{10}$$

We ignore conditioning on action-set $\eta = Pa(V') \cup I$ since we are intervening on it. Now, we have a joint

distribution of focus-set and remain-set with action-set as an intervention.

$$\begin{aligned}
&\implies P_\eta(V' \cup S) = \prod_i P_{Pa(C_i) \cup \eta}(C_i) \\
&\text{[Here, } S := \mathcal{V} \setminus \{V' \cup Pa(V') \cup I\} \implies \mathcal{V} \setminus \{Pa(V') \cup I\} = V' \cup S\text{]} \\
&\implies \sum_S P_\eta(V' \cup S) = \sum_S \prod_i P_{Pa(C_i) \cup \eta}(C_i) \\
&\implies \sum_S P_\eta(V' \cup S) = \prod_i \sum_{S(i)} P_{Pa(C_i) \cup \eta}(C_i) \\
&\text{[Since, } S(i) = S \cap C_i \text{ and } \forall(i, j), i \neq j, C_i \cap C_j = \emptyset \implies S_i \cap S_j = \emptyset\text{]}
\end{aligned} \tag{11}$$

Here, $\forall_i, S(i)$ are disjoint partitions of the variable set S and contained in only c-component C_i , i.e., $S(i) = S \cap C_i$. Since $\forall_{i,j}, C_i \cap C_j = \emptyset$, this implies that $S_i \cap S_j = \emptyset$ would occur as well. Intuitively, remain-sets located in different c-components do not intersect. Therefore, each of the probability terms at R.H.S, $P_{Pa(C_i) \cup \eta}(C_i)$ is only a function of $S(i)$ instead of whole S . This gives us the opportunity to push the marginalization of $S(i)$ inside the product and marginalize the probability term. After marginalizing $S(i)$ from the joint, we define rest of the variables as active c-components C_i^+ . The following Figure 13 helps to visualize all the sets.

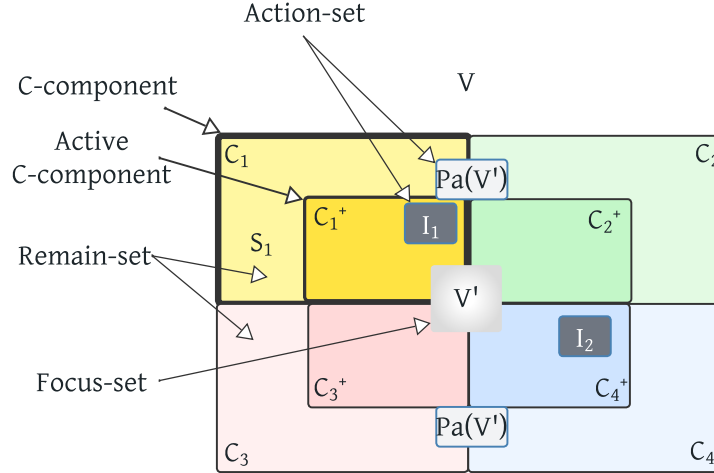


Figure 13: Visualization of focus-sets, action-sets, and remain-sets

We continue the derivation as follows:

$$\begin{aligned}
&\implies P_{Pa(V') \cup I}(V') = \prod_i P_{Pa(C_i) \cup Pa(V') \cup I}(C_i^+) \\
&\text{[Here, } C_i^+ = C_i \setminus S(i)\text{, i.e., active c-component: focus-set elements located in } C_i\text{]} \\
&= \prod_i P_{Pa(C_i^+) \cup I \cup \{Pa(C_i) \setminus Pa(C_i^+)\} \cup Pa(V')}(C_i^+) \\
&= \prod_i P_{X \cup Z}(C_i^+) \text{ [Let, } X = Pa(C_i^+) \cup I \text{ and } Z = \{Pa(C_i) \cup Pa(V')\} \setminus X\text{]}
\end{aligned} \tag{12}$$

Here, we have variable set C_i^+ in the joint distribution. Now, if we intervene on the parents $Pa(C_i^+)$ and I , rest of the intervention which is outside C_i^+ becomes ineffective. Therefore, we have $X = Pa(C_i^+) \cup I$, the intervention which shields the rest of the interventions, $Z = \{Pa(C_i) \cup Pa(V')\} \setminus X$. Therefore, we can apply do-calculus rule 3 on Z and remove those interventions. Finally,

$$\implies P_{Pa(V') \cup I}(V') = \prod_i P_{Pa(C_i^+) \cup I}(C_i^+) \text{ [We apply Rule 3 since } C_i \perp\!\!\!\perp Z | X_{C_{\bar{X}}}\text{]} \tag{13}$$

□

Corollary D.8, suggests that Tian’s factorization can be applied on the h-nodes of $H^I \in \mathcal{H}$.

Corollary D.8. Consider a causal graph G . Let $\{C_i\}_{i \in [t]}$ be the c-components of $G_{\bar{T}}$. For some intervention target I , let $H^I = (V_{\mathcal{H}^I}, E_{\mathcal{H}^I})$ be the h-graph constructed by Algorithm 6 where $V_{\mathcal{H}^I} = \{H_k^I\}_k$. Suppose H_k^I is some node in \mathcal{H}^I . We have that $H_k^I = \{C_i\}_{i \in T_k^I}$ for some $T_k^I \subseteq [t]$. With slight abuse of notation we use H_k^I interchangeably with the set of nodes that are in H_k^I . Then,

$$P_{Pa(H_k^I) \cup I}(H_k^I) = \prod_{i \in [t]} P_{Pa(C_i) \cup I}(C_i) \quad (14)$$

Proof. Let, $V' = H_k^I$, $C_i^+ = C_i \setminus \emptyset = C_i$. Then, this corollary is direct application of Lemma D.7. □

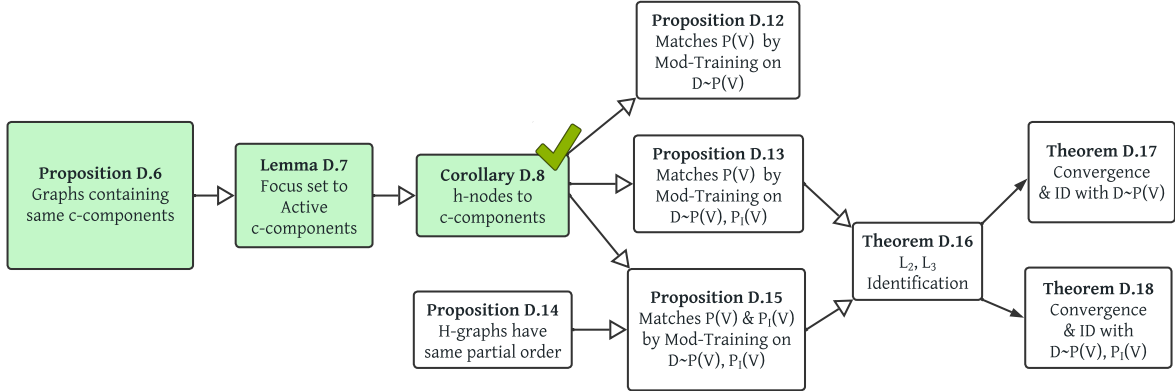


Figure 14: Flowchart of proofs

D.5 Theoretical Proofs of Distributions Matching by Modular-DCM Modular Training

We provide Definition D.2: \mathcal{H}^I -graph here again.

Definition D.9 (\mathcal{H}^I -graph). For a post-interventional graph $G_{\bar{T}}$, let the set of c-components in $G_{\bar{T}}$ be $\mathcal{C} = \{C_1, \dots, C_t\}$. Choose a partition $\{H_k^I\}_k$ of \mathcal{C} such that the \mathcal{H}^I -graph $\mathcal{H}^I = (V_{\mathcal{H}^I}, E_{\mathcal{H}^I})$, defined as follows, is acyclic: $V_{\mathcal{H}^I} = \{H_k^I\}_k$ and for any s, t , $H_s^I \rightarrow H_t^I \in E_{\mathcal{H}^I}$, iff $P(H_t^I | \text{do}(pa(H_t^I) \cap H_s^I)) \neq P(H_t^I | pa(H_t^I) \cap H_s^I)$, i.e., do-calculus rule-2 does not hold. Note that one can always choose a partition of \mathcal{C} to ensure \mathcal{H}^I is acyclic: The \mathcal{H}^I graph with a single node $H_1^I = \mathcal{C}$ in $G_{\bar{T}}$. Even though \mathcal{H}^I for different I might have different partial order, during training, every \mathcal{H}^I follows the partial order of \mathcal{H}^\emptyset . Since its partial order is valid for other H-graphs as well.

Training order, \mathcal{T} : We define a training order, $\mathcal{T} = \{\sigma_0, \dots, \sigma_m\}$ where $\sigma_i = \{H_k\}_k$. If $H_{k_1}^I \rightarrow H_{k_2}^I, H_{k_1}^I \in \sigma_i, H_{k_2}^I \in \sigma_j$ then $i < j$.

Definition D.10 (Notation for distributions). $Q(\cdot)$ is the observational distribution induced by the deep causal SCM. $P(\cdot)$ is the true (observational/interventional) distribution. With a slight abuse of notation, if we have $P(\mathbf{V})$ and intervention I , then $P_I(\mathbf{V})$ indicates $P_I(\mathbf{V} \setminus I)$. Algorithm 7 is said to have converged if training attains zero loss every time line 14 is visited.

Definition D.11 (Ancestor set \mathcal{A}_I in G_I). Let parents of a variable set \mathbf{V} be $Pa(\mathbf{V}) = \bigcup_{V \in \mathbf{V}} Pa(V) \setminus \mathbf{V}$.

Now, for some h-node $H_k^I \in \mathcal{H}^I$ -graph, we define $\mathcal{A}_I :=$ the minimal subset of ancestors exists in the causal graph G_I with intervention I such that the following holds,

$$p(H_n^I \cup \mathcal{A}_I | do(pa(H_n^I \cup \mathcal{A}_I)), do(I)) = p(H_n^I \cup \mathcal{A}_I | pa(H_n^I \cup \mathcal{A}_I), do(I)) \quad (15)$$

For training any h-node in the training order $\mathcal{T} = \{\sigma_0, \dots, \sigma_m\}$, i.e., $H_k^0 \in \sigma_j$, $0 < j \leq m$, if only observational data is available, i.e., $I = \emptyset$, we search for an ancestor set \mathcal{A}_\emptyset such that \mathcal{A}_\emptyset satisfies modularity condition for H_k^0 :

$$P(H_k^0 \cup \mathcal{A}_\emptyset | do(pa(H_k^0 \cup \mathcal{A}_\emptyset))) = P(H_k^0 \cup \mathcal{A}_\emptyset | pa(H_k^0 \cup \mathcal{A}_\emptyset)) \quad (16)$$

Similarly, for $I \in An_G(H_k^I)$, i.e., intervention on ancestors, we can learn $P_{pa(H_k^0)}(H_k^0)$ from available interventional datasets since $H_k^I = H_k^0$, i.e., contains the same c-factors, according to \mathcal{H}^I -graphs construction. These c-factor distributions are identifiable from $P_I(V)$ as they can be calculated from the c-factorization of $P_I(V)$. Thus we have,

$$P_{pa(H_k^I)}(H_k^I) = P_{pa(H_k^0)}(H_k^0) \quad (17)$$

Therefore, to utilize ancestor interventional datasets, We search for smallest ancestor set $\mathcal{A}_I \subseteq An_{G_I}(H_k^I)$ in G_I such that do-calculus rule-2 applies,

$$P(H_k^I \cup \mathcal{A}_I | do(pa(H_k^I \cup \mathcal{A}_I)), do(I)) = P(H_k^I \cup \mathcal{A}_I | pa(H_k^I \cup \mathcal{A}_I), do(I)) \quad (18)$$

Then we can train the mechanisms in H_k^0 to learn the $P(\mathcal{V})$ c-factors by matching the following alternative distribution from D^I dataset,

$$\begin{aligned} P(H_k^I \cup \mathcal{A}_I | pa(H_k^I \cup \mathcal{A}_I), do(I)) &= Q(H_k^I \cup \mathcal{A}_I | do(pa(H_k^I \cup \mathcal{A}_I)), do(I)) \\ \implies P(H_k^I \cup \mathcal{A}_I | do(pa(H_k^I \cup \mathcal{A}_I)), do(I)) &= Q(H_k^I \cup \mathcal{A}_I | do(pa(H_k^I \cup \mathcal{A}_I)), do(I)) \end{aligned} \quad (19)$$

Matching the alternative distributions with D^I will imply that we match $P(\mathcal{V})$ c-factor as well. Formally:

$$\begin{aligned} Q_{pa(H_k^I)}(H_k^I) &= P_{pa(H_k^I)}(H_k^I) \\ Q_{pa(H_k^I)}(H_k^I) &= P_{pa(H_k^0)}(H_k^0) \end{aligned} \quad (20)$$

D.5.1 Matching Observational Distributions with Modular Training on $D \sim P(\mathcal{V})$

Now, we provide the theoretical proof of the correctness of Modular-DCM Modular Training matching observational distribution by training on observational dataset D^0 . Since, we have access to only observational data we remove the intervention-indicating superscript/subscript and address \mathcal{H}^0 as \mathcal{H} , ancestor set \mathcal{A}_I as \mathcal{A} and dataset D^0 as D .

Proposition D.12. *Suppose Algorithm 2: **Modular-DCM Modular Training** converges for each h-node in \mathcal{H}^0 -graph constructed from $G = (\mathcal{V}, \mathcal{E})$. Suppose the observational distribution induced by the deep causal model is $Q(\mathcal{V})$ after training on data sets $D \sim P(\mathcal{V})$. Then,*

$$P(\mathcal{V}) = Q(\mathcal{V}) \quad (21)$$

Proof Sketch. After expressing the observational distribution $P(\mathcal{V})$ as c-factorization expression, we can combine multiple c-factors located in the same h-node as $\prod_{C_i \in H_k} P_{pa(C_i)}(C_i) = P_{pa(H_k)}(H_k)$ according to

Corollary D.8. Therefore, if we can match $P_{pa(H_k)}(H_k), \forall k$, this will ensure that we have matched all c-factors $P_{pa(C_i)}(C_i), \forall i$ and as a result $P(\mathcal{V})$ as well. For the h-nodes which does not have any parents (i.e., root nodes) in the \mathcal{H} -graph, we know $P_{pa(H_k)}(H_k) = P(H_k | Pa(H_k))$ due to the construction of H-graph. Therefore, Modular-DCM trains mechanism in those h-nodes by matching $P(H_k | Pa(H_k)) = Q_{Pa(H_k)}(H_k)$.

For the h-nodes which are not root h-nodes in the \mathcal{H} -graph, we match $P_{pa(H_k)}(H_k)$ by matching an alternative distribution $P(H_k \cup \mathcal{A} | do(Pa(H_k \cup \mathcal{A})))$. This alternative distribution factorizes as $P(H_k \cup \mathcal{A} | do(Pa(H_k \cup \mathcal{A})))$.

$\mathcal{A})) = P_{pa(H_k)}(H_k) * \prod_{H_S \in \mathcal{A}} \prod_{C_j^+ \subseteq H_S} P_{Pa(C_j^+)}(C_j^+)$. Therefore, $P_{Pa(H_k)}(H_k) = \frac{P(H_k \cup \mathcal{A} | \text{do}(Pa(H_k \cup \mathcal{A})))}{\prod_{H_S \in \mathcal{A}} \prod_{C_j^+ \subseteq H_S} P_{Pa(C_j^+)}(C_j^+)}$. The

numerator is already matched as that is the alternative distribution we have matched while training h-node H_k . As we are following the topological order of the \mathcal{H} -graph, the denominator is matched while training the ancestor h-nodes of H_k . Therefore, Modular-DCM modular training matches $P_{pa(H_k)}(H_k), \forall k$ and thus $P(V) = Q(V)$. We provide the detailed proof below. \square

Proof. According to Tian's factorization we can factorize the joint distributions into c-factors as follows:

$$P(\mathcal{V}) = P(\mathcal{H}) = \prod_{H_k \in \mathcal{H}} \prod_{C_i \in H_k} P_{pa(C_i)}(C_i) \quad (22)$$

We can divide the set of c-components $\mathcal{C} = \{C_1, \dots, C_t\}$ into disjoint partitions or h-nodes as $H_k = \{C_i\}_{i \in T_k}$ for some $T_k \subseteq [t]$. Following Corollary D.8, we can combine the c-factors in each partitions and rewrite it as:

$$\prod_{H_k \in \mathcal{H}} \prod_{C_i \in H_k} P_{pa(C_i)}(C_i) = P_{pa(H_0)}(H_0) \times P_{pa(H_1)}(H_1) \times \dots \times P_{pa(H_n)}(H_n) \quad (23)$$

Now, we prove that we match each of these terms according to the training order \mathcal{T} .

For any root h-nodes $H_k \in \sigma_0$:

Due to the construction of \mathcal{H} graphs in Algorithm 6, the following is true for any root nodes, $H_k \in \sigma_0$.

$$P(H_k | Pa(H_k)) = P_{Pa(H_k)}(H_k) \quad (24)$$

Modular-DCM training convergence for the DCM in $H_k \in \sigma_0$. (Algorithm 2, line 8) ensures that the following matches:

$$\begin{aligned} P(H_k | Pa(H_k)) &= Q_{Pa(H_k)}(H_k) \\ \implies P_{Pa(H_k)}(H_k) &= Q_{Pa(H_k)}(H_k) \end{aligned} \quad (25)$$

Since, Equation 24 is true, observational data is sufficient for training the mechanisms in $H_k \in \sigma_0$. Thus, we do not need to train on interventional data.

For the h-node $H_k \in \sigma_1$:

Now we show that we can train mechanisms in H_k by matching $P(\mathcal{V})$ c-factors with $D \sim P(\mathcal{V})$ data set. Let us assume, $\exists \mathcal{A} \subseteq \sigma_0$ such that $\mathcal{A} = An(H_k)$, i.e., ancestors set of H_k in the \mathcal{H} -graph that we have already trained with available D dataset. To apply Lemma D.7 in causal graph G , consider $V' = H_k \cup \mathcal{A}$ as the focus-set, $Pa(V')$ as the action-set. Thus, active c-components: $C_j^+ := C_j \cap V'$

Then we get the following:

$$\begin{aligned} P(H_k \cup \mathcal{A} | \text{do}(Pa(H_k \cup \mathcal{A}))) &= \prod_{C_i \in H_k} P_{pa(C_i)}(C_i) \times \prod_{H_S \in \{\mathcal{A}\}} \prod_{C_j^+ \subseteq H_S} P_{Pa(C_j^+)}(C_j^+) \\ &\quad \text{[Here, 1st term is the factorization of the current h-node} \\ &\quad \text{and 2nd term is the factorization of the ancestors set.]} \end{aligned} \quad (26)$$

$$\implies P(H_k \cup \mathcal{A} | \text{do}(Pa(H_k \cup \mathcal{A}))) = P_{pa(H_k)}(H_k) * \prod_{H_S \in \mathcal{A}} \prod_{C_j^+ \subseteq H_S} P_{Pa(C_j^+)}(C_j^+)$$

Here according to Corollary D.8, we combine the c-factors $P_{pa(C_i)}(C_i)$ for c-components in H_k to form $P_{pa(H_k)}(H_k)$. We continue the derivation as follows:

$$\begin{aligned} \implies P_{Pa(H_k)}(H_k) &= \frac{P(H_k \cup \mathcal{A} | \text{do}(Pa(H_k \cup \mathcal{A})))}{\prod_{H_S \in \mathcal{A}} \prod_{C_j^+ \subseteq H_S} P_{Pa(C_j^+)}(C_j^+)} \\ \implies P_{Pa(H_k)}(H_k) &= \frac{Q(H_k \cup \mathcal{A} | \text{do}(Pa(H_k \cup \mathcal{A})))}{\prod_{H_S \in \mathcal{A}} \prod_{C_j^+ \subseteq H_S} Q_{Pa(C_j^+)}(C_j^+)} \end{aligned} \quad (27)$$

Here the R.H.S numerator follows from previous line according to Equation 19. For the denominator at R.H.S, $\forall H_S \in \mathcal{A}$, we have already matched $P(H_S \cup \mathcal{A} | \text{do}(pa(H_S \cup \mathcal{A})))$, during training of $\mathcal{A} = An(H_k)$ h-nodes. According to Lemma D.7, matching these distribution is sufficient to match the distribution at R.H.S denominator. Therefore, our DCM will produce the same distribution as well. This implies that from Equation 27 we get,

$$\begin{aligned} P_{pa(H_k)}(H_k) &= Q_{pa(H_k)}(H_k) \\ \implies P_{pa(H_k)}(H_k) &= Q_{pa(H_k)}(H_k) \quad [\text{According to Equation 17}] \end{aligned} \quad (28)$$

Similarly, we train each h-node following the training order \mathcal{T} and match the distribution in Equation 23. This finally shows that,

$$P(V) = \prod_{j \leq n} P_{pa(H_j)}(H_j) = \prod_{j \leq n} Q_{pa(H_j)}(H_j) = Q(V) \quad (29)$$

□

D.5.2 Matching Observational Distributions with Modular Training on $\mathbf{D} \sim P_I(\mathcal{V}), \forall I \in \mathcal{I}$

Now, we provide the theoretical proof of the correctness of Modular-DCM Modular Training matching observational distribution from multiple datasets $D^I, \forall I \in \mathcal{I}$.

Notations: When we consider multiple interventions $I \in \mathcal{I}$, we add I as subscript to each notation to indicate the intervention that notation correspond to. The following notations are mainly used in Proposition D.13, Proposition D.14 and Proposition D.15.

- \mathbf{D}^I : the interventional dataset collected with intervention on node I .
- $P_I(V), Q_I(V)$: the interventional joint distribution after intervening on node I representing respectively the real data and the generated data produced from the Modular-DCM DCM.
- $G_{\bar{I}}$ and \mathcal{H}^I : the causal graph and the H-graph after $\text{do}(I)$ intervention. \mathcal{H}^0 or only \mathcal{H} implies the H-graph for the original causal graph.
- H_k^I : the k -th hnode in the \mathcal{H}^I -graph.
- \mathcal{A}_I : the ancestor set in $G_{\bar{I}}$ -graph, required to construct the alternative distribution for the c-component in consideration. Thus, \mathcal{A}_\emptyset or only \mathcal{A} refers to the observational case.
- σ_0, σ_1 : the root hnodes and the non-root hnodes in the H-graph in consideration.

Proposition D.13. *Suppose Algorithm 7: **Modular-DCM Modular Training** converges for each h-node in \mathcal{H}^0 -graph constructed from $G = (\mathcal{V}, \mathcal{E})$. Suppose the observational distribution induced by the deep causal model is $Q(\mathcal{V})$ after training on data sets $\mathbf{D}^I, \forall I \in \mathcal{I}$. Then,*

$$P(\mathcal{V}) = Q(\mathcal{V}) \quad (30)$$

Proof Sketch. The proof of this Proposition follows the same route as Proposition D.12. In both cases, Modular-DCM matches the observational distribution $P(V)$. The only difference between the two setups is that Modular-DCM has access to multiple interventional datasets in this setup which enables matching observational distribution efficiently by utilizing a smaller ancestor set with the joint. An important fact is that even if we have access to $\text{do}(I), \forall I \in \mathcal{I}$ datasets and we construct multiple \mathcal{H}^I -graphs, we still follow the topological order of \mathcal{H}^0 -graph, i.e, H-graph with no intervention. This is valid according to Proposition D.14 since a topological order of \mathcal{H}^0 works for all \mathcal{H}^I -graphs even though \mathcal{H}^I are sparser. Also, any node in H_k^I contains the same set of nodes as in H_k^0 for all k .

We can consider any h-node to be either a root h-node or a non-root h-node. Since for the root h-nodes, the ancestor set is empty, we follow the same approach as the observational case and the proof of correctness follows from Proposition D.12. Now, suppose a h-node is not a root node and intervention I is not located inside it. To match the alternative distribution, instead of searching for the ancestor set in only H^0 -graph

created for observational data, Modular-DCM looks at all H^I -graphs created based on intervention I and chooses the smallest ancestor set. We assume that a smaller ancestor set will make it easy to match the corresponding alternative distribution. More precisely, instead of matching $P(H_k \cup \mathcal{A}_\emptyset | \text{do}(Pa(H_k \cup \mathcal{A}_\emptyset)))$ from observational H -graph, Modular-DCM matches $P(H_k \cup \mathcal{A}_I | \text{do}(Pa(H_k \cup \mathcal{A}_I)), \text{do}(I))$ where \mathcal{A}_I is smallest across all H^I -graphs. Since intervention I is not located inside the h-node, $P(H_k \cup \mathcal{A}_I | \text{do}(Pa(H_k \cup \mathcal{A}_I)), \text{do}(I)) = P(H_k \cup \mathcal{A}_I | Pa(H_k \cup \mathcal{A}_I), I)$, i.e, the interventional alternative distribution is same as an observational conditional distribution. Thus, we train on the interventional dataset to match $P_{pa(H_k^I)}(H_k^I)$ which is equivalent to $P_{pa(H_k^\emptyset)}(H_k^\emptyset)$ for h-nodes that contain no intervention.

Following the above approach, to match $P_{pa(H_k^\emptyset)}(H_k^\emptyset)$ for all h-nodes will eventually match $P(V)$. The rest follows the same proof as Proposition D.12. We provide the detailed proof below. \square

Proof. According to Tian's factorization we can factorize the joint distributions into c-factors as follows:

$$P(\mathcal{V}) = P(H^\emptyset) = \prod_{H_k^\emptyset \in H^\emptyset} \prod_{C_i \in H_k^\emptyset} P_{pa(C_i)}(C_i) \quad (31)$$

We can divide the set of c-components $\mathcal{C} = \{C_1, \dots, C_t\}$ into disjoint partitions or h-nodes as $H_k^\emptyset = \{C_i\}_{i \in T_k}$ for some $T_k \subseteq [t]$. Following Corollary D.8, we can combine the c-factors in each partitions and rewrite it as:

$$\prod_{H_k^\emptyset \in H^\emptyset} \prod_{C_i \in H_k^\emptyset} P_{pa(C_i)}(C_i) = P_{pa(H_0^\emptyset)}(H_0^\emptyset) \times P_{pa(H_1^\emptyset)}(H_1^\emptyset) \times \dots \times P_{pa(H_n^\emptyset)}(H_n^\emptyset) \quad (32)$$

Now, we prove that we match each of these terms according to the training order \mathcal{T} .

For any root h-nodes $H_k^\emptyset \in \sigma_0$:

Due to the construction of \mathcal{H}^\emptyset graphs in Algorithm 6, the following is true for any root nodes, $H_k^\emptyset \in \sigma_0$.

$$P(H_k^\emptyset | Pa(H_k^\emptyset)) = P_{Pa(H_k^\emptyset)}(H_k^\emptyset) \quad (33)$$

Modular-DCM training convergence for the DCM in $H_k^\emptyset \in \sigma_0$. (Algorithm 7, line 14) ensures that the following matches:

$$\begin{aligned} P(H_k^\emptyset | Pa(H_k^\emptyset)) &= Q_{Pa(H_k^\emptyset)}(H_k^\emptyset) \\ \implies P_{Pa(H_k^\emptyset)}(H_k^\emptyset) &= Q_{Pa(H_k^\emptyset)}(H_k^\emptyset) \end{aligned} \quad (34)$$

Since, Equation 33 is true, observational data is sufficient for training the mechanisms in $H_k^\emptyset \in \sigma_0$. Thus, we do not need to train on interventional data.

For the h-node $H_k^\emptyset \in \sigma_1$:

Now we show that we can train mechanisms in H_k^\emptyset by matching $P(\mathcal{V})$ c-factors with either \mathcal{L}_1 or \mathcal{L}_2 datasets. Let us assume, $\exists \mathcal{A}_I \subseteq \sigma_0$ such that $\mathcal{A}_I = An_{G_{\overline{\mathcal{T}}}}(H_k^I)$, i.e., ancestors set of H_k^I in the \mathcal{H}^I -graph that we have already trained with available D^I dataset. To apply Lemma D.7 in $G_{\overline{\mathcal{T}}}$ with $|I| \geq 0$, consider $V' = H_k^I \cup \mathcal{A}_I$ as the focus-set, $\{Pa(V') \cup I\}$ as the action-set. Thus, active c-components: $C_j^+ := C_j \cap V'$

Then we get the following:

$$\begin{aligned} P(H_k^I \cup \mathcal{A}_I | \text{do}(Pa(H_k^I \cup \mathcal{A}_I)), \text{do}(I)) &= \prod_{C_i \in H_k^I} P_{pa(C_i)}(C_i) \times \prod_{H_S^I \in \{\mathcal{A}_I\}} \prod_{C_j^+ \subseteq H_S^I} P_{Pa(C_j^+) \cup I}(C_j^+) \\ &\quad \text{[Here, 1st term is the factorization of the current h-node} \\ &\quad \text{and 2nd term is the factorization of the ancestors set.]} \quad (35) \\ \implies P(H_k^I \cup \mathcal{A}_I | \text{do}(Pa(H_k^I \cup \mathcal{A}_I)), \text{do}(I)) &= P_{pa(H_k^I)}(H_k^I) * \prod_{H_S^I \in \mathcal{A}_I} \prod_{C_j^+ \subseteq H_S^I} P_{Pa(C_j^+) \cup I}(C_j^+) \end{aligned}$$

Here according to Corollary D.8, we combine the c-factors $P_{pa(C_i)}(C_i)$ for c-components in H_k^I to form $P_{pa(H_k^I)}(H_k^I)$. We continue the derivation as follows:

$$\begin{aligned} \implies P_{Pa(H_k^I)}(H_k^I) &= \frac{P(H_k^I \cup \mathcal{A}_I | \text{do}(Pa(H_k^I \cup \mathcal{A}_I)), \text{do}(I))}{\prod_{H_S^I \in \mathcal{A}_I} \prod_{C_j^+ \subseteq H_S^I} P_{Pa(C_j^+) \cup I}(C_j^+)} \\ \implies P_{Pa(H_k^I)}(H_k^I) &= \frac{Q(H_k^I \cup \mathcal{A}_I | \text{do}(Pa(H_k^I \cup \mathcal{A}_I)), \text{do}(I))}{\prod_{H_S^I \in \mathcal{A}_I} \prod_{C_j^+ \subseteq H_S^I} Q_{Pa(C_j^+) \cup I}(C_j^+)} \end{aligned} \quad (36)$$

Here the R.H.S numerator follows from previous line according to Equation 19. For the denominator at R.H.S, the intervention is an ancestor of the current hnode, i.e., $I \in \{An(H_k^I) \setminus H_k^I\}$. Now, $\forall H_S^I \in \mathcal{A}_I$, we have already matched $P(H_S^I \cup \mathcal{A}_I | \text{do}(pa(H_S^I \cup \mathcal{A}_I)), \text{do}(I))$, during training of $\mathcal{A}_I = An(H_k^I)$ h-nodes. According to Lemma D.7, matching these distribution is sufficient to match the distribution at R.H.S denominator. Therefore, our DCM will produce the same distribution as well. This implies that from Equation 36 we get,

$$\begin{aligned} P_{pa(H_k^I)}(H_k^I) &= Q_{pa(H_k^I)}(H_k^I) \\ \implies P_{pa(H_k^0)}(H_k^0) &= Q_{pa(H_k^0)}(H_k^0) \quad [\text{According to Equation 17}] \end{aligned} \quad (37)$$

Similarly, we train each h-node following the training order \mathcal{T} and match the distribution in Equation 32. This finally shows that,

$$P(V) = \prod_{j \leq n} P_{pa(H_j^0)}(H_j^0) = \prod_{j \leq n} Q_{pa(H_j^0)}(H_j^0) = Q(V) \quad (38)$$

□

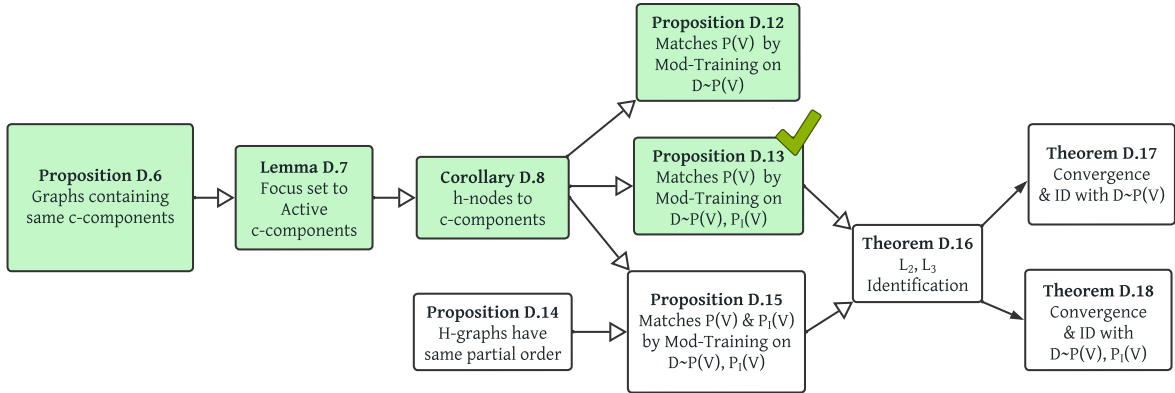


Figure 15: Flowchart of proofs

D.5.3 Matching Interventional Distributions with Modular Training on $D \sim P_I(V), \forall I \in \mathcal{I}$

Before showing our algorithm correctness with both observational and interventional data, we first discuss the DAG property of \mathcal{H} -graphs. Please check the **notations** in the previous section defined for multiple interventions.

Proposition D.14. *Any \mathcal{H} -graph constructed according to Definition D.2 is a directed acyclic graph (DAG) and a common partial order \mathcal{T} , exists for all \mathcal{H}^I -graphs, $\forall I \in \mathcal{I}$.*

Proof. We construct the \mathcal{H} -graphs following Algorithm 6. By checking the modularity condition we add edges between any two h-nodes. However, if we find a cycle $H_j^I, H_k^I \rightarrow \dots \rightarrow H_j^I$, then we combine all h-nodes in the cycle and form a new h-node in \mathcal{H}^I . This new h-node contains the union of all outgoing edges to other h-nodes. Therefore, at the end of the algorithm, the final \mathcal{H} -graph, \mathcal{H}^I will always be a directed acyclic graph. Note that one can always choose a partition of the c-components \mathcal{C} to ensure \mathcal{H}^I is acyclic: The \mathcal{H}^I graph with a single node $H_1^I = \mathcal{C}$.

Next in Algorithm 7, training is performed according to the partial order of \mathcal{H}^\emptyset which corresponds to the original graph G without any intervention. This is the most dense \mathcal{H} -graph and thus imposes the most restrictions in terms of the training order. Let I be an intervention set. For any intervention I , suppose \mathcal{H}^I -graph is obtained from $G_{\bar{I}}$ and I is located in H_k^\emptyset h-node of \mathcal{H}^\emptyset -graph obtained from G . The only difference between \mathcal{H}^\emptyset and \mathcal{H}^I is that the h-node H_k^\emptyset might be split into multiple new h-nodes in \mathcal{H}^I and some edges with other h-nodes that were present in \mathcal{H}^\emptyset , might be removed in \mathcal{H}^I .

However, according to Algorithm 7, we do not split these new h-nodes rather bind them together to form H_k^I that contain the same nodes as H_k^\emptyset . Therefore, no new edge is being added among other h-nodes. This implies that the partial order of \mathcal{H}^\emptyset is also valid for \mathcal{H}^I . After intervention no new edges are added to the constructed \mathcal{H} -graphs, thus we can safely claim that,

$$An_{G_{\bar{I}}}(H_k^I) \subseteq An_G(H_k^\emptyset), \forall I \in \mathcal{I} \quad (39)$$

Since all \mathcal{H} -graphs are DAGs and the above condition holds, any valid partial order for \mathcal{H}^\emptyset is also a valid partial order for all $\mathcal{H}^I, \forall I \in \mathcal{I}$, i.e., they have a common valid partial order. \square

In general, for $I \in H_k^I$, i.e., when the intervention is inside H_k^I , we utilize interventional datasets and search for minimum size variable set $\mathcal{A}_I \subseteq An_{G_{\bar{I}}}(H_k^I)$ in $G_{\bar{I}}$ such that do-calculus rule-2 satisfies,

$$P(H_k^I \cup \mathcal{A}_I | pa(H_k^I \cup \mathcal{A}_I), do(I)) = P(H_k^I \cup \mathcal{A}_I | do(pa(H_k^I \cup \mathcal{A}_I)), do(I)) \quad (40)$$

Then we can train the mechanisms in H_k^I to match the following distribution,

$$\begin{aligned} P(H_k^I \cup \mathcal{A}_I | pa(H_k^I \cup \mathcal{A}_I), do(I)) &= Q(H_k^I \cup \mathcal{A}_I | do(pa(H_k^I \cup \mathcal{A}_I)), do(I)) \\ \implies P(H_k^I \cup \mathcal{A}_I | do(pa(H_k^I \cup \mathcal{A}_I)), do(I)) &= Q(H_k^I \cup \mathcal{A}_I | do(pa(H_k^I \cup \mathcal{A}_I)), do(I)) \end{aligned} \quad (41)$$

Proposition D.15. *Suppose Algorithm 7: **Modular-DCM Modular Training** converges for each h-node in \mathcal{H}^\emptyset -graph constructed from $G = (\mathcal{V}, \mathcal{E})$. Suppose the interventional distribution induced by the deep causal model is $Q_I(V)$ after training on data sets $\mathbf{D}^I, \forall I \in \mathcal{I}$. then,*

$$P_I(V) = Q_I(V) \quad (42)$$

Proof Sketch. The proof of this Proposition follows the same route as Proposition D.12. However, we have now access to both observational and interventional datasets and Modular-DCM is trained on all these datasets modularly to match every interventional joint distribution. An important fact is that even if we have access to $do(I), \forall I \in \mathcal{I}$ datasets and we construct multiple \mathcal{H}^I -graphs, we still follow the topological order of \mathcal{H}^\emptyset -graph, i.e, H-graph with no intervention. This is valid according to Proposition D.14 since a topological order of \mathcal{H}^\emptyset works for all \mathcal{H}^I -graphs even though \mathcal{H}^I are sparser. Also, any node in H_k^I contains the same set of nodes as in H_k^\emptyset for all k .

Tian's factorization allows us to express the interventional joint distribution $P_I(V)$ in terms of multiple c-factors. We divide the c-components corresponding to these c-factors into two sets. Set-1: the c-component containing the intervention and the c-components in the same h-node. Set-2: the rest of the c-components without any intervention. We combine the c-factors in both sets as H_k^I and $H_{k'}^I \in \{\mathcal{H}^I \setminus H_k^I\}$. Therefore, according to Corollary D.8, $P_I(V)$ can be written as: $P_{pa(C_i) \cup I}(C_i) \times \prod_{H_k^I \in \mathcal{H}^I} \prod_{C_{i'} \in H_k^I} P_{pa(C_{i'})}(C_{i'}) =$

$P_{pa(H_k^I) \cup I}(H_k^I) \times \prod_{H_{k'}^I \in \{\mathcal{H}^I \setminus H_k^I\}} P_{pa(H_{k'}^I)}(H_{k'}^I)$. During the modular training with interventional datasets,

Modular-DCM matches each of these c-factors and thus matches the interventional joint distribution.

We can consider any h-node H_k^I as $H_k^I \in \sigma_0$, i.e., to be either a root h-node of \mathcal{H}^I or $H_k^I \in \sigma_1$ i.e., to be a non-root h-node of \mathcal{H}^I . For both of these cases, we follow the same approach as the observational case except the fact that we consider h-nodes in the \mathcal{H}^I graph (but the same topological order as \mathcal{H}^0), the ancestor set \mathcal{A}_I in $G_{\bar{I}}$ and the $\text{do}(I)$ dataset while matching the interventional distribution for h-nodes. Now, for $H_k^I \in \sigma_0$, by the construction of the \mathcal{H}^I graph, we can say $P(H_k^I | Pa(H_k^I), \text{do}(I)) = P_{Pa(H_k^I) \cup I}(H_k^I)$. Thus, we match $P_{Pa(H_k^I) \cup I}(H_k^I)$ by training the DCM mechanisms in H_k^I by matching $P(H_k^I | Pa(H_k^I), \text{do}(I)) = Q_{Pa(H_k^I) \cup I}(H_k^I)$.

For h-nodes $H_k^I \in \sigma_1$, we perform modular training to train these mechanisms by matching an alternative interventional joint distribution $P(H_k^I \cup \mathcal{A}_I | \text{do}(Pa(H_k^I \cup \mathcal{A}_I)), \text{do}(I))$ with the $\text{do}(I)$ interventional data. This alternative distribution can be expressed as: $P_{Pa(H_k^I) \cup I}(H_k^I) \times \prod_{H_S^I \in \mathcal{A}_I} \prod_{C_{i'}^+ \in H_S^I} P_{Pa(C_{i'}^+)}(C_{i'}^+)$. Here the first term

correspond to the distribution involving the current h-node H_k^I we are training. The second term corresponds to the partial c-factors located in the ancestors \mathcal{A}_I . They are partial C_i^+ because \mathcal{A}_I are ancestors of H_k^I in $G_{\bar{I}}$ satisfying the modularity condition D.1 and not necessarily containing the full c-component C_i . We can equivalently write: $P_{Pa(H_k^I) \cup I}(H_k^I) = \frac{P(H_k^I \cup \mathcal{A}_I | \text{do}(Pa(H_k^I \cup \mathcal{A}_I)), \text{do}(I))}{\prod_{H_S^I \in \mathcal{A}_I} \prod_{C_j^+ \subseteq H_S^I} P_{Pa(C_j^+)}(C_j^+)}$. We match the numerator at the

current training step. Since we follow the topological order of the H-graph, the denominator distributions are matched while training the ancestor h-nodes mechanisms in \mathcal{H}^I . Therefore, Modular-DCM DCM can match the interventional distribution $P_{Pa(H_k^I) \cup I}(H_k^I)$. More precisely, $Q_{Pa(H_k^I) \cup I}(H_k^I) = P_{Pa(H_k^I) \cup I}(H_k^I)$.

Modular-DCM follows the topological order of \mathcal{H}^0 and trains all mechanisms in any H_k^0 . While training the k -th h-node, Modular-DCM enforces the mechanisms in the h-node to learn all interventional distribution $P_{Pa(H_k^I) \cup I}(H_k^I), \forall I \in \mathcal{I}$. Therefore, after training the last node in the topological order, Modular-DCM modular training matches the joint interventional distribution $P_I(V)$. We provide the detailed proof below. \square

Proof. Suppose, intervention I belongs to a specific c-component C_i , i.e., $I \in C_i$. According to Tian's factorization, we can factorize the $\text{do}(I)$ interventional joint distributions for $G_{\bar{I}}$ causal graph, into c-factors as follows:

$$P_I(V) = P_I(\mathcal{H}^I) = P_{pa(C_i) \cup I}(C_i) \times \prod_{H_k^I \in \mathcal{H}^I} \prod_{C_{i'} \in H_k^I} P_{pa(C_{i'})}(C_{i'}) \quad (43)$$

The difference between the c-factorization for $P(V)$ and $P_I(V)$ is that when intervention I is located inside c-component C_i , we have $P_{pa(C_i) \cup I}(C_i)$ instead of $P_{pa(C_i)}(C_i)$. We can divide c-components $\mathcal{C} = \{C_1, \dots, C_t\}$ into disjoint partitions or h-nodes as $H_k^0 = \{C_i\}_{i \in T_k}$ for some $T_k \subseteq [t]$.

Let, the c-component C_i that contains intervention I belong to hnode H_k^I , i.e., $C_i \in H_k^I$. Following Corollary D.8, we can combine the c-factors in each partitions and rewrite R.H.S of Equation 43 as:

$$P_{pa(C_i) \cup I}(C_i) \times \prod_{H_k^I \in \mathcal{H}^I} \prod_{C_{i'} \in H_k^I} P_{pa(C_{i'})}(C_{i'}) = P_{pa(H_k^I) \cup I}(H_k^I) \times \prod_{H_{k'}^I \in \{\mathcal{H}^I \setminus H_k^I\}} P_{pa(H_{k'}^I)}(H_{k'}^I) \quad (44)$$

Now, we prove that we match each of these terms in Equation 44 according to the training order \mathcal{T} .

For any root h-nodes $H_k^I \in \sigma_0$:

Due to the construction of \mathcal{H}^I graphs in Algorithm 6, the following is true for any root nodes, $H_k^I \in \sigma_0$.

$$P_I(H_k^I | Pa(H_k^I)) = P_{Pa(H_k^I) \cup I}(H_k^I) \quad (45)$$

Modular-DCM training convergence for the mechanisms in $H_k^I \in \sigma_0$. Algorithm 7, line 14 ensures that the following matches:

$$\begin{aligned} P_I(H_k^I | Pa(H_k^I)) &= Q_{Pa(H_k^I) \cup I}(H_k^I) \\ \implies P_{Pa(H_k^I) \cup I}(H_k^I) &= Q_{Pa(H_k^I) \cup I}(H_k^I) \end{aligned} \quad (46)$$

For the h-node $H_k^I \in \sigma_1$ with $I \in H_k^I$:

Now we show that we can train mechanisms in H_k^I by matching $P_I(V)$ c-factors with \mathcal{L}_1 and \mathcal{L}_2 datasets. Let

us assume, $\exists \mathcal{A}_I \subseteq \sigma_0$ such that $\mathcal{A}_I = An_{G_{\mathcal{T}}}(H_k^I)$, i.e., ancestors of H_k^I in the \mathcal{H}^I -graph that we have already trained with available D^I dataset, $\forall I \in \mathcal{I}$.

To apply Lemma D.7 in $G_{\mathcal{T}}$ with $|I| \geq 0$, consider $V' = H_k^I \cup \mathcal{A}_I$ as the focus-set, $\{Pa(V') \cup I\}$ as the action-set. Thus, active c-components: $C_j^+ := C_j \cap V'$. We apply the lemma as below:

$$P(H_k^I \cup \mathcal{A}_I | do(Pa(H_k^I \cup \mathcal{A}_I)), do(I)) = \prod_{C_i \in H_k^I} P_{pa(C_i) \cup I}(C_i) \times \prod_{H_S^I \in \mathcal{A}_I} \prod_{C_{i'}^+ \in H_S^I} P_{Pa(C_{i'}^+)}(C_{i'}^+) \quad (47)$$

Here, the 1st term is the factorization of the current h-node and the 2nd term is the factorization of the ancestors set. The intervened variable I is located in the current h-node H_k^I . Therefore, the factorized c-components, i.e., $C_i \in H_k^I$ has I as intervention along with their parent intervention. The above equation implies:

$$P(H_k^I \cup \mathcal{A}_I | do(Pa(H_k^I \cup \mathcal{A}_I)), do(I)) = P_{pa(H_k^I) \cup I}(H_k^I) \times \prod_{H_S^I \in \mathcal{A}_I} \prod_{C_{i'}^+ \in H_S^I} P_{Pa(C_{i'}^+)}(C_{i'}^+) \quad (48)$$

According to Corollary D.8, we combine the c-factors $P_{pa(C_i) \cup I}(C_i)$ for c-components in H_k^I to form $P_{pa(H_k^I) \cup I}(H_k^I)$. We continue the derivation as follows:

$$\begin{aligned} \implies P_{pa(H_k^I) \cup I}(H_k^I) &= \frac{P(H_k^I \cup \mathcal{A}_I | do(Pa(H_k^I \cup \mathcal{A}_I)), do(I))}{\prod_{H_S^I \in \mathcal{A}_I} \prod_{C_j^+ \subseteq H_S^I} P_{Pa(C_j^+)}(C_j^+)} \\ \implies P_{pa(H_k^I) \cup I}(H_k^I) &= \frac{Q(H_k^I \cup \mathcal{A}_I | do(Pa(H_k^I \cup \mathcal{A}_I)), do(I))}{\prod_{H_S^I \in \mathcal{A}_I} \prod_{C_j^+ \subseteq H_S^I} Q_{Pa(C_j^+)}(C_j^+)} \end{aligned} \quad (49)$$

Here the R.H.S numerator follows from previous line according to Equation 41 since training has converged for the current h-node. For the R.H.S, denominator, $\forall H_S^I \in \mathcal{A}_I$ appear before H_k^I in the partial order. When we trained h-nodes $H_S^I \in \mathcal{A}_I$ on $P(\mathcal{V})$ and $P_I(\mathcal{V})$ datasets, we matched the joint distribution $P(H_S^I \cup \mathcal{A}_I | do(pa(H_S^I \cup \mathcal{A}_I)), do(I))$, $\forall H_S^I \in \mathcal{A}_I$. According to Lemma D.7, matching these distribution is sufficient to match the distribution at the R.H.S denominator. Therefore, our DCM will produce the same distribution as well. This implies that from Equation 49 we get,

$$P_{pa(H_k^I) \cup I}(H_k^I) = Q_{pa(H_k^I) \cup I}(H_k^I) \quad (50)$$

Similarly, we train each h-node following the training order \mathcal{T} and match the distribution in Equation 44. We train the c-factor that contains interventions with our available interventional dataset and the c-factors that do not include any interventions can be trained with $P(V)$ dataset. This finally shows that,

$$\begin{aligned} P_I(V) &= P_{pa(H_k^I) \cup I}(H_k^I) \times \prod_{H_{k'}^I \in \{H^I \setminus H_k^I\}} P_{pa(H_{k'}^I)}(H_{k'}^I) \\ &= Q_{pa(H_k^I) \cup I}(H_k^I) \times \prod_{H_{k'}^I \in \{H^I \setminus H_k^I\}} Q_{pa(H_{k'}^I)}(H_{k'}^I) \\ &= Q_I(V) \end{aligned} \quad (51)$$

□

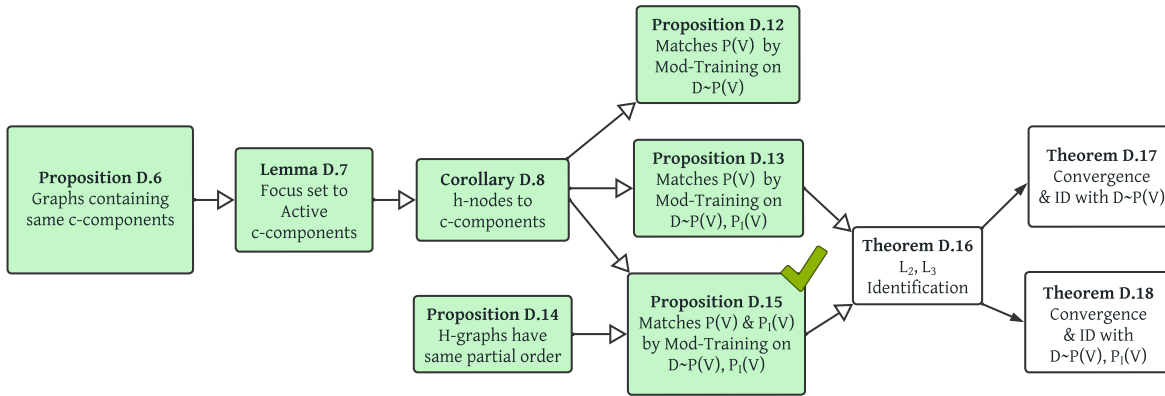


Figure 16: Flowchart of proofs

D.6 Identifiability of Algorithm 7: Modular-DCM Modular Training

Theorem D.16. *Let \mathcal{M}_1 be the true SCM and Algorithm 7: **Modular-DCM Modular Training** converge for each h-node in \mathcal{H} constructed from $G = (\mathcal{V}, \mathcal{E})$ after training on data sets $\mathbf{D} = \{\mathcal{D}^I\}_{I \in \mathcal{I}}$ and output the DCM \mathcal{M}_2 . Then for any $\mathcal{L}_2, \mathcal{L}_3$ causal query $\mathcal{K}_{\mathcal{M}_1}(\mathcal{V})$, identifiable from \mathbf{D} , $\mathcal{K}_{\mathcal{M}_1}(\mathcal{V}) = \mathcal{K}_{\mathcal{M}_2}(\mathcal{V})$ holds.*

Proof. Let $\mathcal{M}_1 = (G = (\mathcal{V}, \mathcal{E}), \mathcal{N}, \mathcal{U}, \mathcal{F}, P(\cdot))$ be the true SCM and $\mathcal{M}_2 = (G, \mathcal{N}', \mathcal{U}', \mathcal{F}', Q(\cdot))$ be the deep causal generative model represented by Modular-DCM. For any $H_k^I \in \mathcal{H}^I, I \in \mathcal{I}$, we observe the joint distribution $P(H_k^I \cup \mathcal{A}^I \cup Pa(H_k^I \cup \mathcal{A}^I), do(I))$ in the input D^I datasets. Thus we can train all the mechanisms in the current h-node H_k^I by matching the following distribution from the partially observable datasets:

$$P(H_k^I \cup \mathcal{A}_I | pa(H_k^I \cup \mathcal{A}_I), do(I)) = Q(H_k^I \cup \mathcal{A}_I | do(pa(H_k^I \cup \mathcal{A}_I)), do(I)) \quad (52)$$

Now, as we are following a valid partial order of the \mathcal{H}^0 -graph to train the h-nodes, we train the mechanisms of each h-node to match the input distribution only once and do not update it again anytime during the training of rest of the network. As we move to the next h-node of the partial order for training, we can keep the weights of the Ancestor h-nodes fixed and only train the current one and can successfully match the joint distribution in Equation 52. In the same manner, we would be able to match the distributions for each h-node and reach convergence for each of them. Modular-DCM Training convergence implies that $Q_I(\mathcal{V}) = P_I(\mathcal{V}), \forall I \in \mathcal{I}$ i.e., for all input dataset distributions. Therefore, according to Theorem C.3, Modular-DCM is capable of producing samples from correct interventional or counterfactual distributions that are identifiable from the input distributions. \square

Theorem D.17. *Suppose Algorithm 2: **Modular-DCM Modular Training** converges for each h-node in the \mathcal{H} -graph constructed from $G = (\mathcal{V}, \mathcal{E})$ and after training on observational dataset $D \sim P(\mathcal{V})$, the observational distribution induced by the DCM is $Q(\mathcal{V})$. Then, we have i) $P(\mathcal{V}) = Q(\mathcal{V})$, and ii) for any \mathcal{L}_2 or \mathcal{L}_3 causal query $\mathcal{K}_{\mathcal{M}_1}(\mathcal{V})$ that is identifiable from \mathbf{D} , we have $\mathcal{K}_{\mathcal{M}_1}(\mathcal{V}) = \mathcal{K}_{\mathcal{M}_2}(\mathcal{V})$*

Proof. Theorem 4.5 is restated here. The first part of the theorem is proved in Proposition D.12. The second part can be proved with Theorem D.16. \square

Theorem D.18. *Suppose Algorithm 7: **Modular-DCM Modular Training** converges for each h-node in the \mathcal{H}^0 -graph constructed from $G = (\mathcal{V}, \mathcal{E})$ and after training on observational and interventional datasets $\mathbf{D}^I \sim P_I(\mathcal{V}) \forall I \in \mathcal{I}$, the distribution induced by the DCM is $Q_I(\mathcal{V}), \forall I \in \mathcal{I}$. Then, we have i) $P_I(\mathcal{V}) = Q_I(\mathcal{V})$, and ii) for any \mathcal{L}_2 or \mathcal{L}_3 causal query $\mathcal{K}_{\mathcal{M}_1}(\mathcal{V})$ that is identifiable from $\mathbf{D}^I, \forall I \in \mathcal{I}$, we have $\mathcal{K}_{\mathcal{M}_1}(\mathcal{V}) = \mathcal{K}_{\mathcal{M}_2}(\mathcal{V})$*

Proof. The first part of the theorem is proved in Proposition D.13 and Proposition D.15. Then it is a direct implication of Theorem D.16, This theorem is equivalent to Theorem 4.5 if we consider $\mathcal{I} = \{\emptyset\}$. \square

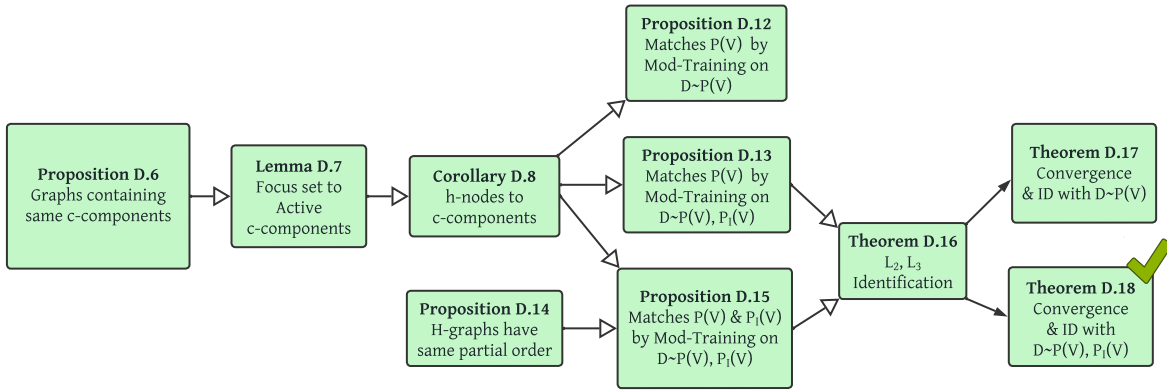


Figure 17: Flowchart of proofs

E Modular Training on Different Graphs

E.1 Modular Training Example 1

We provide an example in Figure 18 to better understand our modular algorithm.

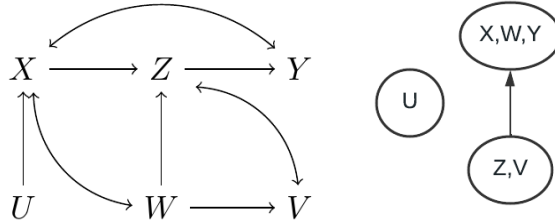


Figure 18: Example graphs for mechanism training

- Train the mechanism of U using $\mathcal{D}_0 \sim p(U)$
- Leverage the fact that $P(z, v | \text{do}(x, w)) = p(z, v | x, w)$ to train the networks of Z, V by intervening on X, W and minimize the loss $\mathcal{L}((Z_{x,w}^F, V_{x,w}^F) || (Z_{x,w}^R, V_{x,w}^R))$
- Consider that $p(x, y, w, z | \text{do}(u)) = p(x, y, w, z | u)$ and that the mechanism of Z was previously trained or we have access to pre-trained network Z . Leverage this fact to train the networks of X, Y, W by intervening on U to minimize the loss $\mathcal{L}((X_u^F, Z_u^F, Y_u^F, W_u^F) || (X_u^R, Z_u^R, Y_u^R, W_u^R))$

E.2 Modular Training Example 2

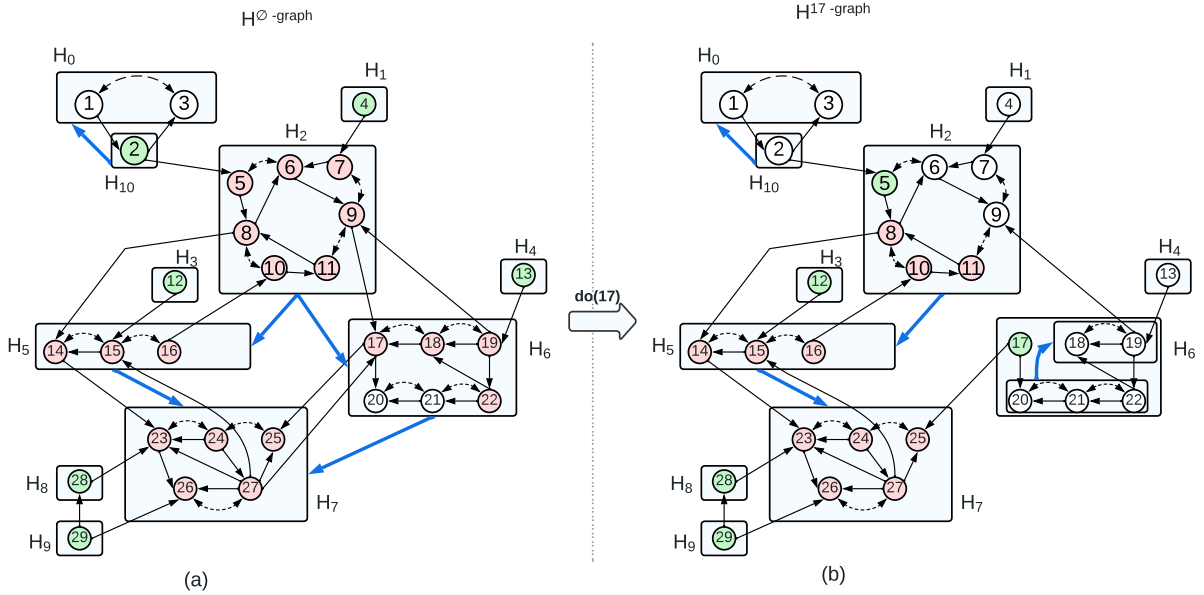


Figure 19: \mathcal{H}^0 -graph and H^{17} -graph construction

In Figure 19, we construct the \mathcal{H}^0 -graph as below. We describe the H-graph edges (thick blue edges) and the backdoor path (thin black edges) responsible for those edges.

$$\begin{aligned}
 H_{10} &\rightarrow H_0 : 3 \leftarrow 2 \leftarrow 1 \\
 H_2 &\rightarrow H_5 : 14 \leftarrow 8 \leftarrow 11 \leftarrow 10 \leftarrow 16, \\
 H_2 &\rightarrow H_6 : 17 \leftarrow 9 \leftarrow 19, \\
 H_5 &\rightarrow H_7 : 23 \leftarrow 14 \leftarrow 15 \leftarrow 27, \\
 H_6 &\rightarrow H_7 : 25 \leftarrow 17 \leftarrow 27
 \end{aligned}$$

In Figure 19, we construct the H^{17} -graph as below:

$$\begin{aligned}
 H_{10} &\rightarrow H_0 : 3 \leftarrow 2 \leftarrow 1 \\
 H_2 &\rightarrow H_5 : 14 \leftarrow 8 \leftarrow 11 \leftarrow 10 \leftarrow 16, \\
 H_5 &\rightarrow H_7 : 23 \leftarrow 14 \leftarrow 15 \leftarrow 27,
 \end{aligned}$$

Now, notice that due to $do(17)$, H_6^{17} gets splitted into two new h-nodes, $[18, 19]$ and $[20, 21, 22]$ with a new edge $[20, 21, 22] \rightarrow [18, 19]$. However, according to our H-graph construction algorithm, we keep these two new h-nodes of H^{17} combined inside H_6^{17} same as \mathcal{H}^0 -graph. Therefore, \mathcal{H}^0 and H^{17} 's common partial order does not change.

For training H_7^0 node: $\{23, 24, 25, 26, 27\}$, we match the following distribution found by applying do-calculus rule 2.

$$P(23, 24, 25, 26, 27, 14, 15, 16, 17, 18, 19, 22, 5, 6, 7, 8, 9, 10, 11, |do(2, 12, 13, 28, 29, 4)) \quad (53)$$

In Figure 19(a), joints are shown as red nodes and their parents as green nodes. However, consider, we have both observational and interventional datasets from $P(\mathcal{V})$ and $P(\mathcal{V}|do(17))$ and we have already trained all the ancestor h-nodes of H_7^{17} . Then we can train the mechanisms that lie in H_7^0 to learn both observational and interventional distribution by matching a smaller joint distribution compared to Equation 53:

$$P(23, 24, 25, 26, 27, 8, 10, 11, 14, 15, 16|do(12, 28, 29, 5, 17)) \quad (54)$$

In Figure 19(b), joints are shown as red nodes and their parents as green nodes. We see that the number of red nodes is less for H^{17} graph compared to \mathcal{H}^0 graph when we were matching the mechanisms in h-node, H_7^0 .

F Experimental Analysis

In this section, we provide implementation details and algorithm procedures of our Modular-DCM training.

F.1 Training Details and Compute

We performed our experiments on a machine with an RTX-3090 GPU. The experiments took 1-4 hours to complete. We ran each experiment for 300 epochs. We repeated each experiment multiple times to observe the consistent behavior. Our datasets contained 20 – 40K samples, and the batch_size was 200, and we used the ADAM optimizer. For evaluation, we generated 20k fake samples after a few epochs and calculated the target distributions from these 20k fake samples and 20k real samples. We calculated TVD and KL distance between the real and the learned distributions. For Wassertein GAN with gradient penalty, we used LAMBDA_GP=10. We had learning_rate = $5 * 1e - 4$. We used Gumbel-softmax with a temperature starting from 1 and decreasing it until 0.1. We used different architectures for different experiments since each experiment dealt with different data types: low-dimensional discrete variables and images. Details are provided in the code. For low-dimensional variables, we used two layers with 256 units per layer and with BatchNorm and ReLU between each layer. Please check our code for architectures of other neural networks such as encoders and image generators

F.2 Image Mediator Experiment

In this section, we provide additional information about the experiment described in Section 5.2. The front-door graph has been instrumental for a long time in the causal inference literature. However, it was not shown before that modular training with high dimensional data was possible, even in the front door graph. This is why we demonstrate the utility of our work on this graph.

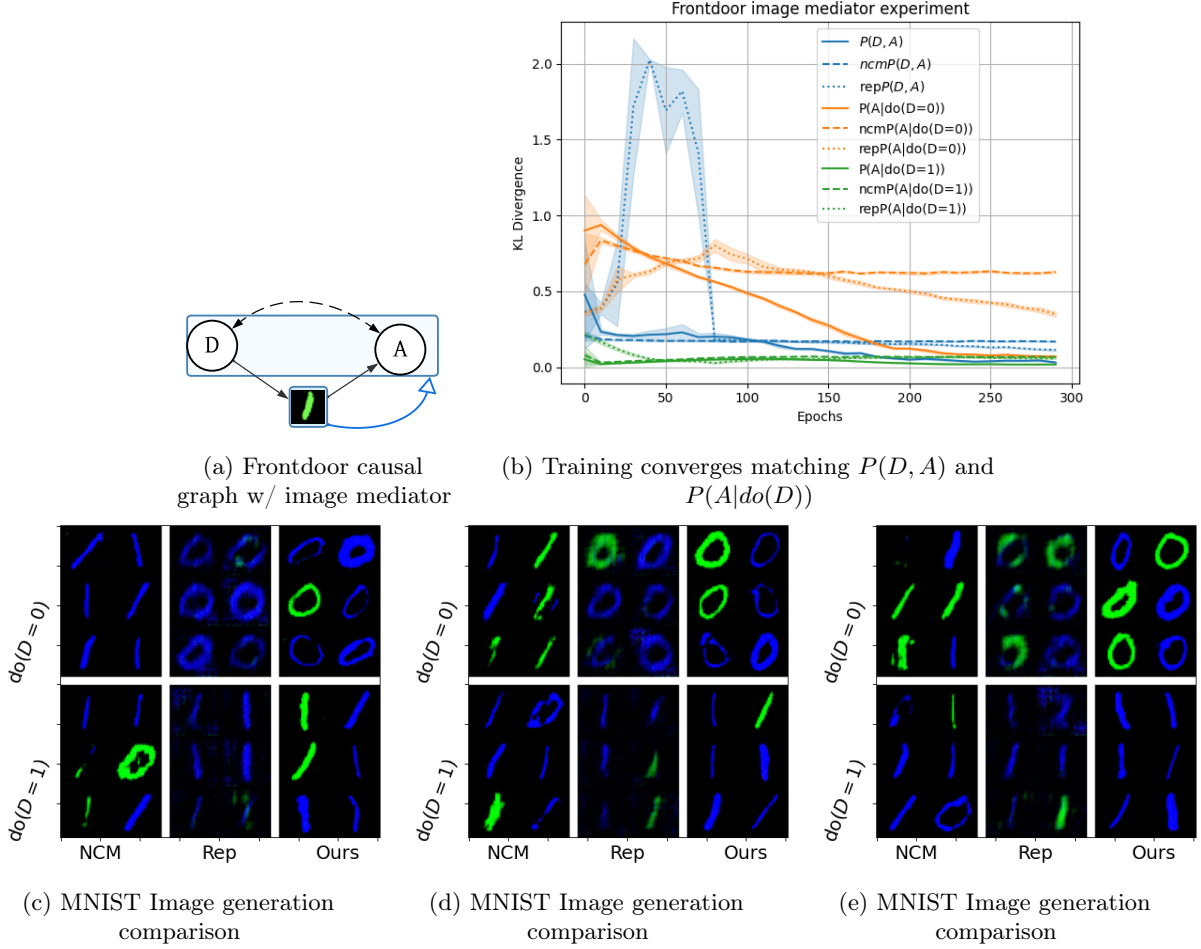


Figure 20: Modular Training on frontdoor causal graph with training order: $\{I\} \rightarrow \{D, A\}$

We have domain $D = [0, 1]$, Image size= $3 \times 32 \times 32$ and $C = [0, 1, 2]$. Let U_0, e_1, e_2, e_3 are randomly generate exogenous noise. $D = U_0 + e_1, Image = f_2(D, e_2), A = f_3(Image, e_3, U_0)$. f_2 is a function which takes D and e_2 as input and produces different colored images showing D digit in it. f_3 is a classifier with random weights that takes U_0, e_3 and $Image$ as input and produces A such a way that $|P(A|do(D = 0)) - P(A|D = 0)|, |P(A|do(D = 1)) - P(A|do(D = 0))|$ and $|P(A|D = 1) - P(A|D = 0)|$ is enough distant. The target is to make sure that the backdoor edge $D \leftrightarrow A$ and the causal path from D to A is active. Since we have access to U_0 as part of the ground truth, we can calculate the true value of $P(A|do(D))$ with the backdoor criterion:

$$P(A|do(D)) = \int_{U_0} P(A|D, U_0)P(D|U_0)$$

During training, U_0 is unobserved but still, the query is identifiable with the front door criterion. Image is a mediator here.

$$P(A|do(D)) = \int_{Image} P(Image|D) \sum_{D'} P(A|D', Image)P(D')$$

However, this inference is not possible with the identification algorithm. But Modular-DCM can achieve that by producing Image samples instead of learning the explicit distribution. If we can train all mechanisms in the Modular-DCM DCM to match $P(D, A, I)$, we can produce correct samples from $P(A|do(D))$. We construct the Modular-DCM architecture with a neural network \mathbb{G}_D having fully connected layers to produce D , a deep convolution GAN \mathbb{G}_I to generate images, and a classifier \mathbb{G}_A to classify MNIST images into variable

A such that D and A are confounded. Now, for this graph, the corresponding \mathcal{H} -graph is $[I] \rightarrow [D, A]$. Thus, we first train \mathbb{G}_I by matching $P(I|D)$. Next, to train \mathbb{G}_D and \mathbb{G}_A , we should match the joint distribution $P(D, A, I)$ since $\{I\}$ is ancestor set \mathcal{A} for c -component $\{D, A\}$. GAN convergence becomes difficult using the joint distribution loss since the losses generated by low and high dimensional variables are not easily comparable and it is non-trivial to find a correct re-weighting of such different loss terms. To the best of our knowledge, no current causal effect estimation algorithm can address this problem since there is no estimator that does not contain explicit image distribution, which is practically impossible to estimate. To deal with this problem, we map samples of I to a low-dimensional representation, RI with a trained encoder and match $P(D, RI, A)$ instead of $P(D, Image, A)$.

Note that, we use the mechanism training order $[I] \rightarrow [D, A]$ specified by the H-graph (Algorithm 1) to match the joint distribution $P(D, Image, A)$. It is not feasible to follow any other sequential training order such as $[D] \rightarrow [Image] \rightarrow [A]$ as training them sequentially with individual losses can not hold the dependence in $D \leftrightarrow A$.

F.3 Performance on Real-world COVIDx CXR-3 Dataset

In this section, we provide some more results of our experiment on COVIDx CXR-3 dataset (Wang et al., 2020). This dataset contains 30,000 chest X-ray images with Covid (C) and pneumonia (N) labels from over 16,600 patients located in 51 countries. The X-ray images are of healthy patients ($C = 0, N = 0$), patients with non-Covid pneumonia ($C = 0, N = 1$), and patients with Covid pneumonia ($C = 1, N = 1$). X-ray images corresponding to COVID non-pneumonia ($C = 1, N = 0$) are not present in this dataset as according to health experts those images do not contain enough signal for pneumonia detection. However, to make the GAN training more smooth we replaced a few ($C = 1, N = 1$) real samples with ($C = 1, N = 0$) dummy samples. We also normalized the X-ray images before training. To obtain the low dimensional representation of both real and fake X-ray images, we used a Covid conditional trained encoder. Instead of training \mathbb{G}_{Xray} from scratch, we use a pre-trained model (Giorgio Carbone, 2023) that can be utilized to produce Xray images corresponding to $C \in [0, 1]$ input. Note that, this pre-trained model takes value 0 for Covid, 1 for normal, and 2 for Pneumonia as input and produces the corresponding images. If a fake Covid sample indicates Covid=1, we map it to the 0 input of the pre-trained GAN. If a fake Covid sample indicates Covid=0, this might be either mapped to 1 (normal) or 2 (Pneumonia). Instead of randomly selecting the value, we use the real Pneumonia sample to decide this (either 1 or 2). After that, we produce X-ray images according to the decided input values. Since we are using the GAN-generated fake samples for Covid=1, the computational graph for auto grad is not broken. Rather the mentioned modification can be considered as a re-parameterization trick.

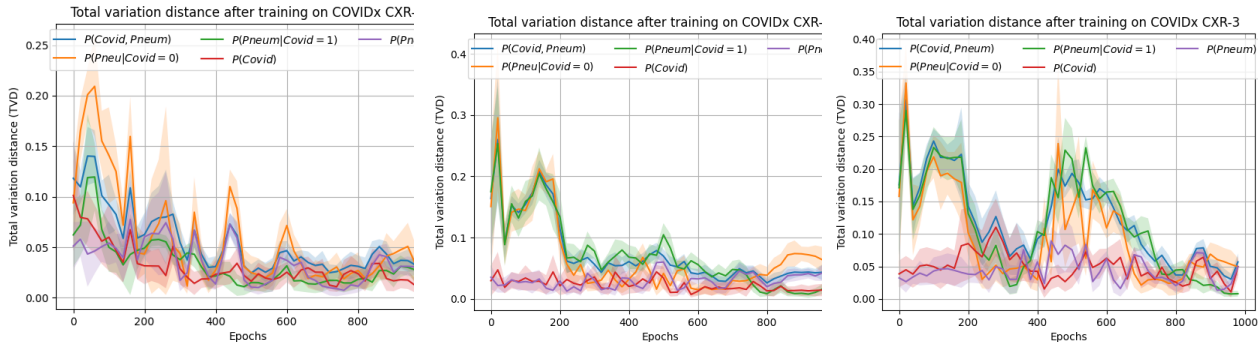


Figure 21: Total variation distance plots show Modular-DCM converges on COVIDx CXR-3 dataset. (consecutive 20 epochs were averaged)

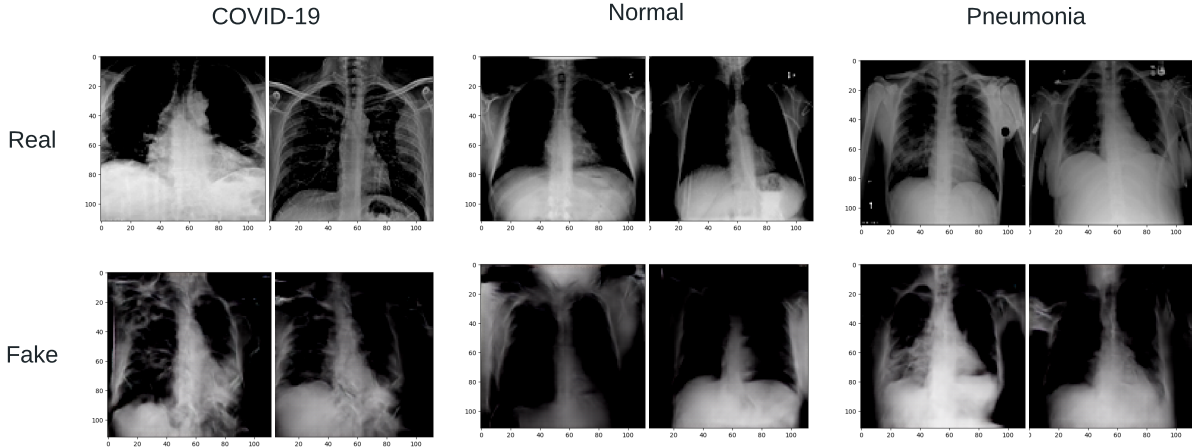


Figure 22: Real images from dataset vs pre-trained GAN generated images

F.4 MNIST Experiment 2: interventional and counterfactual Sampling from MNIST Dataset

In this section, we provide additional information about the experiment described in Section 5.4.

F.4.1 MNIST Experimental Setup

Here, we describe the synthetic SCM that was used for generating the dataset for this experiment.

$$\begin{aligned}
 p(U_1), p(U_2) &\sim \text{Dirichlet}([0.1, 0.1, \dots]) & X_1 &= U_1 + \epsilon_{X_1} \\
 X_2 &= U_2 \% 3 + X_1 * \text{Uniform}[3, 6] + U_1 + \epsilon_{X_2} & W &= X_1 + X_2 + \epsilon_W \\
 Y_1 &= \lfloor W^2 / 10 \rfloor + \epsilon_{Y_1} & Y_2 &= W^2 \% 10 + \epsilon_{Y_2} \\
 Color &= U_2 \% 3 + \epsilon_c & Thick &= \min(\lfloor (W^2 / 10) / 2 \rfloor, 1) + \epsilon_t
 \end{aligned}$$

We sample confounding variable U_1, U_2 and independent exogenous noises, $\epsilon_{X_i}, \forall i$ from Dirichlet distribution. We assign X_1 as a variable of binary uniform distribution in $[0, 1]$. $X_2 \in [0, 8]$, is correlated with U_2 and stays in $[0, 2]$ when $X_1 = 0$, and ranges in $[3, 8]$ when $X_1 = 1$. Also, X_1 and X_2 are confounded with U_1 . Variable $W \in [0, 9]$ is the sum of X_1 and X_2 . Next, $Y_1 \in [0, 9]$ is the first digit of W^2 and $Y_2 \in [0, 9]$ is the 2nd digit of W^2 . $Color \in [0, 2]$ refers to [R=red, G=green, B=blue] respectively and is confounded with X_2 by U_2 . $Thick \in [0, 1]$ referring to [th=thin, **Th**=thick] depends on the first digit of W^2 . We introduce 25% noise with all these relations to prevent them from becoming deterministic functions and also from having zero probabilities for any outcomes so that the strictly positive distribution assumption holds. Finally, we employ a procedure suggested in Castro et al. (2019) to produce $Image_1$ by using Y_1 as the digit parameter and produce $Image_2$ by using Y_2 as the digit parameter besides using $Color$ and $Thick$ as color and thickness parameters for both images. We consider we have access to one observational dataset, $D_1 \sim P(\mathcal{V})$ and two interventional datasets $D_2 \sim P_{X=0}(\mathcal{V}), D_3 \sim P_{X=1}(\mathcal{V})$.

F.4.2 MNIST Low Dimensional Variables

In Figure 23a, each blue box represent the h-nodes of \mathcal{H}^0 . Since h-nodes of $Image_1, Image_2$ are disconnected from other h-nodes, we can first train the low-dimensional mechanisms and use them later to train the Image mechanisms. On the other hand, instead of training, we can also utilize pre-trained models for $Image_1, Image_2$. Without violating the training order, (step-1:) we can first train $[\mathbb{G}_{X_1}, \mathbb{G}_{X_2}, \mathbb{G}_W, \mathbb{G}_{Color}]$ together, with both $\mathcal{L}_1, \mathcal{L}_2$ datasets: D_1, D_2 and D_3 . Next, (step-2:) we train $[\mathbb{G}_{Y_1}, \mathbb{G}_{Y_2}, \mathbb{G}_{Thick}]$ with only \mathcal{L}_1 dataset D_1 . Since intervention X_1 is not in these h-nodes, according to Corollary C.5, Modular-DCM can match both $P(Y_1, Y_2, Thick)$ and $P_{X_1}(Y_1, Y_2, Thick)$.

Modular-DCM training convergence at step-1 and step-2 is shown in Figure 23b. For each distribution in $P(V)$ and $P_{X_1}(V)$, TVD from the true distribution is decreasing. Moreover, both $P(Y_1, Y_2, Thick)$ and $P(Y_1, Y_2, Thick|do(X_1))$ are converging even though we trained this mechanisms with only \mathcal{L}_1 dataset; as expected according to modular training. Furthermore, according to Theorem C.3, after training on D_1, D_2 and D_3 , Modular-DCM can produce correct samples from distributions that are identifiable from $P(V)$ and $P_{X_1}(V)$. In Figure 23d, Modular-DCM illustrates this by producing counterfactual samples from $P_{x_1, x_2}(Color|x'_1, x'_2)$ with small TVD as it is identifiable from available distributions $P(V)$ (see derivation Appendix F.4.4). This experiment verifies that Modular-DCM can produce interventional and counterfactual samples correctly.

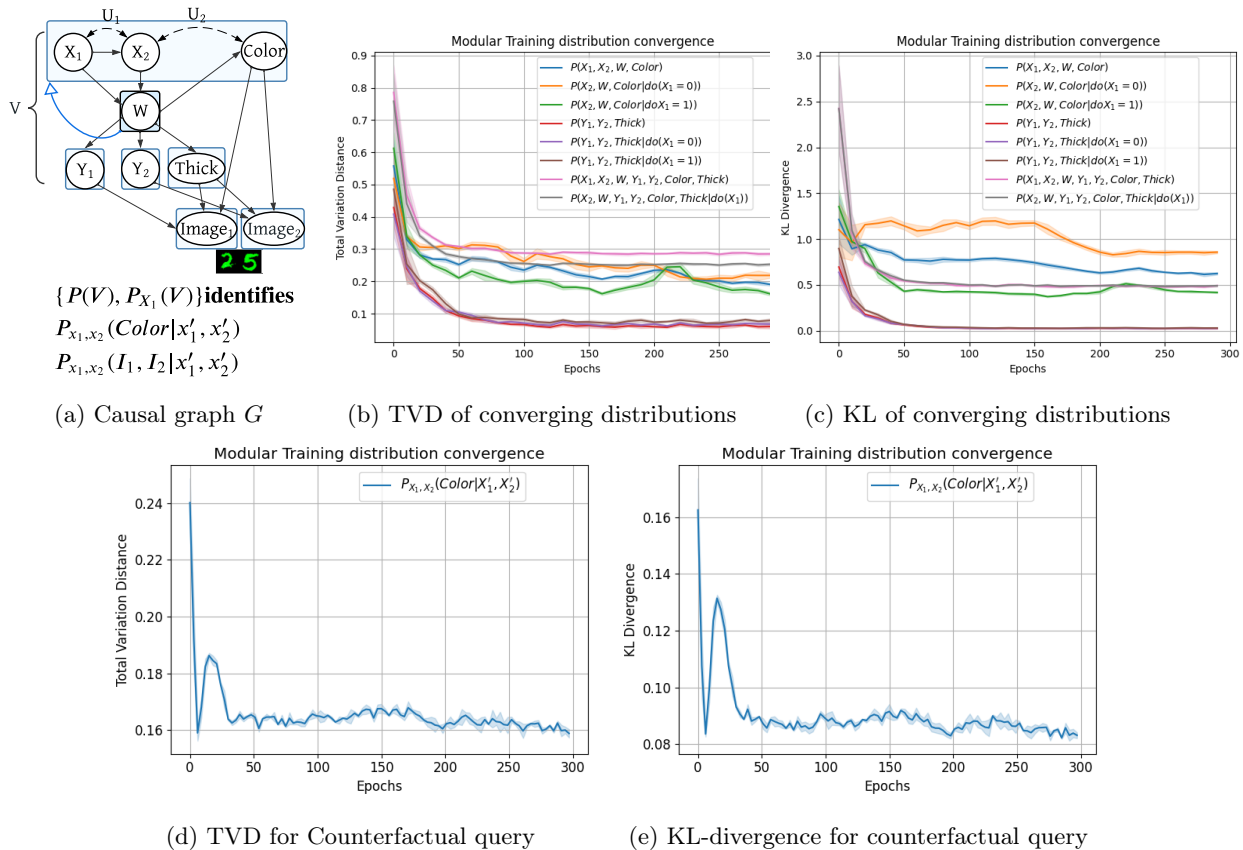


Figure 23: Convergence of \mathcal{L}_1 and \mathcal{L}_2 distributions of MNIST-low dimensional variables.

F.4.3 MNIST High Dimensional Variables

Causal queries	Most probables in SCM	Randomly chosen 10 $[image_1, image_2]$ samples produced from our algorithm Sorted according to probability distribution
Row 1, Layer 1: Observations $P(Y_1, Y_2, Color, Thick X_1=1, X_2=4)$	$[2\ 5\ \mathbf{G}\ \mathbf{Th}]$ $[2\ 5\ \mathbf{B}\ \mathbf{Th}]$ $[7\ 5\ \mathbf{G}\ \mathbf{Th}]$	$p=0.14$ $p=0.08$ $p=0.02$ $p=0.02$ $p=0.01$ $p=0.004$ $p=0.009$ $p=0.006$
Row 2, Layer 2: Interventions $P(Y_1, Y_2, Color, Thick do(X_1=1, X_2=4))$	$[2\ 5\ \mathbf{B}\ \mathbf{Th}]$ $[2\ 5\ \mathbf{G}\ \mathbf{Th}]$ $[7\ 5\ \mathbf{B}\ \mathbf{Th}]$	$p=0.14$ $p=0.11$ $p=0.02$ $p=0.02$ $p=0.02$ $p=0.01$ $p=0.01$ $p=0.003$
Row 3, Layer 3: Counterfactuals $P_{X_1=1, X_2=4}(Y_1, Y_2, Color, Thick X_1=0, X_2=1)$	$[2\ 5\ \mathbf{G}\ \mathbf{Th}]$ $[2\ 5\ \mathbf{B}\ \mathbf{Th}]$ $[7\ 5\ \mathbf{G}\ \mathbf{Th}]$	$p=0.17$ $p=0.085$ $p=0.03$ $p=0.03$ $p=0.02$ $p=0.01$ $p=0.01$ $p=0.005$ $p=1e-5$
Row 4, Layer 1: Observations $P(Y_1, Y_2, Color, Thick X_1=0, X_2=1)$	$[0\ 1\ \mathbf{G}\ \mathbf{th}]$ $[0\ 1\ \mathbf{G}\ \mathbf{Th}]$ $[0\ 7\ \mathbf{G}\ \mathbf{th}]$	$p=0.24$ $p=0.11$ $p=0.01$ $p=0.005$ $p=0.005$ $p=0.004$ $p=0.001$

Figure 24: For each query, the top 3 occurred image samples match with true SCM

In this section, we describe the experiment in Section 5.4 in more detail. After training the mechanisms of $V' = \{X_1, X_2, W, Color, Y_1, Y_2, Thick\}$, we can train $Image_1, Image_2$ mechanisms. We can also utilize pre-trained models of V' if available and use their output values as input to the image mechanisms. After training all the mechanisms in the causal model, we observed the results shown in Figure 24.

In row 1, for query $\in \mathcal{L}_1$, we condition on $X_1 = 1, X_2 = 4$. Therefore, without considering noise, according to the true SCM, we get $W = 5$ and $Y_1 = 5^2/10 = 2, Y_2 = 5^2\%10 = 5$. $Color = X_2\%3 = 1$ due to the confounder between X_2 and $Color$. $Thick = \lfloor (5^2/10)/2 \rfloor = 1$. This represents the highest probable outcome 2,5 with green color and thick=1 which is shown as the first outcome $[2, 5, \mathbf{G}, \mathbf{Th}]$ (column-2). We observe that, our trained gan also produces images of the same outcome with the highest probability, $p = 0.14$. In row 2, for query $\in \mathcal{L}_2$, we intervene on $X_1 = 1, X_2 = 4$. So, X_2 and $Color$ are not confounded anymore and $Color$ will have other outcomes besides green with high probability for example, blue. And as expected, our trained GAN also produces images with blue color with the highest probability.

In row 3, for query $\in \mathcal{L}_3$ we intervene on $X_1 = 1, X_2 = 4$ and X_2 does not have any confounding effect on $Color$. However, since we condition on $X_1 = 0, X_1 = 1$, we would have the corresponding confounder U_2 which will assign $Color = X_1\%3$, i.e, green. Due to this, the most probable counterfactual outcome according to true SCM is $[2\ 5\ \mathbf{G}\ \mathbf{Th}]$. We also find the same outcome with a high probability from our GAN samples. This indicates the ability of Modular-DCM to correctly produce counterfactual samples and differentiate between \mathcal{L}_2 and \mathcal{L}_3 queries. Finally, in the 4th row, we convert the previous \mathcal{L}_3 query into a \mathcal{L}_1 query, by removing the intervention but keeping the same conditions i.e., $X_1 = 0, X_2 = 1$. Our GAN produces green, thin digits of 0,1 with the highest occurrences which is also suggested by the true SCM. This is evidence of the capability of Modular-DCM to separate different causal layers and produce corresponding samples from each layer.

F.4.4 MNIST Derivation

We follow Shpitser and Pearl (2008) to obtain the counterfactual graph and the interventional expression of the counterfactual query for the causal graph shown in Figure 25. For convenience, we combine the variables $\{Y_1, Y_2, Thick, Image_1, Image_2\}$ into variable Y and will consider the counterfactual query $P(Y_{x_1, x_2} = y | x'_1, x'_2)$.

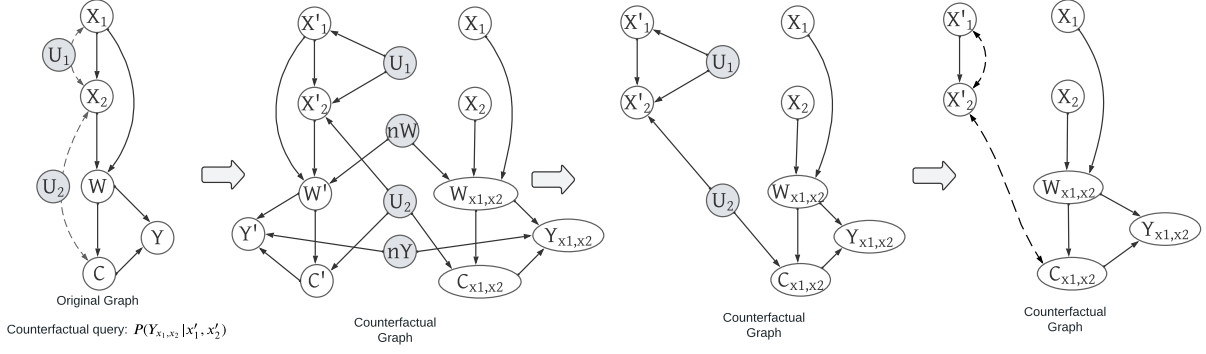


Figure 25: Counterfactual graph construction

In the counterfactual graph, there are three c-components (without fixed nodes: $\{X_1, X_2\}$). They are: $\{X'_1, X'_2, C\}$, $\{W\}$ and $\{Y\}$ (omitting the subscripts). Therefore, the expression is,

$$P(Y_{x_1, x_2} = y | x'_1, x'_2) = \frac{\sum_{w, c} P_w(x'_1, c, x'_2) * P_{x_1, x_2}(w) * P_{w, c}(y)}{\sum_{w, c, y} P_w(x'_1, c, x'_2) P_{x_1, x_2}(w) * P_{w, c}(y)} \quad (55)$$

Using do-calculus rule 2, we can write $P_{x_1, x_2}(w) = P(w | x_1, x_2)$ and $P_{w, c}(y) = P(y | w, c)$. Next the first term,

$$\begin{aligned} P_w(x'_1, c, x'_2) &= P_w(x'_1) * P_w(x'_2 | x'_1) * P_w(c | x'_1, x'_2) && \text{Factorization formula} \\ &= P(x'_1) * P(x'_2 | x'_1) * P_w(c | x'_1, x'_2) && \text{do-calculus rule 3} \\ &= P(x'_1) * P(x'_2 | x'_1) * P(c | x'_1, x'_2, w) && \text{do-calculus rule 2} \end{aligned} \quad (56)$$

So, finally we can write,

$$P(Y_{x_1, x_2} = y | x'_1, x'_2) = \frac{\sum_{w, c} P(x'_1) * P(x'_2 | x'_1) * P(c | x'_1, x'_2, w) * P(w | x_1, x_2) * P(y | w, c)}{\sum_{w, c, y} P(x'_1) * P(x'_2 | x'_1) * P(c | x'_1, x'_2, w) * P(w | x_1, x_2) * P(y | w, c)} \quad (57)$$

Therefore, if we can train Modular-DCM with datasets from only $P(V)$ then we can produce samples from this counterfactual query.

In Shpitser and Pearl (2009), the authors claimed that the counterfactual query $P(Y_{x_1, x_2} = y | x'_1, x'_2)$ is non-identifiable only from $P(V)$ due to the $X_1 \leftarrow U_1 \rightarrow X_2$ edge. After having a conversation with the authors we came to know that the claim was not correct. The counterfactual query is indeed identifiable from $P(V)$ as shown above.

F.5 Asia/Lung Cancer Dataset

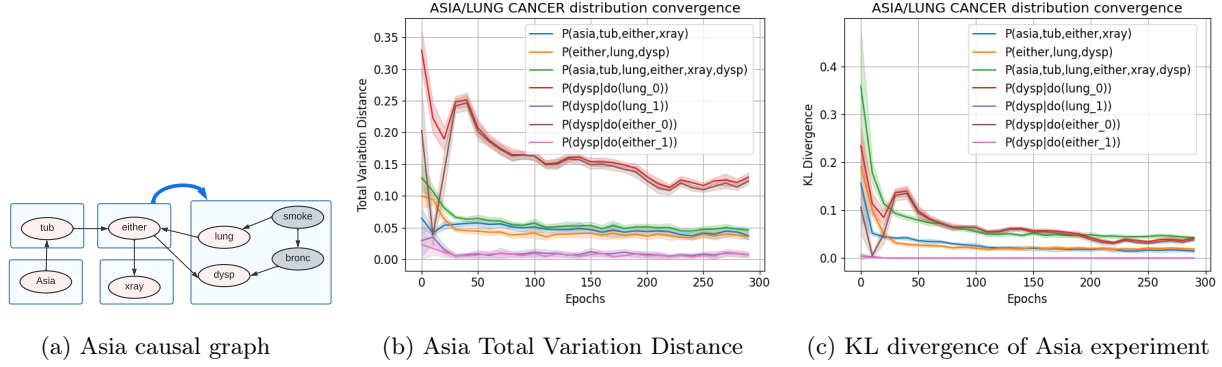


Figure 26: Modular Training on Asia Dataset

Asia Dataset. We evaluate our algorithm performance on ASIA Dataset from bnlearn repository (Scutari and Denis, 2021). The purpose of this experiment is to show that modular training can learn the joint distribution of the Asia dataset formed as semi-Markovian and correctly produces samples from identifiable \mathcal{L}_2 distributions. To check the effectiveness of Modular-DCM for a semi-Markovian causal model, we hide "smoke" and "bronc" variables in the observational dataset as shown in Figure 26a. This action gives us a causal graph with a latent confounder between the "lung" and the "dysp" variables. The \mathcal{H} graph nodes are indicated by the square box containing the variables. According to the algorithm, all \mathcal{H} -nodes are disconnected except $[either] \rightarrow [lung, dysp]$. Therefore, we first start training the mechanisms of $asia, tub, either, xray$ and then separately but in parallel train the mechanisms of $lung, dysp$. Here we can also use pre-trained $either$ while we train $lung, dysp$ to match the distribution $P(lung, dysp, either|tub)$. For evaluation, we generated samples from $P(dysp|do(lung))$ and $P(dysp|do(either))$ distributions from Modular-DCM. We can calculate $P(dysp|do(lung))$ with front-door adjustment and $P(dysp|do(either))$ with back-door adjustment using the real dataset samples. In Figure 26b, 26c, we can see that our partial training is working well with all of the distributions converging to low TVD and KL loss.

F.6 Real-world: Sachs Protein Dataset

For completeness, we test both Modular-DCM and NCM performance on a low-dimensional real-world Sachs dataset (Sachs et al., 2005), which contains a protein signaling causal graph and is given in Figure 27a. The goal is to illustrate Modular-DCM's capability of utilizing multiple partial $\mathcal{L}_1, \mathcal{L}_2$ datasets. We considered the observational dataset $D_1 \sim P(PKA, Mek, Erk, Akt)$ and the interventional dataset $D_2 \sim P(Mek|do(PKA = 2))$. The interventional dataset with $PKA = 2$ is chosen since it has a large number of samples. Here we intentionally hide variable PKC and considered it as a confounder. Hence, $P(Mek|do(PKA = 2)), P(Akt|do(PKA = 2))$ and $P(Erk|do(PKA = 2))$ are non-identifiable from only $P(V)$. According to Corollary C.5, $P(V), P(Mek|do(PKA = 2))$ make these distributions identifiable. More precisely, if we have access to $P(V)$ and $P_{PKA}(Mek)$ only, then it's sufficient to identify, $P_{PKA}(Mek, Erk, Akt)$. We have datasets D_1, D_2 that are sampled from $P(V), P(Mek|do(PKA = 2))$ for training. If we convert the Sachs graph into the train graph \mathcal{H} in Figure 27a, we see that for only the interventional dataset, we have to train the mechanism of Mek. This is because other variables except Mek belong to different hnodes or training components. Here,

$$\begin{aligned}
 & P_{PKA}(Mek, Erk, Akt) \\
 &= P_{PKA}(Mek)P_{PKA}(Erk|Mek)P_{PKA}(Akt|Erk, Mek) \\
 &= P_{PKA}(Mek)P(Erk|Mek, PKA)P(Akt|PKA, Erk, Mek)
 \end{aligned} \tag{58}$$

Therefore, we train Modular-DCM i.e., the DCM to match both $P(V)$ and $P(Mek|do(PKA))$. We *i*) first train $\mathbb{G}_{H_0} = [\mathbb{G}_{PKA}, \mathbb{G}_{Mek}]$ with both D_1 and D_2 , *ii*) next, train $\mathbb{G}_{H_1 \cup H_2} = [\mathbb{G}_{Erk}, \mathbb{G}_{Akt}]$ with only D_1 . In

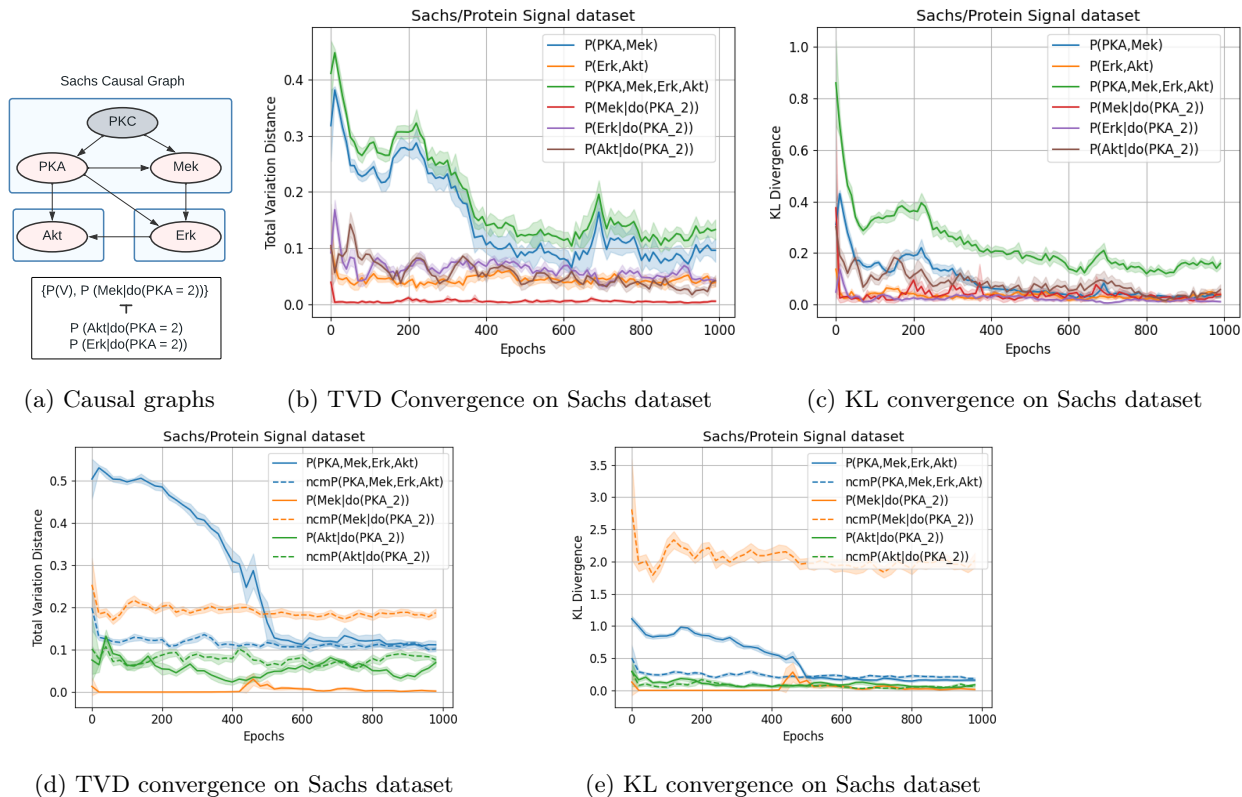


Figure 27: Benchmark and Real-world datasets

Figure 27b and 27c, Modular-DCM converges by training on both $P(V)$ and $P(Mek|do(PKA = 2))$ datasets. We compared the distributions $P(Akt|do(PKA = 2))$ and $P(Erk|do(PKA = 2))$ implicit in Modular-DCM generated samples with the Sachs \mathcal{L}_2 -dataset distributions and observed them matching with low TVD and KL loss. Even though, we don't observe Erk and Akt in D_2 , with modular training, we can still train the mechanisms with $P(V)$ and sample correctly from their \mathcal{L}_2 -distributions. This reflects the transportability of Modular-DCM. During Modular-DCM training, we can use pre-trained models of $\{PKA, Mek\}$, $\{Akt\}$ or $\{Erk\}$ since they are located in different hnodes.

Sachs dataset performance comparison with NCM: In Figure 27d and Figure 27e, we compare and show the convergence of both Modular-DCM and NCM with respect to total variation distance and KL-divergence. We observe that for low-dimensional variables, we perform similarly to DCM or better in some cases. However, they do not have the ability to utilize pre-trained models like we do. Besides, unlike NCM, we do not need to run the algorithm again and again for each identifiable queries. Thus, when queries are identifiable, our algorithm can be utilized as an efficient method to train on datasets involving low-dimensional variables.

F.7 Synthetic Experiment

We measure the performance of the approach where we train all the mechanisms together (Algorithm 3) and Modular-DCM Modular Training (Algorithm 2) on synthetic datasets produced from a random SCM consistent with the causal graph in Figure 28. We produce two observational datasets from the true causal model: $D_1 \sim P(V \setminus \{W_0, Y_0\})$, $D_2 \sim P(V \setminus \{Y_1\})$. We train the causal mechanism of our DCM by following the \mathcal{H}^0 -graph in Figure 28. Here, $H_0 = \{W_0\}$, $H_1 = \{W_1\}$, $H_2 = \{X_0, Y_0\}$, $H_3 = \{X_1, X_2, Y_1\}$. Let $p()$ be the (observational) data distribution. We perform modular training following the \mathcal{H}^0 -graph as following: *i*) Train $\mathbb{G}_{H_0} = [\mathbb{G}_{W_0}]$ with dataset D_2 by matching $p(w_0|x_0)$. *ii*) Train $\mathbb{G}_{H_1} = [\mathbb{G}_{W_1}]$ on D_1 to match $p(w_1|x_1, x_2, x_0)$. *iii*) Train $\mathbb{G}_{H_2} = [\mathbb{G}_{X_0}, \mathbb{G}_{Y_0}]$ with dataset D_2 by comparing $p_1(x_0, w_1, w_0, y_0|do(x_1, x_2))$. Here, we can use pre-trained W_0, W_1 . *iv*) Finally we train the mechanisms in $\mathbb{G}_{H_3} = [\mathbb{G}_{X_1}, \mathbb{G}_{X_2}, \mathbb{G}_{Y_1}]$ together, with dataset D_1 such that after convergence, $p_1(x_1, x_2, w_1, y_1|do(x_0))$ matches. Here, we can use pre-trained W_1 .

We show the experimental result in Figure 28. Here, $P_1()$ represents the sample distributions from Modular-DCM after running Algorithm 3 (i.e. training all the mechanisms together) and $P_2()$ represents the distributions after running Algorithm 2, the Modular Training. We trained each \mathcal{H} -nodes in parallel for 150 epochs. Line 4,5 represents the distribution convergence corresponding to H_4, H_5 in terms of the total variation distance from the true distribution. Line 6 shows the convergence of joint distribution $P_2(V)$ with Modular Training. Line 1,2,3 represent the same distributions but with Algorithm 3. We observe that each partial sample distributions converges with very small total variation distance loss: < 0.10 and joint distribution for modular training also converges with low TVD loss: < 0.16 . For both algorithms, the TVD loss is similarly small, proving the validity of modular training of Modular-DCM.

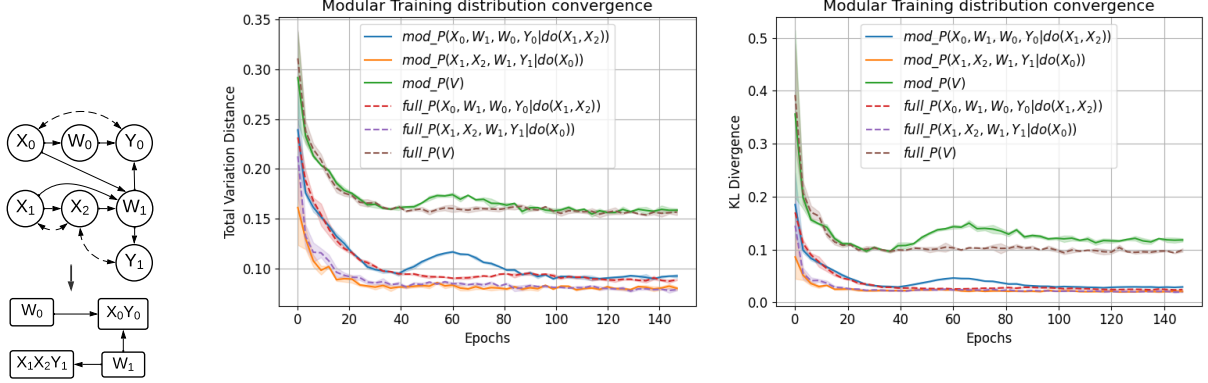


Figure 28: Convergence of full training and modular training on observational datasets.

Training each h-node matches the following distributions of D_1 and D_2 :

$$\begin{aligned}
H_0 &\implies p(w_0|x_0) = q_{x_0}(w_0) \\
H_1 &\implies p(w_1|x_0, x_1, x_2) = q_{x_0, x_1, x_2}(w_1) \\
H_2 &\implies p(x_0, w_0, y_0, w_1|x_1, x_2) = q_{x_1, x_2}(x_0, w_0, y_0, w_1) \\
H_3 &\implies p(x_1, x_2, w_1, y_1|x_0) = p_{x_0}(x_1, x_2, w_1, y_1)
\end{aligned} \tag{59}$$

Therefore, matching each distribution, we match the joint distribution.

$$\begin{aligned}
p(v) &= p_{w_1}(x_1, x_2, y_1) * p_{w_0, w_1}(x_0, y_0) * p_{x_0}(w_0) * p_{x_0, x_1, x_2}(w_1) \\
&= p_{x_0, w_1}(x_1, x_2, y_1) * p_{x_1, x_2, w_0, w_1}(x_0, y_0) \\
&\quad * p_{x_0}(w_0) * p_{x_0, x_1, x_2}(w_1) \\
&= \frac{p_{x_0}(x_1, x_2, w_1, y_1)}{p_{x_0, x_1, x_2}(w_1)} * \frac{p_{x_1, x_2}(x_0, w_0, y_0, w_1)}{p_{x_0, x_1, x_2}(w_0) * p_{x_0, x_1, x_2}(w_1)} \\
&\quad * p_{x_0}(w_0) * p_{x_0, x_1, x_2}(w_1) \\
&= \frac{p(x_1, x_2, w_1, y_1|x_0)}{p(w_1|x_0, x_1, x_2)} * \frac{p(x_0, w_0, y_0, w_1|x_1, x_2)}{p(w_0|x_0, x_1, x_2) * p(w_1|x_0, x_1, x_2)} \\
&\quad * p(w_0|x_0) * p(w_1|x_0, x_1, x_2) \\
&= \frac{q(x_1, x_2, w_1, y_1|x_0)}{q(w_1|x_0, x_1, x_2)} * \frac{q(x_0, w_0, y_0, w_1|x_1, x_2)}{q(w_0|x_0, x_1, x_2) * q(w_1|x_0, x_1, x_2)} \\
&\quad * q(w_0|x_0) * q(w_1|x_0, x_1, x_2) \\
&= q(v)
\end{aligned} \tag{60}$$

G Algorithms & Pseudo-codes

Algorithm 8 $\text{isIdentifiable}(G, \mathcal{I}, query)$

```

1: Input: Causal Graph  $G = (\mathcal{V}, \mathcal{E})$ , Interventions =  $I$ , Causal query distribution =  $query$ 
2: if  $\text{type}(query) = \text{Counterfactual}$  then
3:   Return  $\text{Run\_IDC}(G, query, I)$ 
4: else if  $\text{type}(query) = \text{Interventional}$  then
5:   Return  $\text{Run\_ID}(G, query)$  or  $\text{hasSurrogates}(G, query, I)$ 

```

Algorithm 9 $\text{RunGAN}(G, \mathbb{G}, V_{\mathbf{K}}, I, N)$

```

1: Input: Causal Graph  $G = (\mathcal{V}, \mathcal{E})$ , DCM  $\mathbb{G}$ , target variable set  $V_{\mathbf{K}}$ , Intervention  $I$ , Pre-defined noise  $N$ .
2: for  $V_i, V_j \in V_{\mathbf{K}}$  such that  $i < j$  do
3:   if  $V_i, V_j$  has latent confounder then
4:      $z \sim p(z)$ 
5:      $conf[V_i] \leftarrow \text{Append}(conf[V_i], z)$ 
6:      $conf[V_j] \leftarrow \text{Append}(conf[V_j], z)$  // Assigning same confounding noise [fix for multiple confounders]
7: for  $V_i \in V_{\mathbf{K}}$  in causal graph,  $G$  topological order do
8:   if  $V_i \in I.keys()$  then
9:      $v_i = I[V_i]$  // Assigning intervened value
10:  else
11:     $par = \text{get\_parents}(V_i, G)$ 
12:    if  $V_i \in N.keys()$  then
13:       $exos, conf, gumbel = N[V_i]$ 
14:    else
15:       $exos \sim p(z)$ 
16:       $conf = conf[V_i]$ 
17:       $gumbel = \emptyset$ . //New Gumbel noise will be assigned during forward pass
18:     $v_i = \mathbb{G}_{\theta_i}(exos, conf, gumbel, \hat{\mathbf{v}}_{par})$ 
19:     $\hat{\mathbf{v}} \leftarrow \text{Append}(\hat{\mathbf{v}}, v_i)$ 
20: Return Samples  $\mathbf{v}$  or Fail

```

Algorithm 10 $\text{Evaluate_GAN}(G, \mathbb{G}, \mathcal{I}, query)$

```

1: Input: Causal Graph  $G = (\mathcal{V}, \mathcal{E})$ , DCM =  $\mathbb{G}$ , Available Interventions =  $\mathcal{I}$ , Causal query distribution =  $query$ 
2: if  $\text{isIdentifiable}(G, \mathcal{I}, query) = \text{False}$  then
3:   Return: Fail
4: if  $\text{type}(query) = \text{observation}$  then
5:    $Y = \text{Extract}(query)$ 
6:    $samples \leftarrow \text{RunGAN}(G, \mathbb{G}, [Y], \emptyset, \emptyset)$ 
7: else if  $\text{type}(query) = \text{Intervention}$  then
8:    $Y, (X, x) := \text{Extract}(query)$ 
9:    $samples \leftarrow \text{RunGAN}(G, \mathbb{G}, [Y], \{X : x\}, \emptyset)$ 
10: else if  $\text{type}(query) = \text{Counterfactual}$  then
11:    $Y, (X, x), (X, x') := \text{Extract}(query)$ 
12:    $exos, conf, gumbel \leftarrow \text{RejectionSampling}(\{X : x'\})$ 
13:    $N \leftarrow [exos, conf, gumbel]$ 
14:    $samples \leftarrow \text{RunGAN}(G, [Y], \{X : x\}, N)$ 
15: Return  $samples$ 

```

H Questions and Answers about Modular-DCM

In this section, we answer some questions that might come into readers' minds.

1. **How does our algorithm work for complicated and larger graphs?**

Ans: In Appendix E, we use two graphs with 6 nodes and 27 nodes to show how our algorithm works. We also show our algorithm performance on different graphs in Appendix F. Specifically, in Appendix F.4, we show our performance on a Colored-MNIST experiment where the causal graph contains 7 discrete variable nodes and 2 image nodes. In Appendix F.5, we perform an experiment on the ASIA causal graph from the online bnlearn repository. In Appendix F.6, we show our algorithm performance on the real-world Sachs protein dataset. In Appendix F.7, we show performance on a synthetic experiment with a 7 node causal graph.

2. **What is the benefit of a pre-trained model over training a conditional generator on the observed dataset? Is there a risk that the distribution the pre-trained model was trained on will not match the distribution of the observed dataset?**

Ans: Training a conditional GAN from scratch might require abundant data and resources but if pre-trained, we can use them as black boxes. This gives us the scope to utilize large image-generative models in causality. For example, for the graph $D \rightarrow Image \rightarrow A, D \leftrightarrow A$ in Figure 5a, we could try to match the joint distribution $P(D, Image, A)$ by training all mechanisms together with the same loss from scratch. In that case: i) we could not use any pre-trained models ii) it would not be easy to get convergence due to the contribution of both low and high dimensional variables in the same loss function.

We assume that a pre-trained model correctly captures a part of the joint distribution of which other parts are captured when we train the rest of the network. Specifically, in the $D \rightarrow Image \rightarrow A, D \leftrightarrow A$ graph, we assume the black box \mathbb{G}_{Image} is correctly trained to sample image from the inputs same as $P(Image|D)$. Thus, we can train mechanisms $\mathbb{G}_D, \mathbb{G}_A$ to match $P(D, Image, A)$.

3. **How are the pre-trained generative models playing a role in our algorithm?**

Ans: We follow the partial order of \mathcal{H} -graph to train our DCM in a modular fashion. While we are training the mechanisms in an h-node, we can always use pre-trained models for variables outside the h-node. This gives us the flexibility to plug in any pre-trained large models in our training mechanism instead of training them from scratch.

4. **Which generative models do we use for our algorithm?**

Ans: We use Conditional Generative Adversarial Nets (Mirza and Osindero, 2014) as neural architectures for the variables in the same c-component that share the same confounders. We choose GANs for this purpose since GANs are effective in matching a joint distribution by feeding the same prior noise into multiple generators. For variables that are not confounded with others, we can use any architecture such as diffusion models Ho and Salimans (2022).

5. **How does the GAN convergence impact the theory of our work?**

Ans: We proposed our theorems with the assumption that GAN will properly converge and our algorithm will give correct results. However, due to different issues with GAN training such as mode collapse or convergence failure, it is not unnatural to not converge. As a result, some errors will be introduced in the sampling process. Nonetheless, our algorithm is independent of the method used to train each module and GAN convergence can not break any of our theorems. Thus, one can use state-of-the-art generative models such as style-gan or diffusion models for training each module to improve the GAN training issues.

6. **Can our algorithm intervene with continuous values?**

Ans: Do-calculus does not require discrete variables under certain regularity conditions. One can easily see this from the proofs of the rules from Pearl (1995). Since the Identification algorithm Shpitser and Pearl (2008) and derivatives can be seen as sequential applications of these rules, our proofs follow identically irrespective of the data type. For example, in the experiment described in section 5.2, the generated images are continuous vectors of pixels. Here we can sample from $P(C|do(D)), P(Image|do(D)),$ and $P(C|do(Image))$.